University of Cape Town

Department of Chemical Engineering

Centre for Catalysis Research

The Effect of Metal Type and Loading on n-Paraffin Hydrocracking Conversion and Selectivity

Wynne, Peter D.T.

submitted as partial fulfilment for the degree of

Master of Science in Engineering

December 2013

SYNOPSIS

With the continued decline in global oil reserves, there is a growing need to develop alternative sources of conventional fuels to complement the current dependence on crude oil feedstocks. Natural gas, coal and biomass have been identified for this purpose. The distinctive advantage of using natural (stranded) gas is that it is turned into a useful product, thereby increasing its value and reducing the environmental impact of simply flaring it.

The value-added work up of natural gas is effected by Gas-to-Liquid conversion via the Fischer-Tropsch Synthesis. Long-chain hydrocarbon waxes are produced and these are subsequently hydrocracked into the required middle distillate fuels, preferably diesel, as diesel engines are more efficient than their petrol counterparts.

Hydrocracking may be carried out using a bifunctional catalyst, consisting of metal and acid components. Industrially, hydrocracking is used to crack heavy crude oil fractions into the desired fuel range, however, the catalysts used are sulphided transition metals. These are less suitable for cracking Fischer-Tropsch waxes as they would introduce sulphur into a clean feedstock. Moreover, at reaction temperatures of around 250°C, transition metal sulphide catalysts display little activity. Thus, one may consider noble metals such as palladium or platinum, whilst shape selective zeolites may be used as the acid component.

There is, however, very little published research on the comparative activity of various metals that could be used as the metal function for such a hydrocracking process. Furthermore, the research that has been conducted is not readily comparable for reason of problems associated with differing metal dispersions and cluster formation. Generally, the activity of noble metals can only be compared when all other parameters are kept constant. By removing the noble metal from the acid catalyst and physically separating the two catalyst functions, it is ascertained that the noble metal dispersion does not influence the number and accessibility of acid sites nor does the catalyst acidity influence the dispersion of the noble metal. This allows for an independent evaluation of the acid and metal functions, while removing the associated uncertainties regarding metal dispersion and location.

The aim of this study is to quantify the activity of platinum, palladium, cobalt and nickel, in a hydrocracking environment using n-hexadecane as a representative compound for Fischer-Tropsch wax.

A duplicate experimental apparatus was designed, built and commissioned, each with two trickle phase reactors, so as to test four catalysts at a time. Product analysis was done by online gas chromatography.

It was found that increasing the metal site to acid site ratio increased the overall activity of the bifunctional catalysts; however, at the highest ratios evaluated this became limited, probably due to mass transfer effects. As expected the noble metals were more active than the base metals, platinum being the most active. However, very little useful information could be deduced in respect of selectivities as, in all cases, the product carbon number distributions were indicative of severe overcracking and were essentially indistinguishable regardless of metal type, metal loading or conversion level. It is proposed that this observation is a result of an excessive diffusion (metal site to acid site) distance imposed by the physically mixed catalyst configurations applied and that in all cases the product distributions were wholly controlled by the strong acid function.

From this work it is recommended that future work in this area considers direct metal loading on the zeolite while still attempting to tailor specific metal site to acid site ratios so as to ensure fair comparisons between the four metals.

ACKNOWLEDGEMENTS

I would like to gratefully acknowledge the efforts and support of all those involved in this research, specifically:

Dr Roald Brosius, for all his assistance in the lab, without whose help and insight I would not have been able to get the experimental unit working and producing reliable data. His willingness and time taken to read over this document is also greatly appreciated.

Mr Ross Kukard, for all the time we spent designed, building, setting up and running these experimental units.

Mr Stephen Roberts and Mr Marc Wust, for their guidance in designing and building the experimental apparatus and their continued willingness to help out when asked.

Mr Walter Böhringer, for the large amount of help in preparation of this thesis, supervision and direction in the research and assistance with day-to-day queries regarding the results.

Prof. Jack Fletcher, for the opportunity to carry out this research under his guidance and subsequent support in determining the direction of this work.

Johnson Matthey Technology Centre (UK) for providing the supported metal catalysts that were tested in this work.

University of Cape Town, **Department of Chemical Engineering,** for funding.

University of Cape Town, Postgraduate Funding Office, for funding.

Department of Chemical Engineering colleagues and friends, for always keeping the office atmosphere pleasant, lively and adding to discussions regarding catalysis and everything else.

Friends and family, for supporting me the whole time through this epic and telling me to keep going. Without the chasing up I might have given up a long time ago.

DECLARATION

I, Peter Wynne, declare that all information contained within this dissertation is my own work, with all information obtained from other sources acknowledged and referenced.

Sign: _____ Date: _____

TABLE OF CONTENTS

LIST OF FIGURES

LIST OF TABLES

GLOSSARY

F-T	-	Fischer-Tropsch – A process used to convert syngas (H_2 / CO mixture) into long chained hydrocarbons
JMTC	-	Johnson Mathew Technology Centre
M/A (ratio)	-	Metal site / Acid site ratio – This is the ratio between the number of the metal sites and acid sites and is used to determine the different reactor loadings
P	-	Pressure - for all experiments conducted this was 20 bar
T	-	Temperature - for all experiments conducted this was 225°C
sccm	-	Standard cubic centimetres per minute
WHSV	-	Weight hourly space velocity – This is the amount of feed fed in grams per weight of acid catalyst per hour ($g_{feed}/g_{acid.cat}.hr$)

1 INTRODUCTION

The world currently relies almost solely on conventional crude oil reserves as the source for liquid fuels for automotive and industrial applications. However, these reserves are limited and, therefore, this approach is unsustainable. In an attempt to move away from this reliance on crude oil reserves alternative fuel sources are being considered.

There are large resources of available natural gas and coal. Furthermore, stranded gas found with traditional petroleum reserves is usually vented and flared as it is too expensive to be stored and transported. Gas-to-Liquid conversion is a highly attractive way to prevent this vented gas from being flared and also add monetary value to it by converting it into liquid fuels. This has the added environmental advantage of making use of this gas rather than simply burning it.

As diesel engines are more efficient than their petrol counterparts and, thus, are increasing in demand, a synthetic fuel produced by wax hydrocracking would be desired to fall in the distillate fuels (diesel) range, whilst retaining the low sulphur content typical of Fischer-Tropsch fuels. This would enable the use of other technologies, such as catalytic converters, to aid in the reduction of harmful emissions.

The Gas-to-Liquid or Coal-to-Liquid conversion processes, making use of Fischer-Tropsch synthesis, convert syngas (hydrogen and carbon monoxide mixture) into a range of hydrocarbons. The syngas can be produced by steam reforming of stranded gas or steam gasification of coal.

The Fischer-Tropsch process is, unfortunately, highly unselective, with maximum theoretical distillate fuel yields of only 30 wt%. It is nonetheless possible to produce waxes with high selectivity and to subsequently hydrocrack these waxes into synthetic fuels to achieve, overall, an approximate 80% middle distillate selectivity.

Bifunctional hydrocracking catalysts currently used in the processing of crude oil are less suitable for the hydrocracking of Fischer-Tropsch waxes as they consist of metal sulphides. Though the product would not be highly branched (something that is desirable with respect to diesel cetane number), these catalysts would only serve to add sulphur to a sulphur free feedstock. Metal / acid catalysts that use amorphous silica-alumina as the acid component or

a large pore acid zeolite for the processing of linear waxes would produce a highly branched undesired product. Hence, more shape selective zeolites may be employed instead.

There is very little published research on the comparative activity between the possible metals that could be used for this hydrocracking process, as only a few companies currently operate large scale Fischer-Tropsch refineries. The research that has been conducted so far has been found to be rather inconsistent due to problems associated with differing metal dispersions and metal cluster formation.

Recently, a new testing methodology was developed which allows more accurate tests be carried out on bifunctional hydrocracking catalysts by removing the problems associated with different metal dispersions and cluster formation. The methodology is based on the concept of hydrogen spillover that allows the loading of the metal on a separate inert carrier, just physically mixed with the acid co-catalyst. This enables the independent evaluation of the acid and metal functions. Hence, using this method, the aim is to determine the order of (de)hydrogenation activity of a number of metals in a hydrocracking reaction and to observe the effect of different metal / acid ratios of the combined catalyst system.

2 BACKGROUND

2.1 The Need for New Fuels from Natural Resources other than Crude Oil

Currently, the world relies almost solely on conventional petroleum reserves, namely crude oil, as the source for liquid fuels used in most automotive and industrial applications. However, these reserves have a limited life time which, according to some estimates, maybe 40 to 140 years (Ebenhack, 2001).

In an attempt to move away from this reliance on crude oil reserves, alternative fuel sources are being studied. Ideally, these alternative sources are desired to produce fuels of similar, if not better, quality that that obtained from crude oil. Natural gas and coal have been identified as other possible sources that fit this criterion.

There are significant advantages in gas-to-liquid (GTL) conversion of natural gas to distillate fuels and, thus, there has been growing interest in this field. GTL has been found to be a practical route for adding value to natural gas while being able to obtain high quality products; essentially free from nitrogen, sulphur and aromatic compounds. This is desired as more stringent regulations are passed to reduce harmful exhaust emissions (Calemma *et al.*, 2000). It was found that a virtually unlimited market exists for GTL diesel as it can be used as fuel directly or blended with traditional refinery products to help meet specifications on sulphur content and cetane number. Furthermore, a number of other middle distillate products can be produced including jet fuel and kerosene. Additional benefits are the reduction in greenhouse gas emissions from the flaring of natural gas found with crude oil deposits, while allowing the production of ultra clean products (Collins *et al.*, 2006).

Stranded gas (natural gas) released during the recovery of crude oil is often flared and thus wasted (W. Böhringer, University of Cape Town (UCT), Personal Communication, 2006). This flared gas has a huge potential to be used as a source of fuel, be it as natural gas, or by conversion to liquid fuel stocks. However, the former this is not usually done due to the cost of either compression or chilling (for liquefaction), storage and transportation of this gaseous product. However, this stranded gas can be converted to liquid synthetic fuels by, for example, Fischer-Tropsch Synthesis.

Furthermore, there is a continual desire to reduce harmful emissions from automotive and industrial sources. Recently this has been carried out by using catalytic converters to remove carbon monoxide, nitrous oxides and any remaining hydrocarbons. Unfortunately these

catalytic converters (especially those in diesel-powered vehicles) are vulnerable to poisoning by sulphur compounds (ORNL, 2000), and since all crude oils contain sulphur compounds these need to be removed by expensive hydrotreating. Furthermore, the venting of stranded gas, by burning, is not only a waste of a possible feedstock but this is also a significant source of carbon dioxide.

As diesel engines are approximately 40% more fuel efficient than their petrol counterparts (~35% compared to ~25%), according to some sources (ORNL, 2000), they are gaining popularity in consumer markets. Consequently, the desired synthetic fuels should be in the diesel range (with carbon numbers of 12 to 22), with a high cetane number achieved by having linear, paraffinic hydrocarbon compounds. Additionally, the fuel should contain no sulphur compounds which would increase harmful emissions and possibly negate the use of catalytic converters (ORNL, 2000).

An alternative does exist that involves the conversion of natural gas into methanol (CH_3OH) and then on to petrol in the Methanol-to-Gasoline (MTG) process. However, as diesel engines are more efficient than petrol engines (due to their higher compression ratios) this is not the preferred route, as the overall system efficiency is reduced.

2.2 Gas-To-Liquid (GTL) Conversion using Fischer-Tropsch Synthesis

Fischer-Tropsch (F-T) synthesis is an industrial process in which mainly linear hydrocarbons, both paraffins and olefins, may be synthesised catalytically from carbon monoxide and hydrogen (known as syngas). This syngas feedstock may be produced from a number of sources such as coal gasification or natural gas reforming (Dry, 2003).

The chain length of these hydrocarbons depends on the catalyst and reactor operating conditions, with products ranging from methane (C_1) to waxes ($>C_{45}$). The significant advantage of the hydrocarbons produced using F-T synthesis is the fact that they are clean (i.e. contain no sulphur, nitrogen or heavy metals) as it is easy to remove these undesired compounds from the syngas. Furthermore, the product is essentially linear (Dry, 2003).

Unfortunately, the Fischer-Tropsch process is particularly unselective, with a maximum achievable selectivity towards the desired middle distillate fuels (essentially diesel) being approximately 30 wt% (see Figure 2.1). This is unacceptably low to be of realistic economic feasibility for the sole production of distillate fuels.

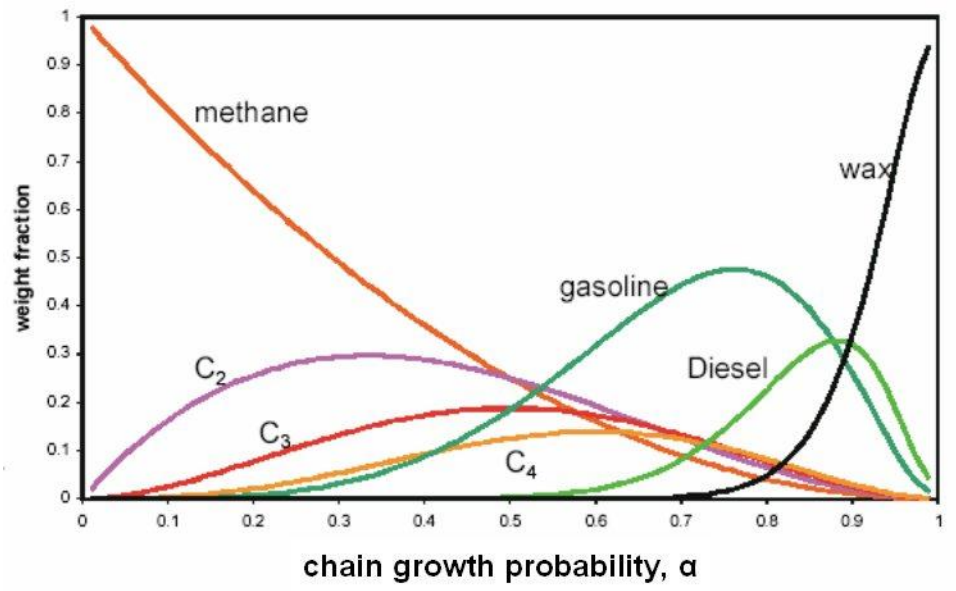

Figure 2.1: Fischer-Tropsch Product Selectivity as a function of Chain Growth Probability (Böhringer et al., 2006b)

Nevertheless, from Figure 2.1, it can be seen that at certain reaction conditions, where the chain growth probability (α) is approximately one, waxes can be produced with high selectivity (~95 wt%).

These waxes form the perfect feedstock for the hydrocracking process, whereby these linear hydrocarbon waxes may be hydrocracked into the required distillate fuel range by using bifunctional catalysts, comprising metal and acid functions, thus producing high quality, clean distillate fuels (Böhringer *et al.*, 2006a). This increases the overall selectivity of distillate fuels from 30% to 80% (Shah *et al*., 1988).

In Figure 2 a simplified block flow diagram depicts the processes involved in the conversion of natural gas into liquid distillate fuels. This research project will focus on the wax hydrocracking stage of the process.

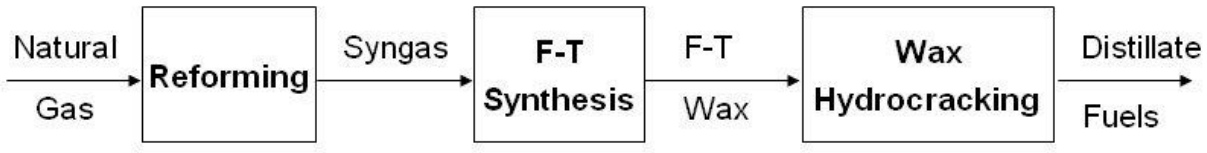

Figure 2.2: Gas-to-Liquid Conversion of Natural Gas to Distillate Fuels by Fischer-Tropsch Synthesis and Hydrocracking (Böhringer et al., 2006b)

2.3 Concepts in Bifunctional Hydrocracking

Essentially, hydrocracking is the breaking down of large organic molecules into smaller saturated hydrocarbon fragments in the presence of hydrogen. In discussing the cracking of hydrocarbons, three principally different reaction mechanisms must be considered. These are:

(i) „true hydrocracking" i.e. acid catalysed hydrocracking over a bi-functional catalyst, consisting of (de)hydrogenation and acid functions,
(ii) non-bond specific hydrogenolysis,
(iii) „methanolysis", a variant of hydrogenolysis that is successively cleaving terminal carbon atoms as methane. The latter two happen over a mono-functional catalyst consisting of pure metal, metal oxide or sulphide (Böhringer *et al.*, 2006).

While these mechanisms may exist simultaneously in the hydrocracking of F-T products in the study, the major mechanism should be „true hydrocracking", commonly known as bifunctional hydrocracking, so as to limit light gas and methane formation.

2.3.1 True Hydrocracking

2.3.1.1 The Classical Mechanism

The traditional bifunctional reaction mechanism over metal / acid catalysts for the hydrocracking of hydrocarbons involves a number of consecutive steps and various intermediates, with reactions occurring on different, physically distinct catalytically active sites. This classical concept, which is widely accepted, was initially proposed by Mills *et al.* (1953) and by Weisz and Swegler (1957).

The classical mechanism involves two different catalyst components, an acid and a dehydrogenation/hydrogenation component, the latter being a noble metal, for instance. Both play a fundamental role in the overall mechanism, with supported metal sites carrying out the dehydrogenation of saturated feed hydrocarbons and the hydrogenation of any formed olefinic fragments, while the skeletal re-arrangements (isomerisation and β-scission) occur on the acid centres (Martens and Jacobs, 1997). Figure 2.3 shows the classical reaction mechanism for the bifunctionally catalysed hydrocracking reaction of a long-chained paraffin over platinum (Pt) supported on an acidic catalyst.

The paraffin is initially dehydrogenated on the metal surface to form an olefin, which travels by gas phase diffusion (Weisz and Swegler, 1957) to the acid site. The carbenium ion formation occurs by the olefin adsorbing to the acidic sites of the acid support. This ion then undergoes isomerisation, alkylation or cracking. Having undergone a number of transformations the products desorb as olefins and diffuse, by fluid phase diffusion, back to the metal component (Park and Ihm, 2000), where they are subsequently hydrogenated. The rate limiting steps in the classical hydrocracking mechanism are both the rearrangement of the original linear alkyl carbenium ions to form species with sufficient branching for easy cracking to proceed and the β-scission of the C-C bond (Martens and Jacobs, 1990).

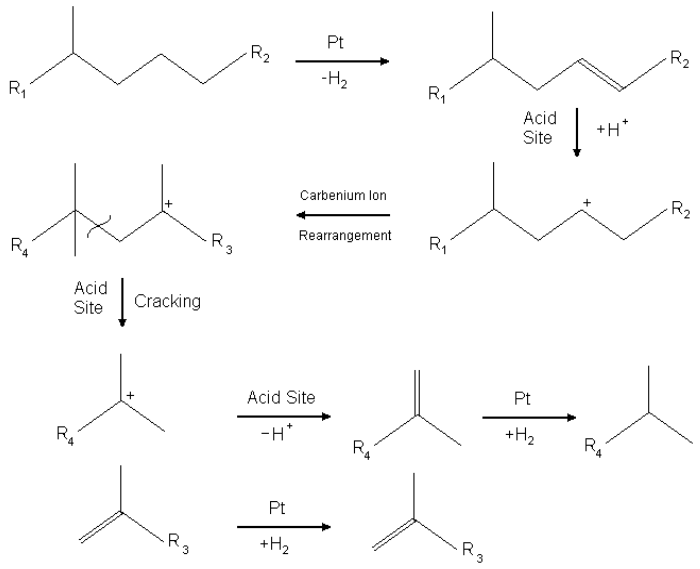

Figure 2.3: Schematic of Bifunctional Catalytic Hydrocracking (Adapted From Martens and Jacobs, 1997; Böhringer et al., 2006b)

2.3.1.2 The Hydrogen Spillover Mechanism

However, a number of results fail to be explained adequately by the classical mechanism. In a series of hydroisomerisation experiments carried out by Roessner and Roland (1996), the different catalyst functions (acid function and metal function) were physically separated using a number of reactor configurations of which two are shown in Figure 2.4.

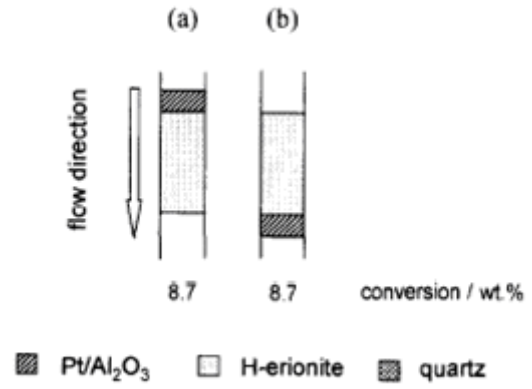

Figure 2.4: Different Physical Arrangements of 0.5wt% Pt/Al_2O_3 (10mg) and H-erionite (1g)

Feed = n-hexane, T = 497 K, T.O.S. = 7 hrs
(a) Layer of Metal Co-Catalyst above the Acid Co-Catalyst
(b) Layer of Metal Co-Catalyst below the Acid Co-Catalyst
(Adapted from Steinberg *et al.*, 1990)

According to the classical mechanism, in system (a) the product should be highly olefinic as there is no hydrogenation function downstream of the acid function. Furthermore, in system (b), it would be expected for there to be no isomerisation / cracking conversion as the feed paraffin, after activation, no longer sees any downstream isomerisation / cracking acid function. However, from the conversions shown (in Figure 2.4), the collaboration between the catalysts is clearly visible, with conversions and selectivities also found to be similar to mechanical mixtures (of the two co-catalysts). Furthermore, the position of the metal supported catalyst, either at the top or bottom of the bed, was found to have little effect.

In theoretical calculations carried out by Kukard and Wynne (2006) it was shown that it was not possible for the product olefins to diffuse up the reactor against the hydrodynamic flow in system (a), therefore olefins would have been expected in the product but this was not the case. Correspondingly, the dehydrogenated paraffins cannot diffuse against the hydrodynamic flow to be isomerised in system (b). This implies some activated species is able to hydrogenate the olefins to paraffins. Furthermore, this species is able to activate the feed n-paraffins so that a carbenium ion is formed which subsequently undergoes the standard isomerisation and cracking reactions defined in the classical mechanism.

As surface diffusion of olefins is improbable and shown not to occur (Kukard and Wynne, 2006), this points to the “surface diffusion of activated hydrogen species” (Roessner and Roland, 1996), a phenomenon known as hydrogen spillover.

The basic concept concerning hydrogen spillover is that gaseous hydrogen adsorbs onto active metal sites, thereby undergoing conversion into some form of activated species. These species are believed to migrate via surface diffusion to the acid sites where they react with the various hydrocarbons to affect either a cracking or isomerisation reaction (Conner and Falconer, 1995). The spillover hydrogen is also able to hydrogenate the product olefins. However, the exact nature of this spillover hydrogen species is not known, but it has been shown to exist. Recently Kukard and Wynne (2006) used this concept to design a testing methodology for bifunctional hydrocracking catalysts where the metal function is provided on an inert carrier (produced as a large batch). Portions of supported metal catalyst are physically mixed with the acid function, thereby avoiding any differences in metal-support interactions in different experiments (see Section 2.4).

2.3.1.3 β-Scission Mechanisms and Intermediate Carbenium Ions

Whether the initial activation of the n-paraffin occurs by the classical mechanism or by hydrogen spillover is not of primary importance. In either case, the reaction proceeds via adsorbed carbenium ion intermediates, with the tertiary carbenium ion being the most stable. Thus, cleavage starting from a tertiary carbenium ion and forming a tertiary carbenium ion is favoured. This is shown in the structures in Figure 2.5. Favourable tertiary – tertiary cracking basically requires the combination of a quaternary carbon and a tertiary carbenium ion in the β-position to each other (type A). Other, less ideal, intermediates possible are shown in Figure 2.5 (B_1 – C), with the rate of β-scission reactions decreasing in the order (Martens and Jacobs, 2001):

$$A >> B_1, B_2 > C .$$

β-Scission comprising a primary carbenium ion intermediate is very unlikely, due to the instability of this ion.

Type A β-scission is only feasible on the central C-C bonds of a paraffin, and from the fourth C-position (on a linear paraffin) onwards with almost equal probability (Dry, 2003). Therefore, for type A hydrocracking to occur, the starting hydrocarbon must contain at least eight carbon atoms (i.e. R_1, $R_2 \geq CH_3$).

As the highly branched carbenium ion intermediates are more reactive towards cracking, the products are usually also highly branched. Intermediate length carbon chains are formed with almost equal probability, with few compounds smaller than C_4 being formed (due to less

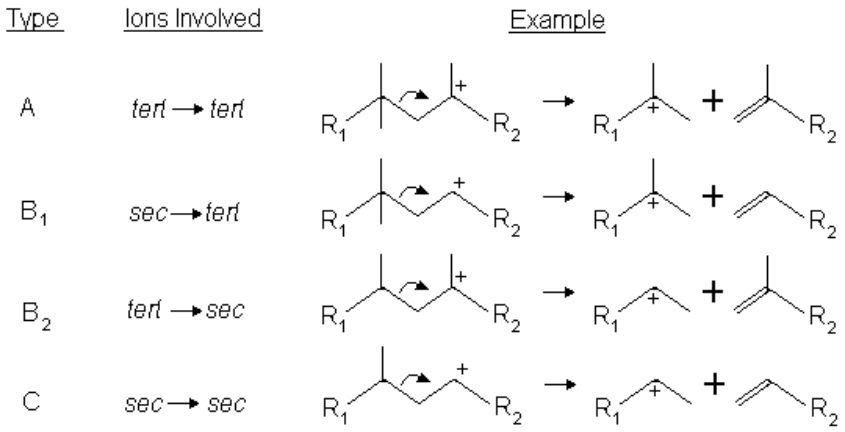

Figure 2.5: Possible β-Scission Mechanisms with Alkylcarbenium Ions (Taken from Martens and Jacobs, 2001)

stable carbenium ion intermediates). However, at more severe conditions and higher conversions, secondary cracking comes into play and the initially equal product carbon number distribution from C_4 onwards (from n-paraffin cracking) shifts towards lower carbon numbers (Böhringer *et al.*, 2006b). The expected distribution, when hydrocracking C_{14} (tetradecane), is shown in Figure 2.6. The curve for secondary cracking represents only a qualitative shift that would occur in the carbon number product distribution.

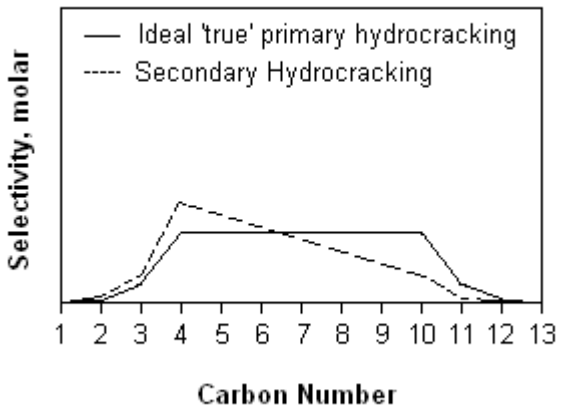

Figure 2.6: Theoretical Carbon-Number Distributions of Products from Bifunctional, Metal / Acid Catalysed 'True Hydrocracking' of n-C_{14} (Taken from Böhringer et al., 2006)

2.3.2 Mechanism of Hydrogenolysis

Unlike true bifunctional hydrocracking as exemplified in the classical mechanism, hydrogenolysis proceeds via adsorbed hydrocarbon radical intermediates, formed by the initial abstraction of a hydrogen radical. Once formed, these chemisorbed hydrogen-deficient

intermediates undergo C-C bond scission. The probability of such β-scission is almost identical for all C-C bonds in the hydrocarbon chain and, in other words, it is non-selective. This is shown in Figure 2.7. Therefore, this pathway has a resultant product carbon-number distribution consisting of practically equal selectivities of hydrocarbons from C_1 upward (Sinfelt, 1973), as shown in Figure 2.8.

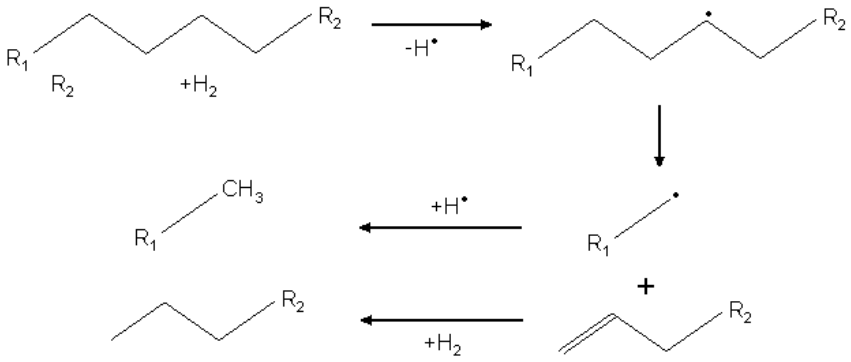

Figure 2.7: Schematic of the Mono-Functional Hydrogenolysis Mechanism (Taken from Böhringer et al., 2006b)

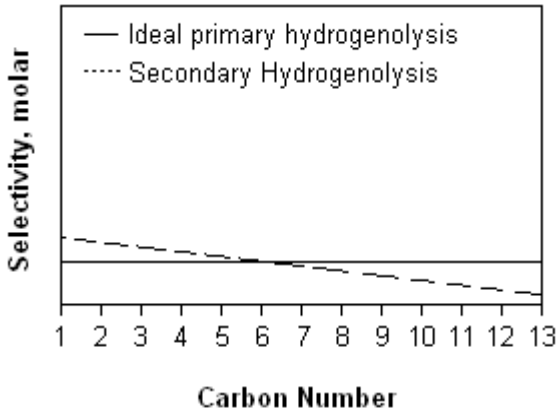

Figure 2.8: Theoretical Carbon-Number Distributions of Products from Hydrogenolysis of n-C_{14} (Taken from Böhringer et al., 2006b)

The resultant hydrocarbon products from this mechanism are essentially unbranched, due to absorbed radical intermediates being involved which results in a low isomerisation activity (as isomerisation is not required to stabilise the intermediates). However, with more severe conditions, secondary hydrogenolysis of the primary fragments occurs and the distribution is shifted towards lower carbon number fractions (Böhringer *et al.*, 2006b). Again only a

qualitative shift in the product distribution upon secondary hydrogenolysis is shown in Figure 2.8.

2.3.3 Mechanism of Methanolysis

Methanolysis is a variation of hydrogenolysis whereby only methyl groups are removed, consecutively, from the ends of the hydrocarbon chains. This reaction proceeds via a specific C-C bond cleavage mechanism (Figure 2.9) such that the terminal C-C bonds of the adsorbed hydrocarbon chains are cleaved with high preference. While some of the long hydrocarbon fragments desorb, others remain on the surface and undergo subsequent demethylation steps. As a result, the overall product carbon number distribution is dominated by methane and the corresponding higher primary fragments, as shown in Figure 2.10.

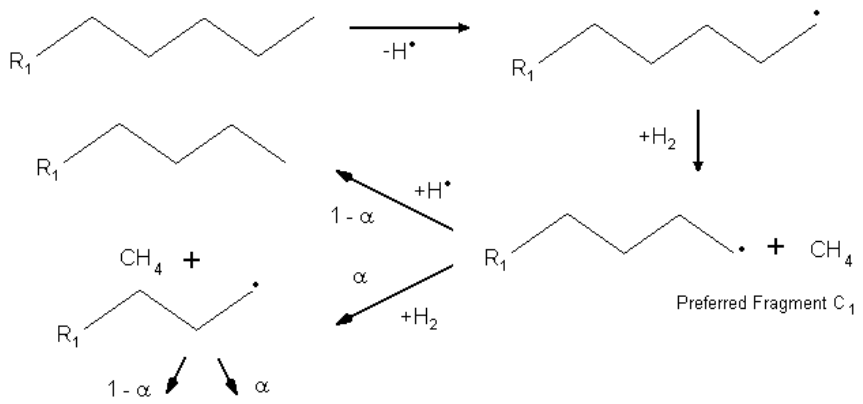

Figure 2.9: Schematic of the Mono-Functional Hydrogenolytic Demethylation Mechanism ('Methanolysis') (Taken from Böhringer et al., 2006b). α = Probability to remain adsorbed and be demethylated again

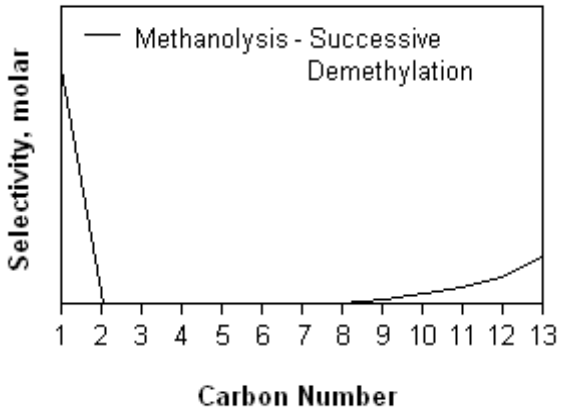

Figure 2.10: Theoretical Carbon-Number Distribution of Products from Methanolysis of n-C_{14} (Taken from Böhringer et al., 2006b)

2.3.4 Combined Mechanistic Effects

Over a bifunctional hydrocracking catalyst, a number of the above reactions can occur in parallel. That is to say hydrogenolysis or methanolysis can occur simultaneously to „true hydrocracking". However, whether it is hydrogenolysis or methanolysis that occurs in parallel, depends on the metal. Platinum is known to promote hydrogenolysis simultaneously to true hydrocracking (Gates *et al.*, 1979) with the expected product distribution as presented in Figure 2.11. In contrast, nickel (Gates *et al.*, 1979), cobalt, palladium and iridium (Sinfelt, 1973) are known to promote methanolysis in parallel with true hydrocracking. The theoretical product distribution is shown in Figure 2.12. Tetradecane (n-C_{14}) has been exemplified in both theoretical product distributions below, so comparisons with the work by Böhringer *et al.* (2006b) (in Figure 2.6, Figure 2.8 and Figure 2.10) can be made.

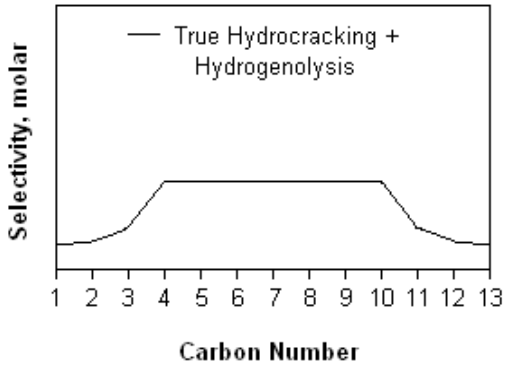

Figure 2.11: Theoretical Carbon Number Distribution for the Combined Product of True Hydrocracking and Hydrogenolysis from n-C_{14}

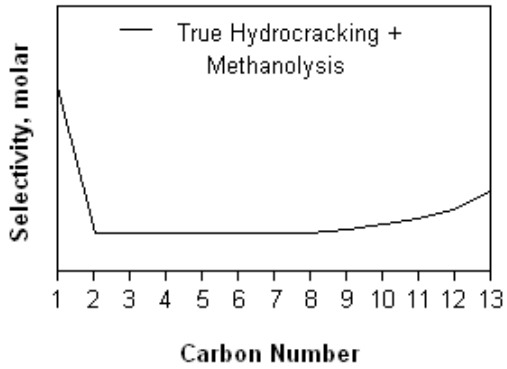

Figure 2.12: Theoretical Carbon Number Distribution for the Combined Product of True Hydrocracking and Methanolysis from n-C_1

2.4 Problems with Catalyst Preparation

It is possible to combine the two different co-catalyst components in one catalyst particle (by impregnation), with the usual practice being to load a suitable metal (such as platinum), on to an acid support (for instance, an acid zeolite). However, applying this type of catalyst preparation technique for comparison of different acid or metal functions suffers from a number of problems including varying metal dispersion, metal crystal size, metal surface area and the location of metal clusters. In Figure 2.13 a number of possibilities are highlighted for a porous support medium (such as an acid zeolite) Please note that the diagram is drawn not to scale but is rather a representation of possible configurations that could be found over various catalysts and supports. As can be seen from the Figure 2.13, this can lead to significant differences in the results, leading to poor reproducibility and an inability to compare different catalysts or different metal loadings in the absence of other effects.

However, it was found in previous research by Kukard and Wynne (2006) that it was possible to prepare the two catalysts separately, with the metal function being loaded on an inert support material, and physically mixing the two components in the catalyst bed in the reactor (see Figure 2.14).

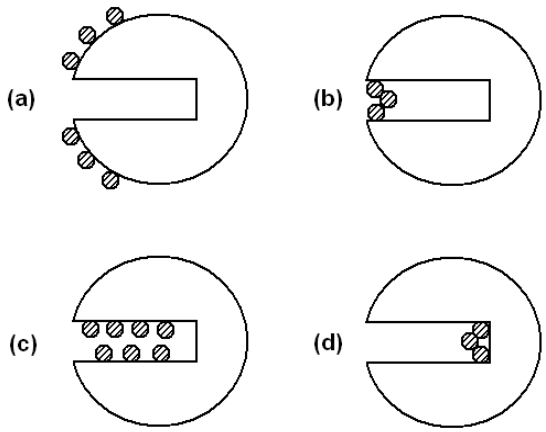

Figure 2.13: Representation of Possible Metal Cluster Distribution on Porous Support Particles

a) Distributions of clusters solely on the external surface of the particle
b) Clusters congregated near the mouth of the pore
c) Even distribution of the clusters throughout the pore system
d) Accumulation of the clusters in the far end of the pores
(Adapted from Kukard and Wynne, 2006)

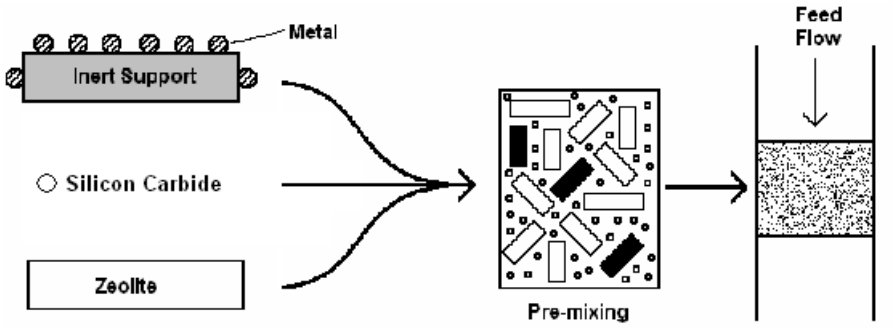

Figure 2.14: Ideal Testing Scenario of Physically Mixed Supported Metal and Zeolite Catalyst Bed

(Adapted from Kukard and Wynne, 2006)

The advantage with this method is the ability to obtain identical metal dispersions while testing different metal loadings, by simply mixing the two different catalysts (always using the same supported metal catalyst) in the correct relative amounts to get the total required metal loading. Furthermore, using this method it is possible to consistently use the same exposed metal surface area for different metal types as the exposed surface area can be determined per gram of inert support. It is then possible to physically mix the zeolite and supported metal, and obtain a known consistent metal surface area for each metal type.

2.5 Current Industrial Status

Originally, hydrocracking was solely utilised to break down large hydrocarbons in the heavy crude oil fractions (such as vacuum gas oils and atmospheric column residues). The aim was to bring these heavy fractions into the petrol and middle distillate range thereby increasing their economic value. It is also applied to upgrade some of the products obtained from other processes. A list of refinery hydrocracking applications (feedstocks and products) are presented in Table 2.1 and Table 2.2. The commercially applied catalysts are sulphided transition metals from group VIA (molybdenum, tungsten) and group VIIIA (cobalt, nickel).

For feeds that are very low in sulphur (~10 ppm), a non-sulphided noble metal based bifunctional catalyst, usually platinum on amorphous silica-alumina, can be applied. Nevertheless, this requires severe pre-treatment of the feedstock to remove the bulk of the sulphur from the oil, using sulphided transition metals; otherwise the platinum is poisoned (Scherzer and Gruia, 1996).

Table 2.1: Hydrocracking Feedstocks (Adapted from Scherzer and Gruia, 1996)

Feedstock
• Straight run gas oils
• Vacuum gas oils
• FCC cycle oils and decant oils
• Coker gas oils
• Thermally cracked stock
• Deasphalted oils
• Straight-run and cracked naphthas

Table 2.2: Hydrocracking Products (Adapted from Scherzer and Gruia, 1996)

Products
• LPG
• Motor gasolines
• Reformer feed
• Jet fuels
• Diesel fuels
• Heating oils
• Olefin plant feedstocks
• Lube oils
• FCC feedstock

However, the hydrocracking of F-T waxes is carried out industrially by only two large companies, namely Sasol (in the Oryx Plants in Qatar) and Shell (in the Shell Middle Distillate Synthesis Process (Eilers *et al.*, 1990) in Bintulu, Malaysia). Due to the novelty of this process not much of the companies" research in the field has been published. Furthermore, considering published findings, it appears as if limited research and development has been committed to the special case of distillate fuel production via F-T wax hydrocracking (Sie *et al*., 1991, Eilers *et al*., 1990). Thus, the reviewed literature is essentially based on work done on similar processes.

2.6 The Effect of Metal Type and State

2.6.1 Sulphided Metal Components

The heavy fractions from crude oil contain a relatively high fraction of sulphur (up to 3%) and nitrogen compounds, therefore the catalysts used have to be resistant to such compounds. Nevertheless, the required hydrocracking can be achieved by combining a large pore zeolite with a sulphided hydrogenation (metal) function. Transition metal sulphides meet the

requirement for high-resistance to poisoning by S- and N- compounds while being effective hydrogenation and hydrodesulphurisation (HDS) catalysts. Industrially most catalysts use combinations of tungsten or molybdenum and cobalt or nickel as bulk metals and promoters respectively. Consequently, most published work has focused on sulphides of these metals. However, a number of other transition metals may be more active for hydrocracking (Welters *et al.*, 1995).

Welters *et al.* (1995) studied the hydrocracking properties of various CaY (zeolite) supported metal (Fe, Co, Ni, Mo, Ru, Rh, Pd, W, Re, Ir, and Pt) sulphide catalysts for the hydroconversion of n-decane at 3 bar pressure and temperatures between 290 and 402°C. It was found that these sulphided metals could be ranked in decreasing (de)hydrogenation strength as Ir > Rh > Pt, Pd, Mo, Re, W > Ru > Fe, Ni, Co. However, this disagrees with the findings of Maxwell (1987) who found the general order as noble metals > sulphided transition metals > sulphided noble metals.

A more important general result was found to be that the hydrocracking activity is determined not only by the (de)hydrogenation properties of the metal but also its position, distribution and dispersion on the zeolite. This needs to be taken into account as the results obtained by Welters *et al.* (2005) may be of limited value because these effects were not considered. In the work by Welters *et al.* (2005), the metal loadings varied between 3.9 wt% and 13.9 wt% while the metal surface areas were not reported. Furthermore, the catalysts used were prepared by impregnation onto the zeolite and, as discussed in Section 2.4, this method potentially has a number of inherent flaws.

2.6.2 Non-Sulphided Metal Components

As F-T waxes do not contain sulphur or nitrogen compounds, the HDS function is not required. It is thus possible to use noble metals, which would have been poisoned by high sulphur concentrations, as the supported metal rather than base metals (Leckel, 2007). A number of studies have looked at using platinum (Alvarez *et al.*, 1996; Calemma *et al.*, 2000; Leckel., 2007) with Leckel finding that higher zeolite acidity and metal dispersion resulted in a more active catalyst for the hydrocracking of n-hexadecane.

The most commonly used metals are platinum, palladium or bimetallic systems. The catalysts loaded with noble metals (Pt, Pd) show a higher selectivity toward hydroisomerisation than catalysts containing non-noble unsulphided transition metals (Ni, Co, Mo, W) (Calemma *et al.*, 2000, and references therein). However, the hydrocracking ability of

these metals has not been compared at similar reactor operating conditions. In research carried out by Böhringer *et al.* (2006b) on the hydrocracking of tetradecane using unsulphided CoMo/SiO_2-Al_2O_3, high methane selectivity was found. It was concluded this was due to metallic Co clusters on the support, resulting in a significant amount of methanolysis (see Section 2.3.3). As methane was the original feed for the steam reformer in the GTL process (Figure 2.2), this is highly undesired as it represents a loss of productivity.

Additionally, increasing attention has been paid to the hydroisomerisation and hydrocracking of long chained paraffins over bifunctional catalysts in the last 20 years using Pt and Pd loaded on zeolites (Calemma *et al.*, 2000, and references therein). It has been found the hydrogenation activity decreases in the order Pt > Pd (Scherzer and Gruia, 1996). However, results reported by Aboul-Gheit *et al.* (2005) for the hydroconversion of cyclohexene show the order of (de)hydrogenation ability of common noble metals to be in the order Pd > Pt > Ir > Re (Re shows very limited activity and was basically inactive). Although these results seemingly contradict each other, the different researchers were using different feedstocks and this may explain the discrepancies in the ordering.

There is also the possibility of using non-sulphided base metals and research has been done using NiMo-SiO_2/Al_2O_3 (Leckel, 2005) and unsulfided Pt/SiO_2-Al_2O_3 catalyst, modified with MoO_3 (Leckel and Liwanga-Ehumbu, 2006) but in both case the effects of the operating conditions were examined in preference to the effect of the metals or metal loadings.

In a number of the papers (for example Blomsma *et al.* (1997)), small chained hydrocarbons (C_7 – C_{10}) are used as the feedstock, although these are not representative of F-T waxes ($>C_{30}$). Using C_7 is an unadvisable choice of feed material as it is unable to undergo type A cracking (see Figure 2.5) which is the fastest and most likely to happen in an industrial system. For research on wax hydrocracking, larger feed hydrocarbons should be used as they will be more representative of waxes.

2.7 The Effect of Metal Loading

The amount of metal loaded onto the zeolite support will affect the overall conversion and selectivity of the system towards hydrocracking. Changing the metal loading (and thus the metal surface area) on the zeolite affects the metal / acid balance in the combined catalyst.

The metal / acid balance is important because it affects the relative amount of isomerisation and hydrocracking. If there is limited metal (or a weak hydrogenating metal) there is more

cracking of the formed alkenes as they are not hydrogenated before they have undergone a number of cracking steps (see Figure 2.3) (Calemma *et al.*, 2000). This results in unwanted small carbon number fractions, and it is termed secondary cracking. This is depicted in Figure 2.6.

However, if the two functions are properly balanced, with the hydrogenation function saturating the olefinic intermediates before they can undergo secondary cracking, the over-cracking is reduced thus the selectivity towards either distillate fuels or gasoline can be optimised (Collins *et al.*, 2006).

Alvarez *et al.* (1996) found that for low ratios of the number of metal sites to the number of acid sites (n_{Pt}/n_A), the activity per acid site is low (due to limited activation of the feed molecules) and the deactivation is rapid. However, if n_{Pt}/n_A is increased the activity per acid site is high (as there is adequate activation of the feed), the deactivation is slowed, and the n-decane is successively transformed into monobranched, dibranched and tribranched isomers plus subsequent cracking products (see Figure 2.15). The authors termed the latter case „ideal hydrocracking" (see carbon number distribution in Figure 2.6), where only one cracking step of the alkene intermediate takes place on an acid site during its diffusion from the platinum site on which it was generated to those where their fragments are hydrogenated. This is the desired case as it results in a high selectivity of the preferred diesel products. Therefore, this is the aim of future diesel hydrocracking catalysts, as conversion and selectivity are optimised to limit overcracking.

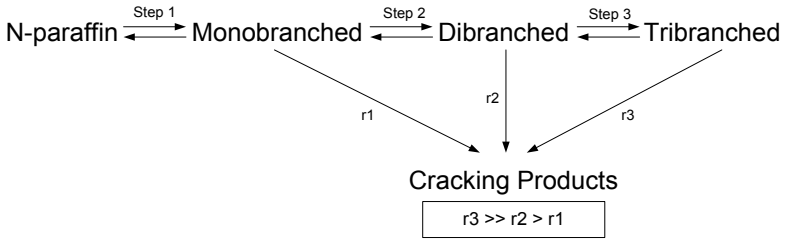

Figure 2.15: Reaction Scheme for the Formation of Feed Isomers and Cracked Products

(Taken from Calemma et al., 2000)

Furthermore, catalysts with a strong (de)hydrogenation function (noble metals) require relatively mild acidity to optimize selectivity to middle distillates while catalysts with a weaker (de)hydrogenation function can tolerate a stronger acid (Collins *et al.*, 2006).

Thus it can be said the metal loading/distribution has a strong influence on the catalytic performance. The activity is improved by an increase in metal surface area, while the isomerisation selectivity increases with the metal content until sufficient metal site density is reached. However, if the metal content becomes too high, the desired selectivity decreases due to the maladjustment in the metal-acid balance with a large portion of the feed remaining in a carbon number fraction above that of the desired product (Rezgui *et al.*, 2005).

In general, the noble metal content of hydrocracking catalysts is usually 1 wt%, while for non-noble metals it is larger: 3-8 wt% for Co and Ni (as the promoters) and 10-30 wt% for Mo and W (as the bulk metal).

2.8 Summary of Findings from Literature

Industrially, sulphided catalysts (mainly mixtures of Co or Ni with Mo or W) are primarily used, as crude oil contains sulphur which would poison noble metals. However, as there is an increasing drive to GTL processes, due to the availability of feedstocks (natural or stranded gas) and the desirability of the final products, there is a need to systematically study the possible catalysts that may be applied for hydrocracking waxes that are produced by the Fischer-Tropsch stage.

It was found that there are different rankings for the (de)hydrogenation strengths of the possible metals but these seem to depend on the feedstock used and the metal form (metal or sulphide) used in the research. Very few authors have reported the same ordering, with limited explanations as to how or why the obtained ordering resulted. Additionally, in the majority of the experiments performed, the actual feedstocks utilised have properties significantly different to those of F-T waxes. Furthermore, little has been published with regard to the different (de)hydrogenation abilities of different possible hydrocracking metals in their metallic form without promoters. The effects of the metal function on hydrocracking have almost exclusively been done with platinum, as this is the currently used hydrocracking metal. However, there may be more active or otherwise more attractive (from a cost basis) (de)hydrogenation metals which have not been tested or optimised.

In principle, there is general agreement on the effect of the metal / acid balance with a number of authors quantifying these effects. However, the conditions used, in particular, the choice of feedstock, were not truly representative of those found industrially. In each case, the metal / acid balance needs to be tailored to the feedstock, the required product spectrum, the strength of the acid function and (de)hydrogenation strength of the metal function.

The classical reaction mechanism as well as other mechanisms (hydrogenolysis and methanolysis) are well known, and so is the effect of the metal / acid balance. However, much of the research on this has not been done at industrially relevant conditions of temperature (225 – 350°C) and pressure (20 – 50 bar). In previous research, small hydrocarbon feedstocks where used, which are not representative of F-T waxes. Therefore, future work needs to focus on obtaining results at industrial conditions, namely pressures of 20 – 40 bar and lower temperatures, using more representative n-alkanes as feed stocks such as hexadecane ($C_{16}H_{34}$).

3 OBJECTIVES OF RESEARCH

The objective of this study are three-fold, as follows:

i. To determine the relative activities of Pt, Pd, Ni and Co hydrocracking catalysts based on a common acid function, viz. H-MFI-90 (H-ZSM5-90),
ii. To determine the effect of metal loading, or more precisely, of metal / acid site ratio (M/A ratio) for each metal type – both in terms of catalyst hydrocracking activity (n-hexadecane conversion) and selectivity (product carbon number distribution) and, where possible, also to determine for each metal the M/A ratio required for ideal hydrocracking,
iii. To determine the effect of metal type on the selectivity to the side reactions, notably towards methanolysis.

4 EXPERIMENTAL

A significant aspect of this study included the design, construction and commissioning of a suitable apparatus for conducting the catalytic experiments, given the intended experimental conditions, the high-boiling nature of n-hexadecane feed and the preference for complete online analysis of the reactor effluent streams.

4.1 Catalysts

Catalysts comprised of physical mixtures of two co-catalysts, a metal co-catalyst on an inert support and a zeolite co-catalyst.

4.1.1 Supported Metal Co-Catalysts

Four metals were selected for this work as they are known to be effective as agents for dehydrogenation / hydrogenation. Two of these were noble metals, platinum and palladium, and two were base metals, nickel and cobalt.

Silica-supported metal catalysts were obtained from Johnson Matthey Technology Centre (JMTC) for use in this work. The silica (SiO_2) was chosen as it is inert (non-acidic) for carbenium ion mediated reactions such as cracking as well as offering no recognised hydrogenation activity.

For all the metals investigated a sufficient quantity of catalysts was prepared as a single batch, such that exactly the same metal function was applied throughout the experimental programme, eliminating variations in respect of metal loading, dispersion, and location of metal within the structure of the support material. According to Johnson Matthey, the 5 wt% supported metal catalysts were prepared via the incipient wetness method. Limited additional information concerning catalyst preparation is provided in Table 4.1 (JMTC).

Table 4.1: Preparation details of the supported metal catalysts

Metal	Precursor compound	Support	Calcination Temperature (°C)	Calcination Time (hr)
Platinum	Platinum (II) Nitrate Solution	Silica (SiO_2)	500	2.0
Palladium	Palladium (II) Nitrate Solution	Silica (SiO_2)	500	2.0
Nickel	Nickel (II) Nitrate Solution	Silica (SiO_2)	500	2.0
Cobalt	Cobalt (II) Nitrate Solution	Silica (SiO_2)	500	2.0

The properties of the supported metals utilised in this investigation are presented in Table 4.2. Carbon monoxide (CO) chemisorption was used to determine such information as the metal dispersion, crystallite size and the active metal sites (those being the surface metal sites). The catalyst was reduced for the CO chemisorption in precisely the same manner as that used for the catalyst reduction in the hydrocracking tests (reactor in-situ activation – Section 4.3.2) so as to ensure accurate and reliable measurements for the metal dispersion. This method involved heating the catalyst up to 350°C at 5°C/min in a 100 sccm stream of 5% hydrogen and 95% nitrogen. Once the required temperature was reached the catalyst was reduced for 16 hours in the same gaseous mixture, before a final two hour period during which pure hydrogen was passed over the catalyst, also at a rate of 100 sccm.

Table 4.2: Physical Properties of the Supported Metal Catalysts

Metal/Support	Supplier	Reported Loading (wt% metal)	Dispersion (%)	Metal Crystallite Diameter (nm)	Surface Metal Sites (sites/g)
Pt/SiO_2	Johnson-Matthey	5.0	18	6.3	2.8E+19
Pd/SiO_2	Johnson-Matthey	5.0	19	5.9	2.8E+19
Ni/SiO_2	Johnson-Matthey	5.0	15	6.7	7.7E+19
Co/SiO_2	Johnson-Matthey	5.0	0.45	220	2.3E+18

The metal loadings are according to Johnson Matthey Technology Centre

4.1.2 Acid Zeolite Co-Catalyst

The acid function used was H-MFI-90 (H-ZSM5-90). Research by Kukard (2008) and a number of preliminary tests in this study showed that using wider pore zeolites and amorphous material resulted in significantly reduced overall activity due to the reduced effect of the acid function.

The H-MFI-90 zeolite was obtained in pure powder form from Sud-Chemie (now Clariant), without the addition of any binding materials that are usually used when extrudates are manufactured. Details of the zeolite catalyst can be found in Table 4.3.

Table 4.3: Physical Properties of the Acid Zeolite

Zeolite	Supplier	Nominal SiO_2/Al_2O_3 Ratio	Acid Site Density (sites/g)
H-MFI	Sud-Chemie	90	1.10E+20

4.1.3 Co-Catalyst Forming

All catalysts, both the zeolite and silica-supported metal catalysts were used as a granulate after pelletizing, crushing and sieving. Approximately 10 grams of catalyst powder (be it the supported-metal or zeolite) was placed in a steel press-die (Specac T25 Electronic Press) and briquetted under 20 tons pressure for five minutes. These co-catalyst briquettes were subsequently crushed using a pestle and mortar, and sieved into the size range of 500 - 800 µm. This size range was selected to minimize the hydrodynamic wall effects - being less than one tenth the diameter of the reactor (Sinnot, 2005) - and resulted in particles that were large enough so as not to be flushed out of the reactor under the flow conditions applied and are stable as a single combined catalyst bed in the reactor isothermal zone. They are, however, not so large as to cause internal transport limitations (Ndimande, 2014). It was further found that, for this size range, the co-catalysts mixed well and could readily be introduced as a single unified catalyst bed into the test reactor.

4.1.4 Combined Metal / Acid Catalyst Formulations

The findings of Alverez *et al*. (1996) which showed that, for the hydroconversion of n-decane over Pt / H-Y at 200°C and 1 bar, a metal / acid site ratio (that is the molar ratio of the respective reactive sites) of between 0.03 and 0.17 ensured that neither the metal or acid function were limiting was taken as the basis for the formulations of this study. Under the conditions outlined in the work done by Alverez *et al*. (1996), a metal / acid ratio of 0.17 resulted in ideal hydrocracking – when each feed molecule is cracked only once before it is hydrogenated and leaves the reactor. This figure was taken as the starting point for the current study. Even so, a key objective of the different formulations was to ensure the metal / acid site ratios were similar for the different metals, while ensuring that a suitable amount of

the combined catalyst - large enough to weigh out accurately yet not too large to fit in the reactor isothermal zone - was used in each test. Likewise, C_{16} feed flow rates needed to fall within the pump"s reliable flow range (Section 4.2.1).

Combined catalyst charge formulations are provided for all experimental runs in Table 4.4 (note: the metal / acid site ratio is determined from the amounts of each co-catalyst included, the metal content and dispersion of the metal co-catalyst and the acid site density of the zeolite co-catalyst – see Appendix C for details). For formulations with the lowest metal loadings (see Table 4.4, for Pt (Pt-1, Pt-2), Pd (Pd-1, Pd-2), and Ni (Ni-1)), and for all Co runs (Co-1 to Co-4), more catalyst was charged into the test reactor so as to ensure it was possible to combine a decent amount of supported metal co-catalyst with the acid zeolite. Additionally, the larger catalyst charges allowed for lower weight hourly space velocities during catalyst testing, so ensuring that conversion levels were kept within the range 20 – 90% (note: the total volume of the catalyst charge differs from experiment to experiment so as to allow for a comparison of different metal functions at the same space velocity and similar conversion levels).

Figure 4.1 shows the different weighed out catalyst charges for the platinum experiments 3 - 6 prior to testing. The different formulations (metal / acid co-catalyst compositions) can be clearly seen with the black particles being the platinum-on-silica co-catalyst and the white particles being the zeolite co-catalyst.

Table 4.4: Combined Catalyst Charges Utilised

Metal	Run Number	Supported Metal Catalyst		Acid Catalyst		Metal Content in combined catalyst (wt %)	Metal Site / Acid Site Ratio *
		Type	Mass (g)	Type	Mass (g)		
Platinum	Pt-1	$Pt/Si0_2$	0.0067	H-MFI-90 (ZSM-5)	4.0006	0.0079	0.0004
	Pt-2		0.0214		4.0004	0.026	0.0013
	Pt-3		0.0159		0.9998	0.078	0.0040
	Pt-4		0.1596		0.9999	0.69	0.040
	Pt-5		0.3978		1.0005	1.4	0.10
	Pt-6		0.6722		0.9997	2.0	0.17
Palladium	Pd-1	$Pd/Si0_2$	0.0030	H-MFI-90 (ZSM-5)	4.0004	0.0041	0.0004
	Pd-2		0.0107		4.0009	0.013	0.0013
	Pd-3		0.0169		2.0003	0.041	0.0041
	Pd-4		0.0831		1.0000	0.38	0.040
	Pd-5		0.2067		0.9995	0.86	0.10
	Pd-6		0.3490		1.0001	1.3	0.17
Nickel	Ni-1	$Ni/Si0_2$	0.0232	H-MFI-90 (ZSM-5)	4.0006	0.028	0.0041
	Ni-2		0.1147		2.0005	0.27	0.040
	Ni-3		0.2860		2.0006	0.63	0.10
	Ni-4		0.4834		2.0001	1.0	0.17
Cobalt	Co-1	$Co/Si0_2$	0.0262	H-MFI-90 (ZSM-5)	4.0005	0.029	0.0001
	Co-2		0.2302		4.0001	0.27	0.001
	Co-3		0.5726		4.0007	0.63	0.003
	Co-4		0.9666		4.0005	1.0	0.01

* - determined from the amounts of each co-catalyst included, the metal content and dispersion of the metal co-catalyst, and the acid site density of the zeolite co-catalyst.

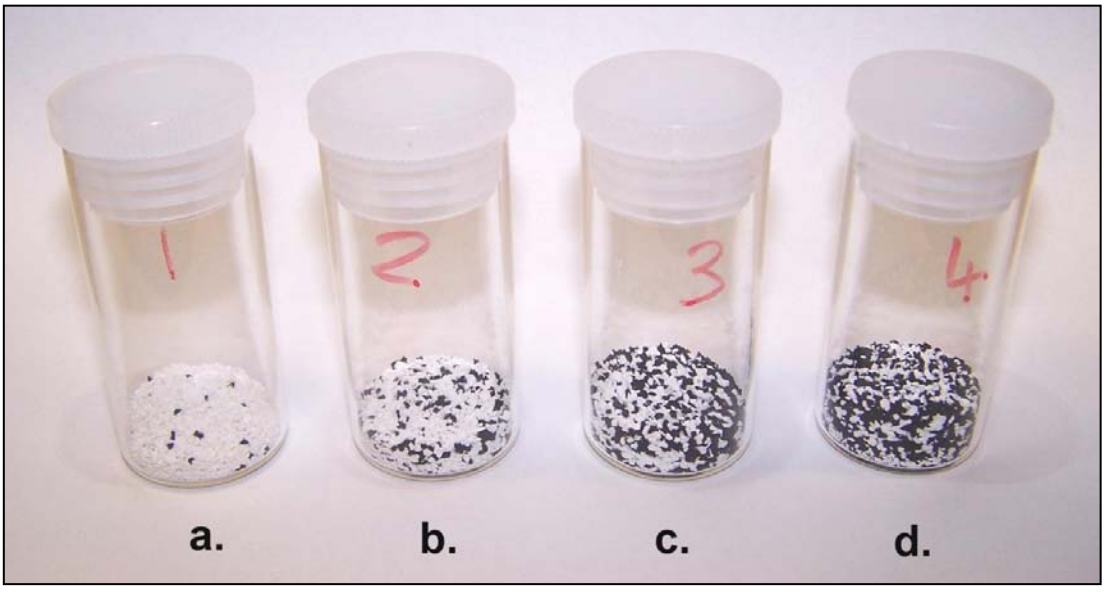

Figure 4.1: Photograph showing Samples of the Supported Platinum Catalyst Physically Mixed with H-MFI-90 for Runs Pt-3 to Pt-6

a. Loading for run Pt-3 (0.0159g Pt/SiO_2 mixed with 0.9998g H-MFI-90)

b. Loading for run Pt-4 (0.1596g Pt/SiO_2 mixed with 0.9999g H-MFI-90)

c. Loading for run Pt-5 (0.3978g Pt/SiO_2 mixed with 1.0005g H-MFI-90)

d. Loading for run Pt-6 (0.6722g Pt/SiO_2 mixed with 0.9997g H-MFI-90)

4.2 Reactor Apparatus

The final test unit configuration used to conduct the catalyst performance evaluation experiments is presented below. It should be noted, nonetheless, that a number of developments and modifications were implemented subsequent to the initial design to establish this final configuration. These developments are considered essential for the determination of accurate and reproducible performance data and a full overview thereof can be found in Appendix A.

The final flow diagram is presented in Figure 4.3 and Figure 4.4 which focus, respectively, on the setup up-stream of the reactor and the gaseous feed section, and on the furnace / reactor sections and subsequent downstream apparatus and analysis equipment.

It must be noted that Figure 4.3 and Figure 4.4 represent a single test unit comprising two reactor tubes but that the overall apparatus (Figure 4.2) consisted of two test units, each comprising two reactor tubes for a total of four catalyst testing reactors (tubes). However, the two product lines from the second unit (the one on the right in Figure 4.2), are routed to a single 6-port selection valve along with the two product lines from the first test unit as shown in lower left quadrant of Figure 4.4. From this point any of the four reactor product lines may be routed to the online gas chromatograph for analysis, while the remaining three reactor product lines are routed to the vent line.

Figure 4.2: Photograph of the Final Experimental Apparatus Setup

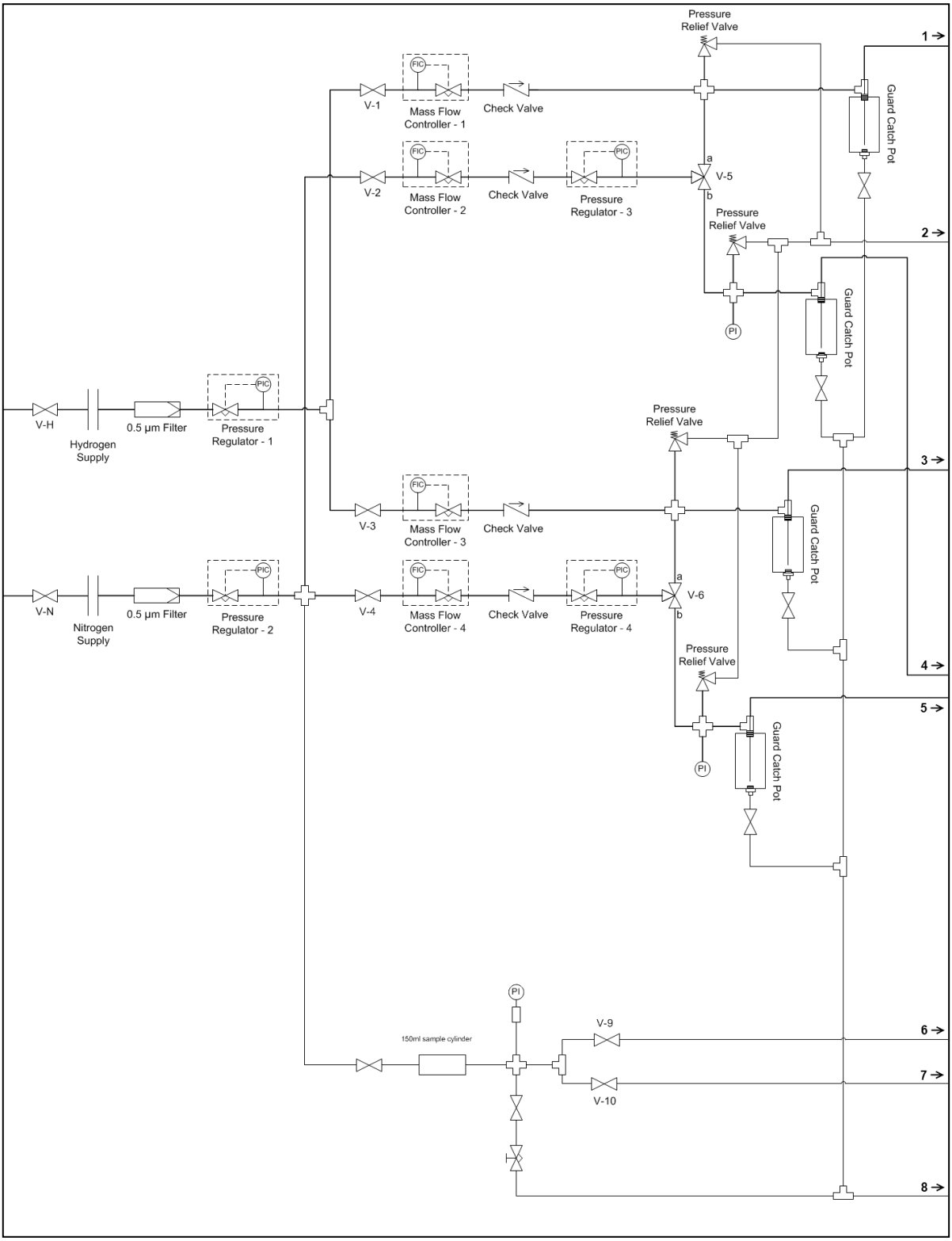

Figure 4.3: Flow Diagram of Catalyst Test Apparatus – Gaseous Feed Section

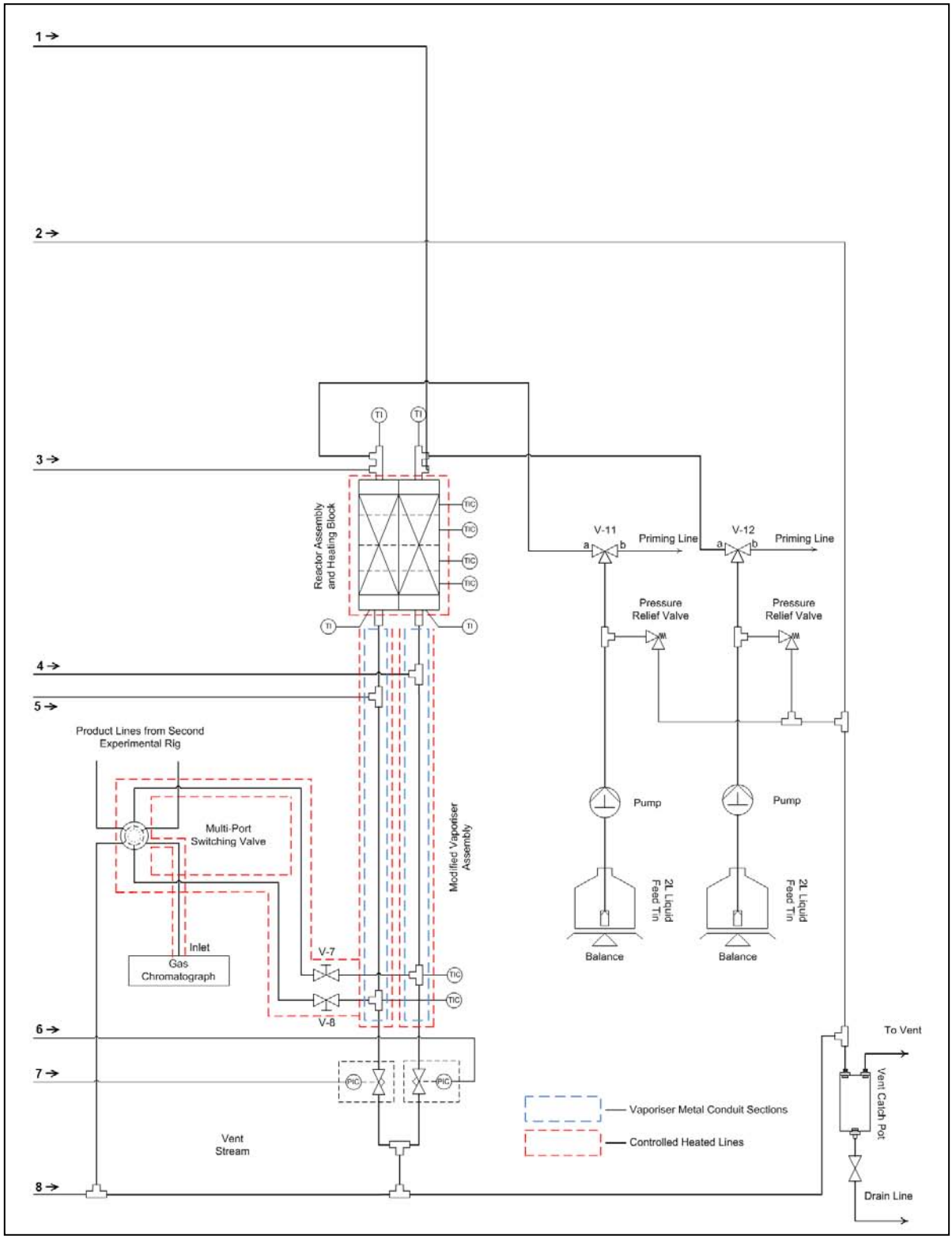

Figure 4.4: Flow Diagram of Catalyst Test Apparatus - Liquid Feed, Reactor and Vaporiser Section

4.2.1 Feed Delivery System and Feed Stocks

n-Hexadecane (n-$C_{16}H_{34}$) was chosen as a model long chain length paraffin to represent F-T wax. It is easy to handle as it is liquid at ambient conditions, whilst being of a significantly long chain length to adequately provide for all possible cracking mechanism as described in Section 2.3 (for which at least 8-carb on chain length is required). The melting and boiling points of n-$C_{16}H_{34}$ are 18°C and 287°C respectively. Additionally, it comprises a single component only making analysis significantly simpler and it is the cheapest of the long-chain paraffins commercially available. The composition of the hexadecane feed is provided in Table 4.5 and a sample chromatogram may be seen in Figure 4.7.

Liquid feed if pumped from a metal feed vessel via a LabAlliance Series 1 chromatography pump to the liquid injection on the reactor head assembly. The delivery line includes both a purge and pressure relief valves for pump priming and system overpressure release, respectively. The feed vessels rest on laboratory balances which allow for determining of the feed mass flow rate. Although n-hexadecane solidifies only at 18°C, the feed pot, pump head and all lines through which it flows are heated to 60°C to ensure it remains liquid should the laboratory temperature decrease below the melting point for some reason – besides ensuring smooth execution of experiments, this is also a safety precaution to ensure the liquid does not solidify in the feed delivery system resulting in large pressure excursions due to line blockage.

Table 4.5: n-Hexadecane Feed Compound Analysis

Compound	Molar Distribution (%)
n-C_{15}	0.53
i-C_{15}	Trace
n-C_{16}	99.47
i-C_{16}	Trace
n-C_{17}	Trace
i-C_{17}	Negligible

The other major feedstock is hydrogen, which is provided at 100 bar from the laboratory supply. After filtration and pressure reduction on the test unit, the gas is supplied via mass flow controllers (Brookes), check valves and guard catch pots to the gas injection point on

the reactor head assembly. The latter two devices serve to protect the system against possible backflow of liquids through the flow controllers (and possibly into the gas ring main in the event of flow blockage within the test unit).

As the product from the reactor comprises both liquid and vapour, a diluent, nitrogen, is required to allow complete vaporisation of the entire product at the conditions prevailing in the vaporiser unit downstream of each reactor tube. A 250 sccm stream of nitrogen is added into the product stream immediately after the reactor, and then both streams enter the vaporiser. Ensuring the entire stream is vaporised, even at low conversion (i.e. when there is still a large portion of $C_{16}H_{34}$ unreacted) ensure the final analysis, done by online sampling of the vaporous product, to be accurate.

4.2.2 Reactor Assembly

The reactor is a vertically orientated packed bed trickle-phase reactor comprising a cylindrical reactor body (316 stainless steel, 16 mm internal diameter) and reactor head assembly to which gaseous and liquid feed lines are attached. The head and body are joined via a 1” VCR connection. The reactor is housed in a brass furnace comprising four independent heating zones so as to provide an isothermal zone of sufficient length for the catalyst bed and to pre-heat the feed, as indicated in Figure 4.5 for a target reactor temperature of 225°C. Reaction pressure is maintained at 20 bar by the use of a back pressure regulator placed downstream of the reactor and vaporiser sections

Gas and liquid feeds are mixed in the heating zone above the catalyst bed in the top portion of the reactor. The catalyst is placed in the isothermal zone, approximately in the centre of the reactor (see Figure 4.5), where it is held in place by granulated silicon carbide support beds both above and below the catalyst bed.

4.2.3 Product Vaporiser

The vaporiser is comprised of a heated packed bed of silicon carbide at a temperature that increases steadily along the length of the tube from 200°C at the top to 270°C at the bottom where a small sample stream is taken by means of a needle valve. The bottom temperature ensures that the entire product stream, which has been diluted with nitrogen injection between the reactor and the vaporiser, is vaporised prior to sampling for chromatographic analysis.

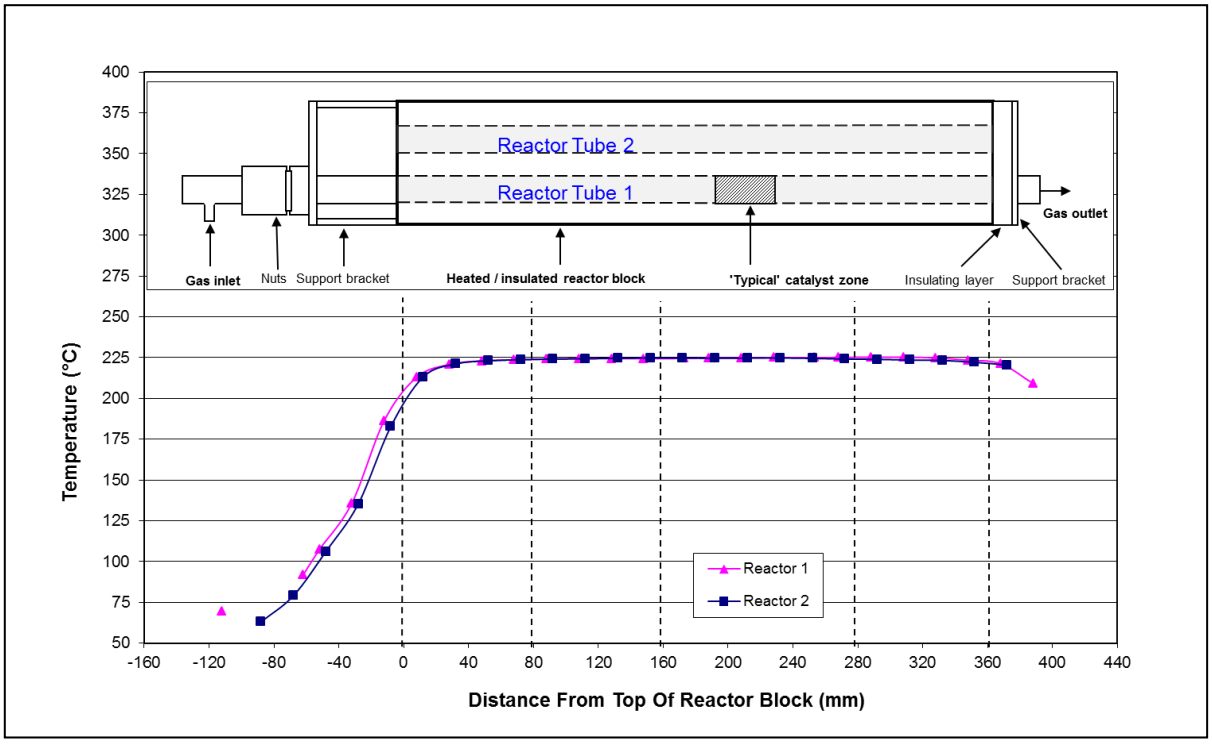

Figure 4.5: Reactor Temperature Profiles for the Two Reactors in the Test Unit One

The design and operation of the vaporiser as well as associated elements of the flow path between the reactor exit and the back pressure regulator (downstream of the vaporiser) are considered crucial to the quality of the experimental data, as detailed in Appendix A.2.

4.2.4 Sampling and Analysis System

The experimental apparatus is set up so that the samples from the four reactors can be analysed online and in sequence. The different product streams are sent in turn to the gas chromatograph (GC) by means of a multi-port switching valve („Vici Valve" made by Valco Instruments). All product lines (one from each of the four reactors used) enter the valve with one line going to the GC for analysis and the other three going to vent. When one sample has been analysed the valve selects a subsequent reactor product for GC analysis. Each reactor product stream is sampled every four hours with each individual gas chromatographic analysis taking 50 minutes.

The Gas Chromatograph employed is a Varian 3900 with a flame ionisation detector (FID) with a Varian PONA type GC capillary column installed. This is capable of separating out the products as no oxygen containing compounds are found in the product streams. The analytical and data work-up procedures are detailed in Section 4.4.

4.3 Hydrocracking Test Procedures

4.3.1 Reactor Loading

The two co-catalysts are weighed on a four decimal place balance according to the test requirements as shown in Table 4.4. Once weighed-out, the two co-catalysts are physically combined and gently mixed to ensure a homogenous mix of the two components (Figure 4.1). The cleaned reactor tube is plugged with glass wool (to prevent loss of reactor packing when in use) and partially filled with inert silicon carbide (SiC) to ensure the subsequent catalyst bed is located suitably in the isothermal zone of the reactor (Figure 4.5). The mixed co-catalyst is carefully loaded, into a single level bed, after which the reactor is completely filled up with additional SiC. The reactor head assembly is attached via the main VCR fitting, after which the assembled reactor is positioned into the furnace block and the gaseous feed, liquid feed and product lines are attached and secured, also via VCR fittings.

4.3.2 Catalyst Activation

After installing the reactor into the furnace (Section 4.3.1), the catalyst was activated by reduction under hydrogen flow (both co-catalysts having been calcined in air by the respective suppliers prior to receipt) as per the sequence below.

The reactor temperature was ramped from room temperature to the reduction temperature at a rate of 5°C/min under a 100 sccm stream of 5% hydrogen and 95% nitrogen, after which the catalyst was held at the reduction temperature for 16 hours before switching pure hydrogen at 100 sccm for a further two hours. This was followed by cooling under hydrogen flow to reaction temperature. Final reduction temperatures are listed for each catalyst in Table 4.6 and Figure 4.6 depicts the temperature ramping profile for the platinum and palladium catalyst. Once the system has cooled to reaction temperature, the run is initiated with the introduction of n-hexadecane and adjustment of the H_2 flowrate as per the sequence outlined in Section 4.3.3.

Table 4.6: The Reduction Conditions for the Supported Metal Catalysts

Metal/Support	Reduction Temperature (°C)	Temperature Ramp (°C/min)	Reduction Time (hrs)	Gas
$Pt/Si0_2$	350	5.0	18.0	Hydrogen
$Pd/Si0_2$	350	5.0	18.0	Hydrogen
$Ni/Si0_2$	450	5.0	18.0	Hydrogen
$Co/Si0_2$	250	5.0	18.0	Hydrogen

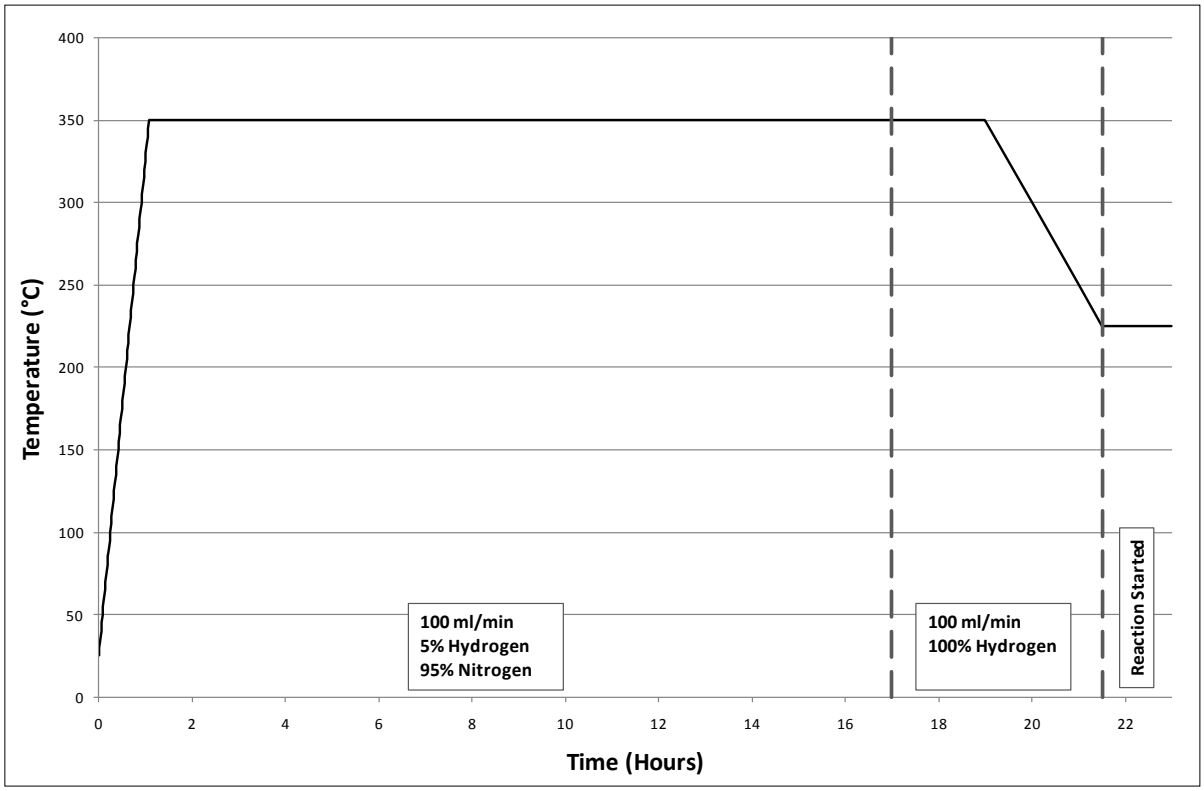

Figure 4.6: The Reduction Temperature Programme for Platinum Catalysts

Whereas the final reduction temperatures for the noble metals come from well establish practice for these metals, those for nickel (450°) and cobalt (250°C) were determined from temperature programmed reduction analysis (Appendix B). In the case of cobalt the minimum possible reduction temperature (250°C) was applied in order to maximise the metal surface area in this particularly poorly dispersed system. In all cases the reduction temperatures used were above the reaction temperature thus ensuring the nature of the supported metal was not thermally altered during the reaction.

4.3.3 Reaction Conditions

General research in the area of hydrocracking has considered a wild range of conditions with temperatures from 130 – 260°C, pressures from 5 – 100 bar and molar hydrogen to hydrocarbon ratios of 3 – 300 (Alverez *et al*., 1996; Martens *et al*., 2001).

However given the undemanding nature of the hexadecane feedstock and the general aim of the research programme within which this study was conducted, viz the combination of F-T synthesis and wax hydrocracking into a single process unit, the reactor conditions employed reflect those typical of both F-T wax hydrocracking (200 – 250°C) and the typical low temperature cobalt catalysed F-T synthesis (230°C, 20 bar).

Also, assuming an 80% F-T conversion of syngas to hydrocarbons, a F-T chain growth probability of 0.8 and assuming, for the sake of argument, that the F-T product consists of pure n-hexadecane, the F-T product H_2:C_{16} molar ratio would be approximately 10:1, a value consistent with previous work suggesting that to ensure hydrogen does not limit the extent of the reaction it is fed at a H_2:C_{16} molar ratio of 10:1 (Nakamura *et al*., 1997).

Consequently, the conditions that were utilised in this study are presented in Table 4.7.

Table 4.7: Summary of Experimental Conditions

Temperature (°C)	225
Pressue (bar)	20
H_2:n-$C_{16}H_{34}$ ratio (molar)	10:1
"Wax" Feedstock	n-Hexadecane n-$C_{16}H_{34}$
Gas Feed	Hydrogen
Gas Diluent (post reactor)	Nitrogen 250 ml/min

4.3.4 Start-Up Procedure

The start-up procedure is carried out simultaneously for all four of the reactor tubes operated.

i. Determine loadings to be used based on required metal site / acid site ratios (Table 4.4) and load and install the reactors as per Section 4.3.1 above
ii. Pressurise the reactors to 20 bar, using pure nitrogen, and check for leaks around reactor fittings
iii. Set nitrogen and hydrogen flows to those required for catalyst reduction and conduct the reduction process as per section (see Section 4.3.2) At the same time turn on the heating lines around the vaporiser conduit (set temperature of 270°C)

    Note: the heating lines from the sample tee off point to the gas chromatograph remain on at all times

iv. Set hydrogen, diluent nitrogen and n-hexadecane flows to required valves (Table 4.7) and turn on piston pump
v. Start gas chromatograph (FID) to analyse hydrocarbon product (see Section 4.4 for analysis and data work-up procedures).

4.3.5 Procedures Applied During Catalytic test Runs

vi. Take and analyse samples until stable results are obtain, which indicate that the initial settling in and primary de-activation period is over
vii. Once steady results are obtained record a number of GC analyses for error analysis purposes
viii. Adjust the flow rates of both hydrogen and n-hexadecane according to the WHSV settings in Table 4.8 (ensuring the molar ratio remains at 10:1) and allow to stabilise
ix. Again, once stable, record a number of GC analyses
x. Once sufficient different WHSVs have been set and necessary data has been recorded stop feed flows.

4.3.6 Shut-Down Procedure

As the reactors are in pairs in the brass furnaces on the test units, experiments for both tubes must be completed before the unit is finally shut down. It is possible to turn the flows off to one reactor once the required data is obtained, without affecting the flows to the other reactor on the same unit.

xi. Halt n-hexadecane flow at the piston pump
xii. Turn off the heating bands around the reactors
xiii. Halt hydrogen flows to the reactors
xiv. Introduce nitrogen flow to the top of each reactor to flush the remaining un-reacted and products feed from the reactor and to flush the lines after the reactor
xv. Once completed, turn off vaporiser heating lines and allow system to cool completely under nitrogen flow.
xvi. Shut down all gas flows
xvii. Remove and clean reactors.

4.3.7 Emergency Shut Down Procedure

In the event that a problem occurs with the apparatus, resulting in an emergency such as a fire or unacceptable pressure build up, it is possible to shut all down electrical systems and gas flows very simply.

i. Turn off power with the large red cut-out switch on main power box – this shuts off power to the entire test unit. The mass flow controllers for the gas supply will close (or shut down) and the pump will stop if the power goes off.
ii. If possible, additionally turn off gas flows at the valves attached to the house gas lines located behind the unit – the two valves will close off the nitrogen and hydrogen supply.

4.4 Chromatographic Analysis and Data Workup

The analytical arrangement (gas chromatography) and sampling procedures are presented in Section 4.2.4. A typical product chromatogram is presented in Figure 4.7, where the n-paraffins are clearly identified.

Given the flame ionisation detector (FID) employed, the area under a peak in the chromatogram is proportional to the number of carbon atoms contained in each specific compound, i.e. the FID is a mass-sensitive detector. Thus,

$$Area_x \sim No\ of\ carbon\ atoms\ present\ in\ Product\ Species\ x$$

$Area_x = Integrated\ chromatographic\ peak\ area\ of\ Product\ Species\ x$

To get the proportional number of moles of a specific compound, the area of the peak is divided by the number of carbon atoms per molecule of the respective compound, i.e.,

$$N.C_X = \frac{Area_x}{Number\ of\ carbon\ atoms\ in\ C_x}$$

$C_x = Hydrocarbon\ with\ carbon\ number\ x$
$N.C_X = No\ of\ atoms\ of\ product\ species\ C_X$

Selectivity

Another variable that is of importance is the selectivity of products and also the product carbon number distribution. From the carbon number distribution it is easy to determine different trends and the extent of the cracking for each metal. For this to be drawn up, the product selectivity (on a molar basis) is needed. This is calculated as follows:

$$S_X = \frac{N.C_X}{\sum_{x=1}^{15} N.C_x}$$

$S_x = Selectivity\ of\ hydrocarbon\ with\ carbon\ number\ x$
$N.C_X = No\ of\ atoms\ of\ product\ species\ C_X$

Conversion

There are two different conversions that can be looked at to analyse the results obtained from the GC read outs. These are the overall conversion of the feed compound, n-$C_{16}H_{34}$, and the cracking conversion of the feed. These two conversions are defined in the two equations below (as percentage values).

$$Overall\ conversion\ of\ C_{16} = \left(1 - \frac{N.C_{16}}{\sum_{x=1}^{16} N.C_x}\right) \cdot 100$$

$$Cracking\ conversion\ of\ C_{16} = \left(1 - \frac{N.C_{16}}{\sum_{x=1}^{15} N.C_x}\right) \cdot 100$$

$C_x = Hydrocarbon\ with\ carbon\ number\ x$
$N.C_x = No\ of\ atoms\ of\ product\ species\ C_x$

The acid zeolite readily isomerises the feed compound before it is cracked to smaller products, but the work is focusing on the cracking of the feed, and while the isomerisation is required to initiate the process, if the feed is not cracked it is not part of the area of interest. Therefore, the area of concern is cracking conversion – that is the n-C_{16} that is cracked down into smaller products.

It must be noted that at the reaction conditions (essentially the high temperature and the strength of the acid sites) the isomerised n-hexadecane feed is extremely reactive and therefore is almost completely cracked. It was found that the overall conversion and the cracking conversion were essentially the same at these conditions.

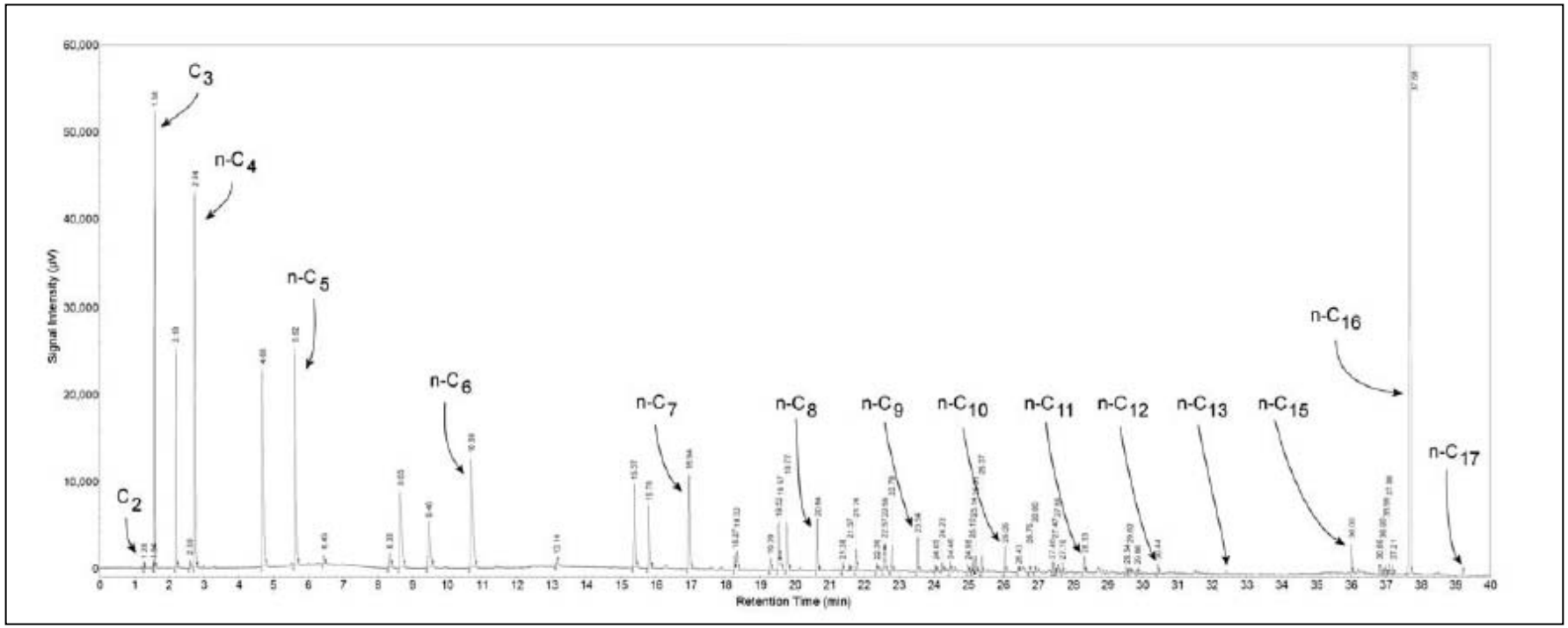

Figure 4.7: Sample Chromatogram from Catalyst Comprising of 0.119g Pt/SiO_2, 0.800g H-MFI-90, and 0.667g SiO_2 (Temperature = 250°C, Pressure = 40 bar, Molar Feed Ratio (H_2:C_{16}) = 10:1) (Adapted from Kukard, 2008)

4.5 Experimental Programme

Table 4.8 provides a summary of the experiments and experimental conditions evaluated (see Table 4.4 for the detailed catalyst loadings). In all cases, weight hourly space velocity (WHSV) was calculated based on the amount of acid catalyst charged to the reactor. As the same acid function was used in each catalyst, it is convenient to use the mass, rather than the number of acid sites.

$$Weight\ Hourly\ Space\ Velocity_{Acid} = \frac{Mass_{Feed}}{Mass_{Acid\ catalyst} \times hour}$$

Table 4.8: Experimental Programme in terms of Weight Hourly Space Velocities Utilised

Metal	Run Number	WHSV ($g_{feed}/g_{acid.cat}$.hr) (T = 225°C, P = 20 bar, H_2/C_{16} ratio = 10:1)													
Platinum	Pt-1	0.11	0.23	0.34	0.46		0.69								
	Pt-2	0.11	0.23	0.34	0.46		0.69								
	Pt-3				0.46			0.92		1.38					
	Pt-4							0.92		1.38		1.84		2.76	
	Pt-5							0.92		1.38		1.84		2.76	
	Pt-6							0.92		1.38		1.84		2.76	
Palladium	Pd-1	0.11	0.23	0.34	0.46		0.69								
	Pd-2	0.11	0.23	0.34	0.46		0.69								
	Pd-3		0.23		0.46		0.69	0.92							
	Pd-4							0.92		1.38		1.84	2.30	2.76	3.22
	Pd-5							0.92		1.38		1.84	2.30	2.76	3.22
	Pd-6							0.92		1.38		1.84	2.30	2.76	3.22
Nickel	Ni-1	0.11	0.23	0.34	0.46	0.57									
	Ni-2		0.23		0.46		0.69	0.92	1.15	1.38	1.61				
	Ni-3		0.23		0.46		0.69	0.92	1.15						
	Ni-4		0.23		0.46		0.69	0.92	1.15	1.38	1.61				
Cobalt	Co-1	0.11	0.23		0.46										
	Co-2	0.11	0.23		0.46										
	Co-3	0.11	0.23		0.46										
	Co-4	0.11	0.23		0.46										

Selection of the WHSV evaluated was determined while the experiments were being run. The settings depended on the conversions previously observed so as to determine performance over the full conversion range and, in so doing, to allow for the comparison of selectivities at similar conversion levels amongst the catalysts. The finally achieved conversion range was ~ 12% to 99%. It should be noted that these conversion ranges were not achieved with all the metals, particularly not for cobalt, as the combination of lowest feed flow rates and minimum catalyst charge could not achieve the full conversion range for certain catalysts.

5 RESULTS

5.1 Preliminary Findings

5.1.1 Blank Runs

A blank run employing only inert silicon carbide as the packing in each reactor was conducted for purposes of determining any activity resulting from the reactor walls / packing or if any thermal cracking occurred at the conditions at which the experiments were carried out.

In each case, the blank runs did not show any activity (no conversion of n-hexandecane was measured). From this result it is possible to conclude that at the reaction conditions, neither the metal wall of the reactor nor the SiC packing is contributing to the overall conversion, nor is thermal cracking.

5.1.2 Typical Time-On-Stream Data

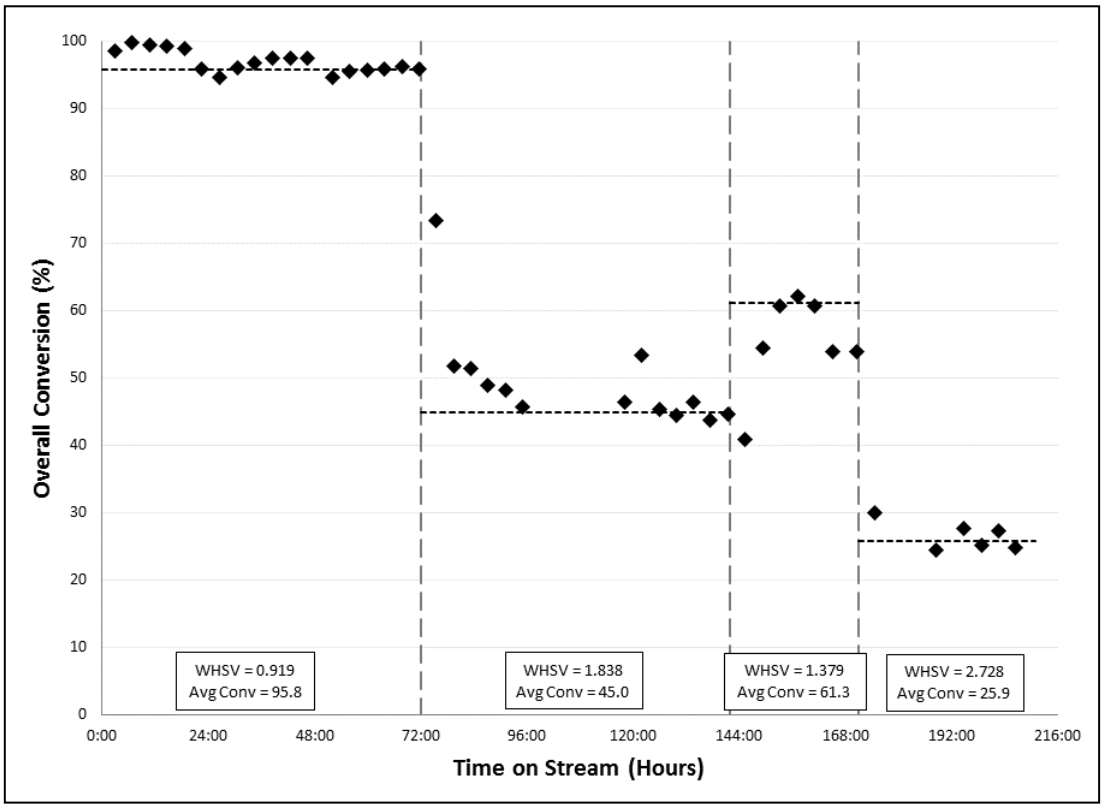

Figure 5.1: Platinum Time-on-Stream Data (M/A = 0.10)

Figure 5.1 presents typical conversion with the time-on-stream (ToS) data with vertical dashed lines indicating a change in experimental conditions, in this case a change in the space velocity (WHSV). Average conversions for each experimental condition were calculated only from data points after the system had re-attained steady state subsequent to each change (i.e. when consecutive data points so indicated). Likewise, the average steady-state values for each compound in the product stream were determined and, hence, steady-state selectivities and carbon number distributions where calculated.

5.1.3 Zeolite (H-MFI-90) Only Performance

After completion of the experimental work of this study, a study (Ndimande, 2014) was conducted to determine the performance of pure H-MFI-90 at the same reaction conditions. Although not conducted in the identical apparatus of this study, the findings are considered representative and directly applicable to this study, and are presented in Figure 5.2.

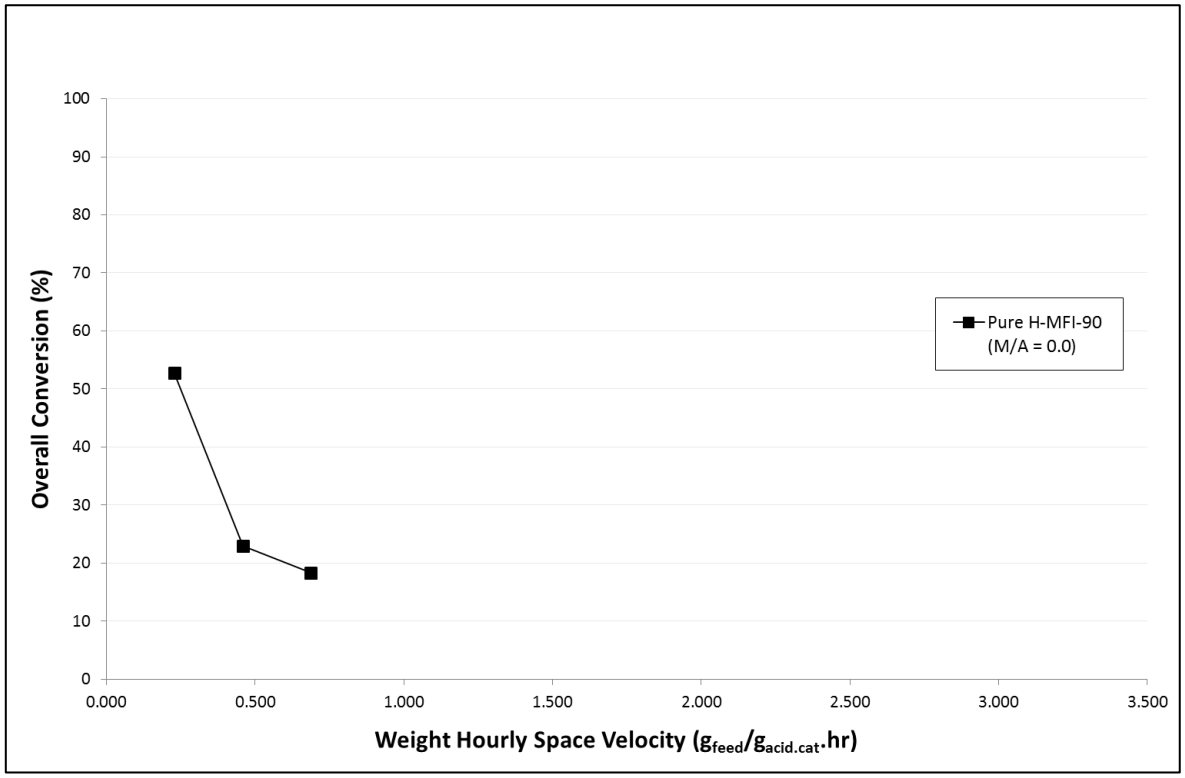

Figure 5.2: The Effect of WHSV on Overall Conversion for Pure H-MFI-90

It must be noted that the product was slightly more olefinic in nature (average 12% olefins) compared to that for the bi-functional catalysts (7 – 8% olefins), as may be expected for an acid catalysed cracking mechanism. Although the zeolite-only activity is substantially lower than that of the catalysts involving appreciable metal contents, this „background" zeolite

catalysed performance must be kept in mind for the lowest metal / acid (M/A) ratios of this study. The complete product distribution for the H-MFI-90 only tests was not reported with only the olefinic nature being compared to that found in this study. It should be noted that the product was more aromatic in composition as well due to the acid catalysed reaction that occurs on the zeolite.

5.2 Activity

5.2.1 Effect of Metal Type and Metal / Acid Site Ratio on Overall Conversion

Figure 5.3 to Figure 5.6 present the effect of varying metal loading (and, hence, M/A ratios) with increasing space velocity for each of the metals, respectively. In all cases it can be seen that increasing the M/A ratio increases the overall combined catalyst activity. Additionally, increasing WHSV reduces the conversion as expected.

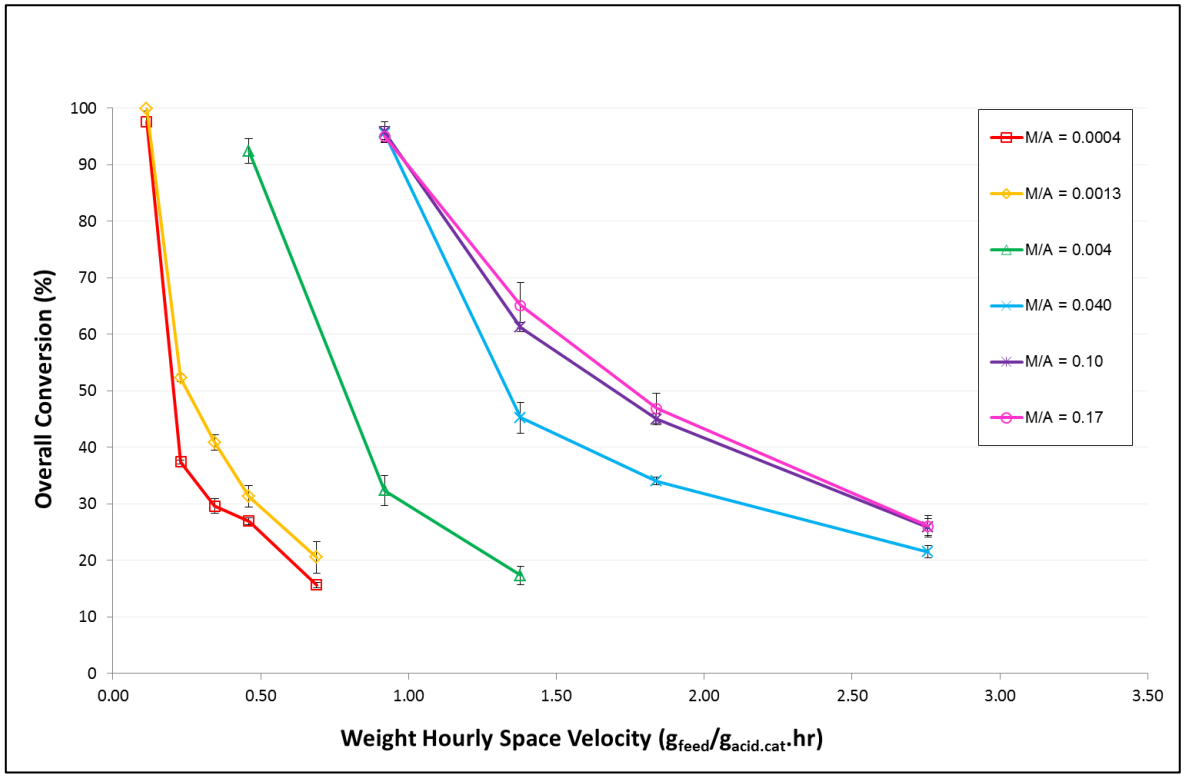

Figure 5.3: The Effect of Increasing Platinum Metal Site / Acid Site Ratios on Overall Conversion

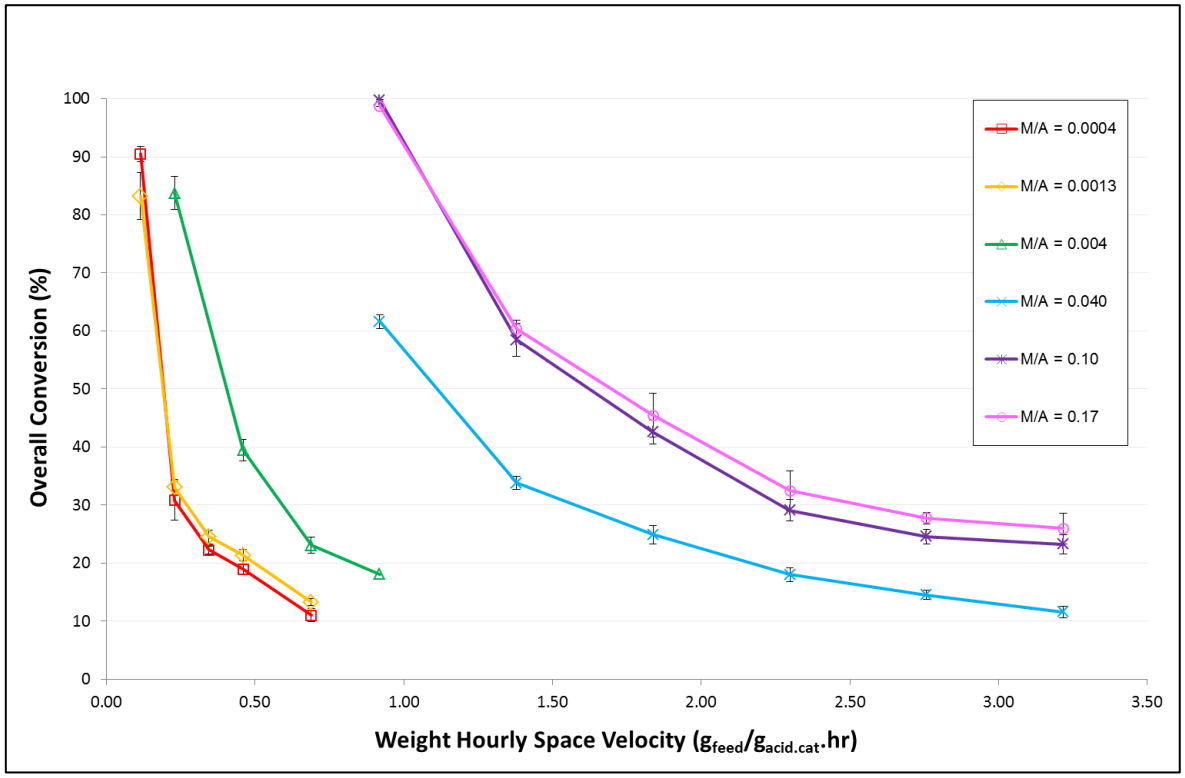

Figure 5.4: The Effect of Increasing Palladium Metal Site / Acid Site Ratios on Overall Conversion

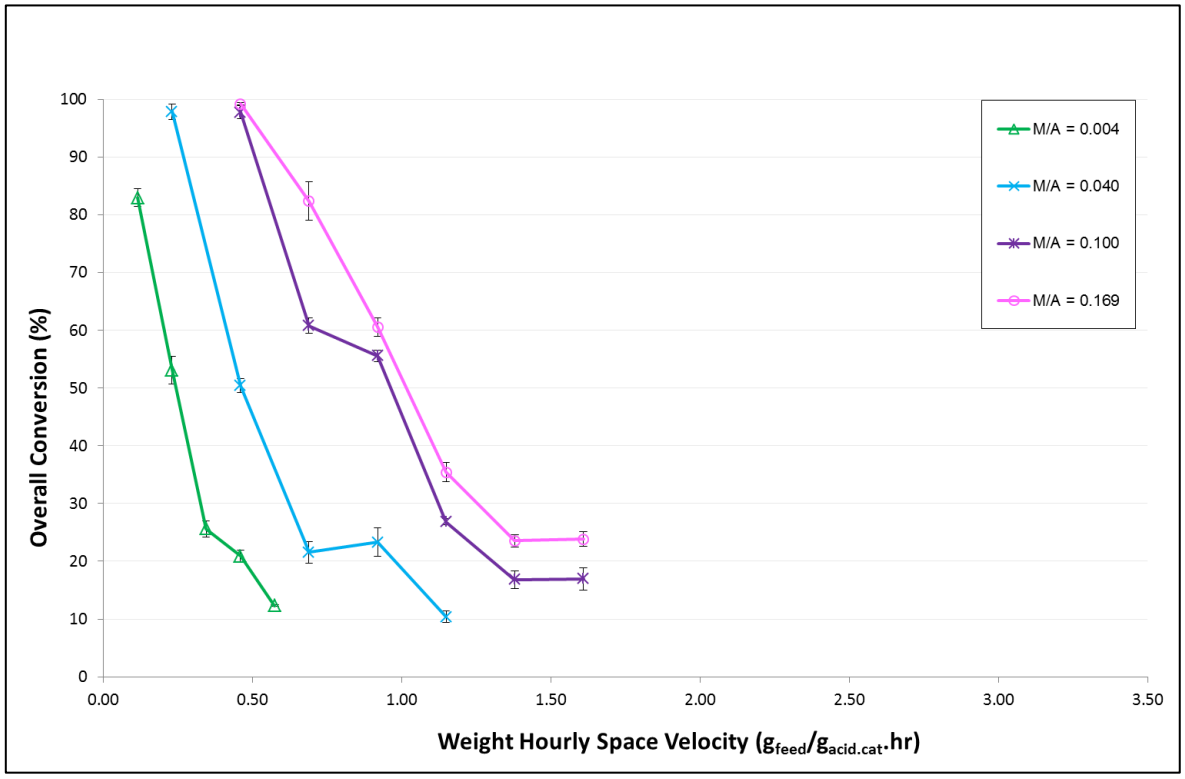

Figure 5.5: The Effect of Increasing Nickel Metal Site / Acid Site Ratios on Overall Conversion

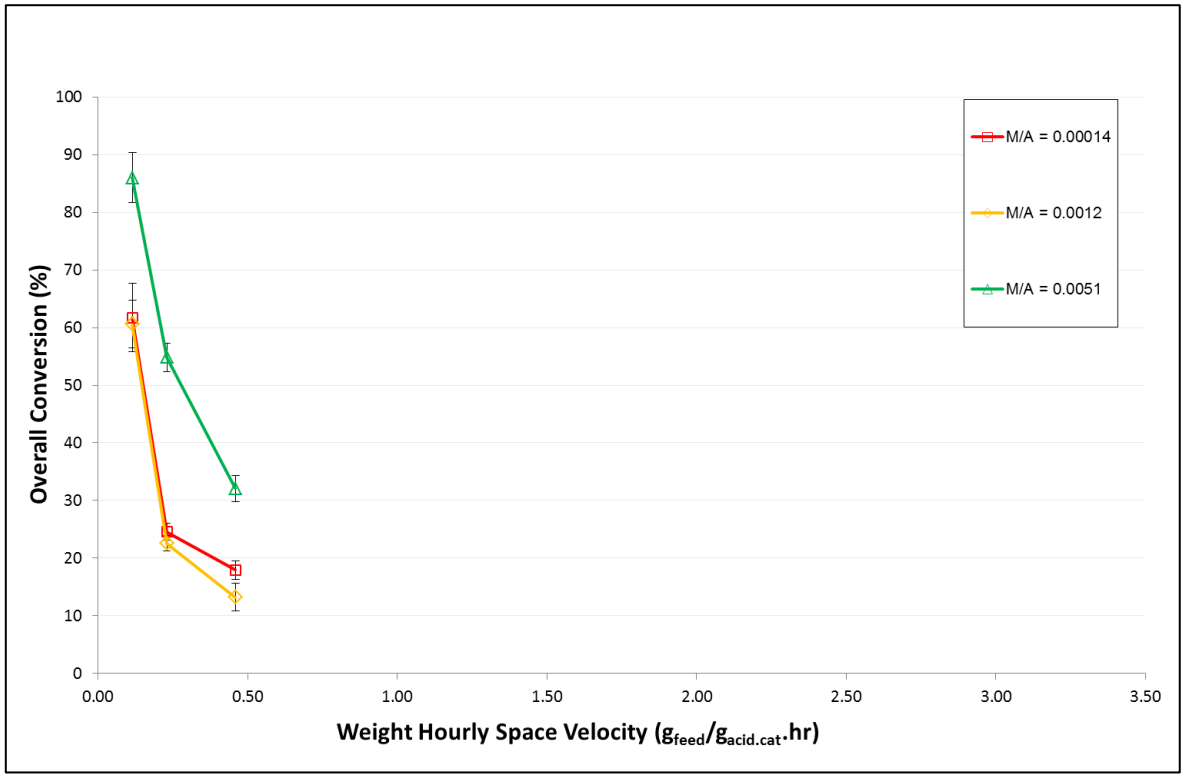

Figure 5.6: The Effect of Increasing Cobalt Metal Site / Acid Site Ratios on Overall Conversion

A comparison of metal type on activity is shown for two different M/A ratios in Figure 5.7 and Figure 5.8 from which it can be seen that metal activity increase as Co ~ Ni < Pd < Pt. As the cobalt ratios were significantly lower, cobalt data only appears in Figure 5.7 (*note*: the cobalt M/A ratio is 0.005 while the other metal M/A ratios are 0.004) as the higher ratios were not possible (due to impracticalities in loading volumes – see Section 4.1.4).

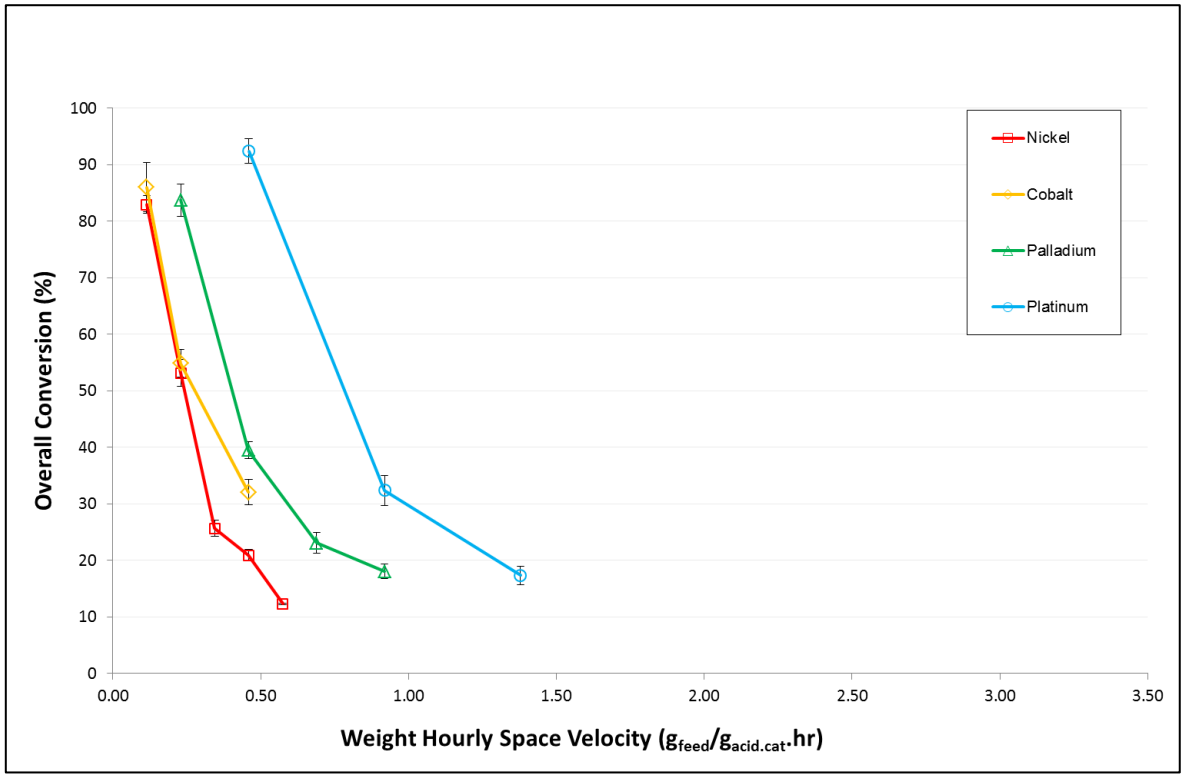

Figure 5.7: The Effect of Different Metal Types and WHSV on Overall Conversion (Metal site / Acid Site Ratio of 0.004 (Note: Cobalt metal site to acid site ratio of 0.005))

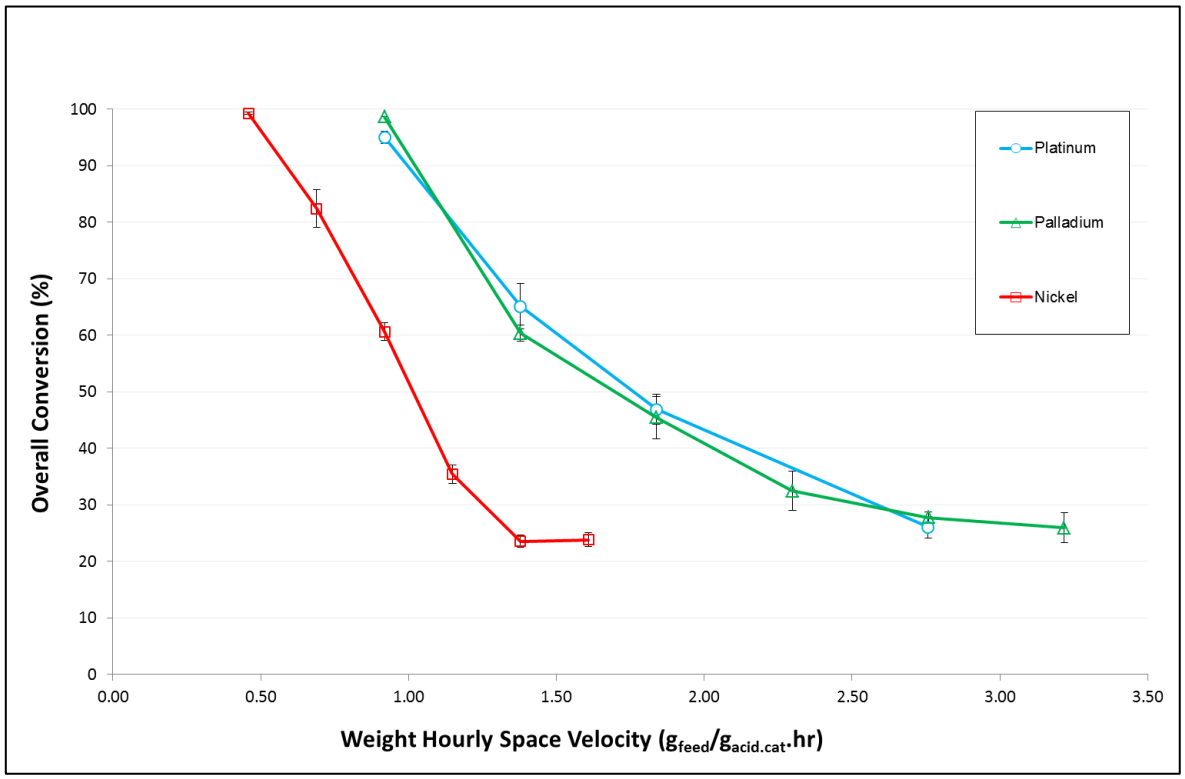

Figure 5.8: The Effect of Different Metal Types and WHSV on Overall Conversion (Metal Site / Acid Site Ratio of 0.169)

5.2.2 Effect of Metal Type and Metal / Acid Site Ratio on Reaction Rate

For a more direct comparison between catalyst, their activity is presented per metal in Figure 5.9 to Figure 5.11 as the actual reaction rate at the different WHSVs (*note: this was not done for cobalt due to the particularly low M/A ratios*). In all cases increasing the metal loading increases the reaction rate up until a certain level at which point the reaction rates levels off – although in some cases that point of levelling off was not yet reached.

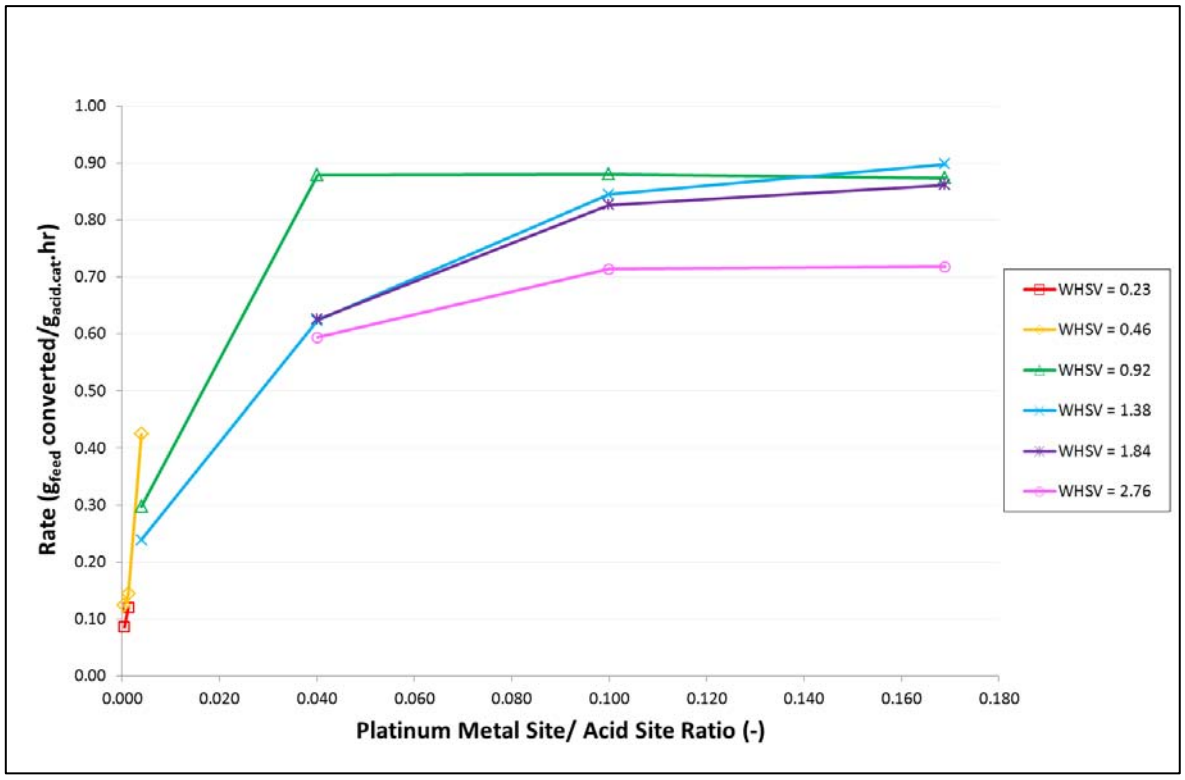

Figure 5.9: The Effect of Platinum Metal Site / Acid Site Ratios on Reaction Rates with increasing Weight Hourly Space Velocity

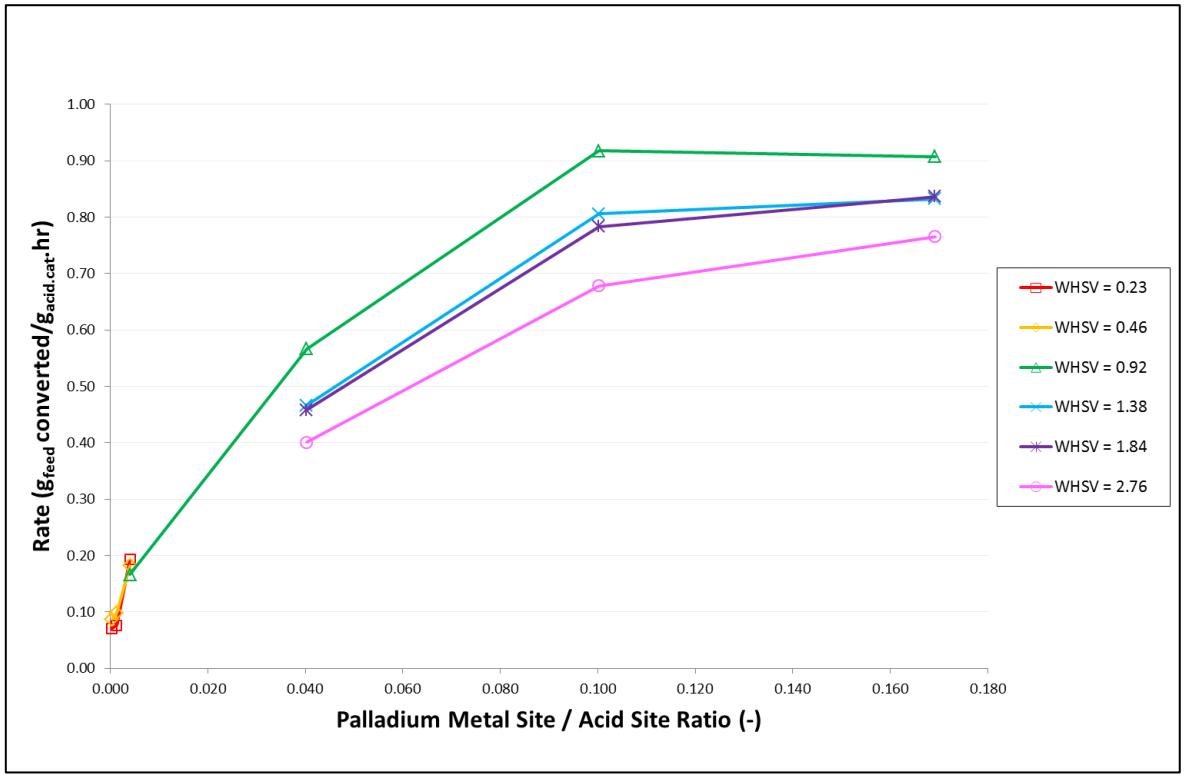

Figure 5.10: The Effect of Palladium Metal Site / Acid Site Ratios on Reaction Rates with increasing Weight Hourly Space Velocity

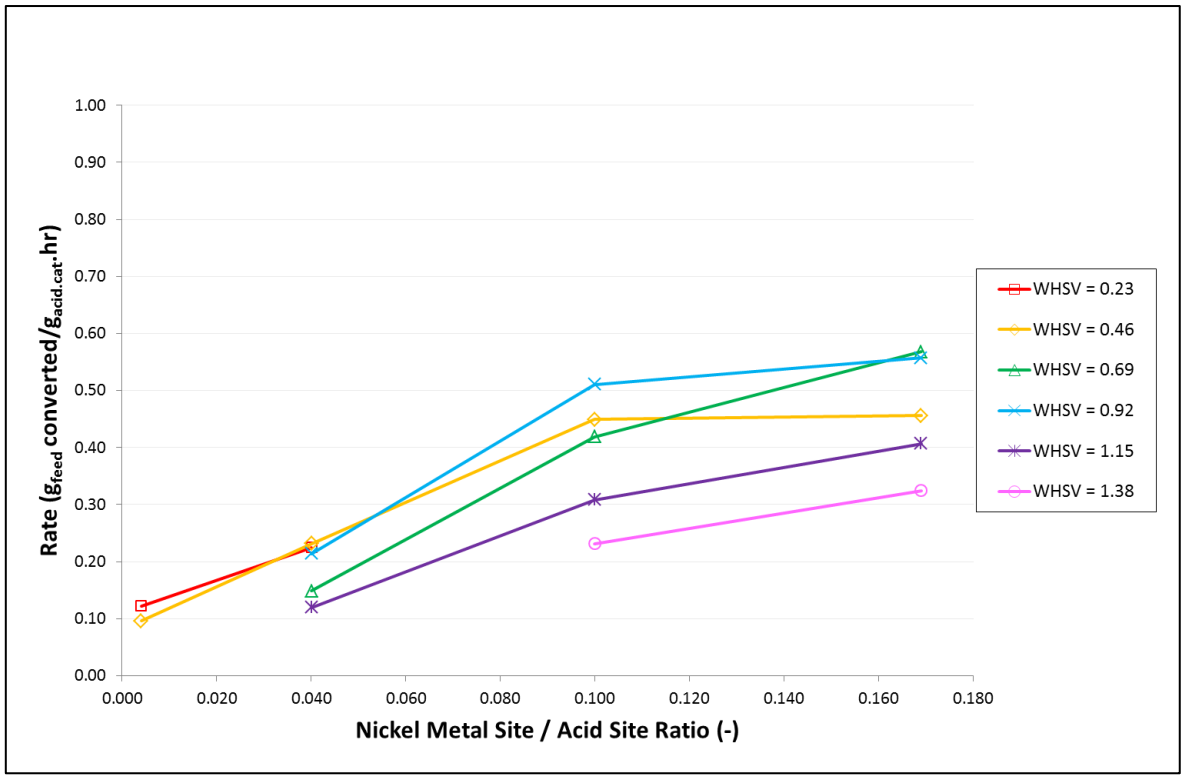

Figure 5.11: The Effect of Nickel Metal Site / Acid Site Ratios on Reaction Rates with increasing Weight Hourly Space Velocity

Combining the above graphs using a chosen WHSV (1.38 $g_{feed}/g_{acid.cat}.hr$) produces the curves in Figure 5.12. The nickel catalyst shows a significantly lower activity than the noble metals. The cobalt curve has not been plotted here as the M/A ratios were too low in comparison with regards to activity.

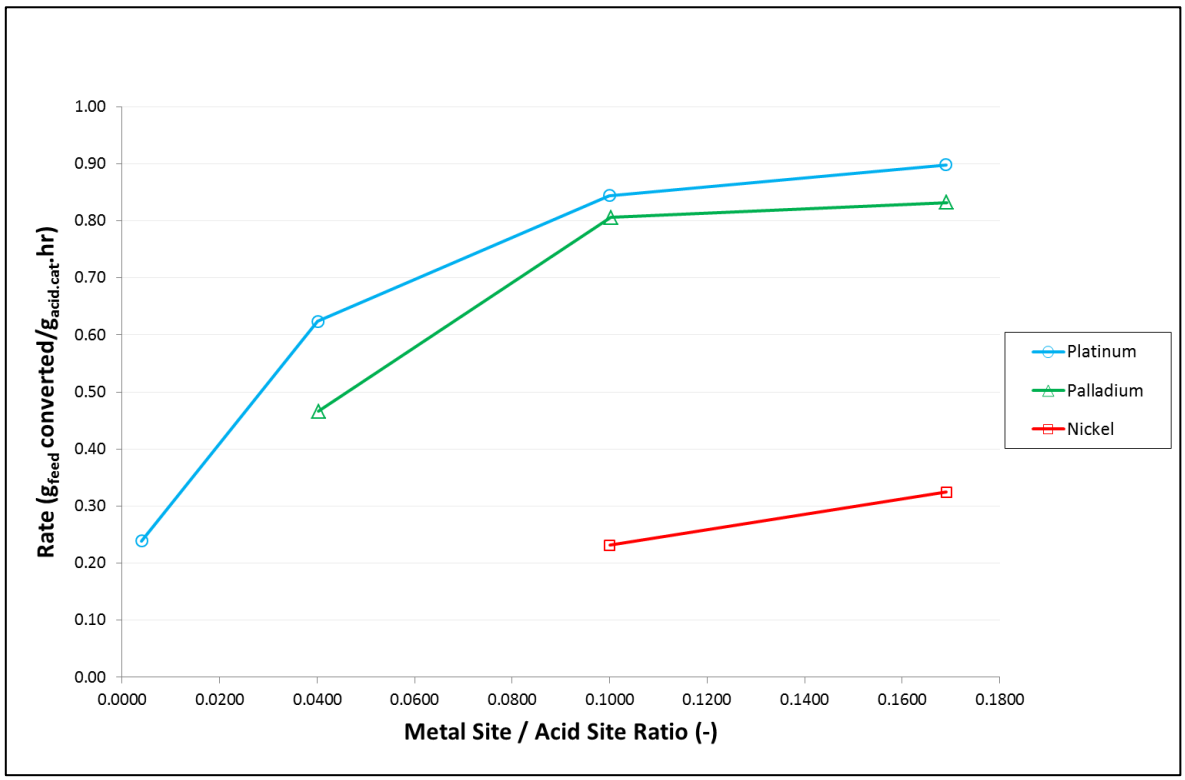

Figure 5.12: The Effect of Different Metal Types and Metal Site /Acid Site Ratios on Overall Reaction Rates (WHSV = 1.38 $g_{feed}/g_{acid.cat}$.hr)

5.3 Selectivity

5.3.1 Effect of Conversion on Selectivities

Figure 5.13 and Figure 5.14 present the product carbon number distributions from platinum and palladium at increasing conversion (achieved by reducing WHSV) at a constant M/A ratio of 0.169 in both cases. It is important to note that the distributions do not alter significantly as the conversion changes (the small changes are due to averaging data). While not shown here, the same trends occur at the other M/A ratios across all the metals and metal loadings tested.

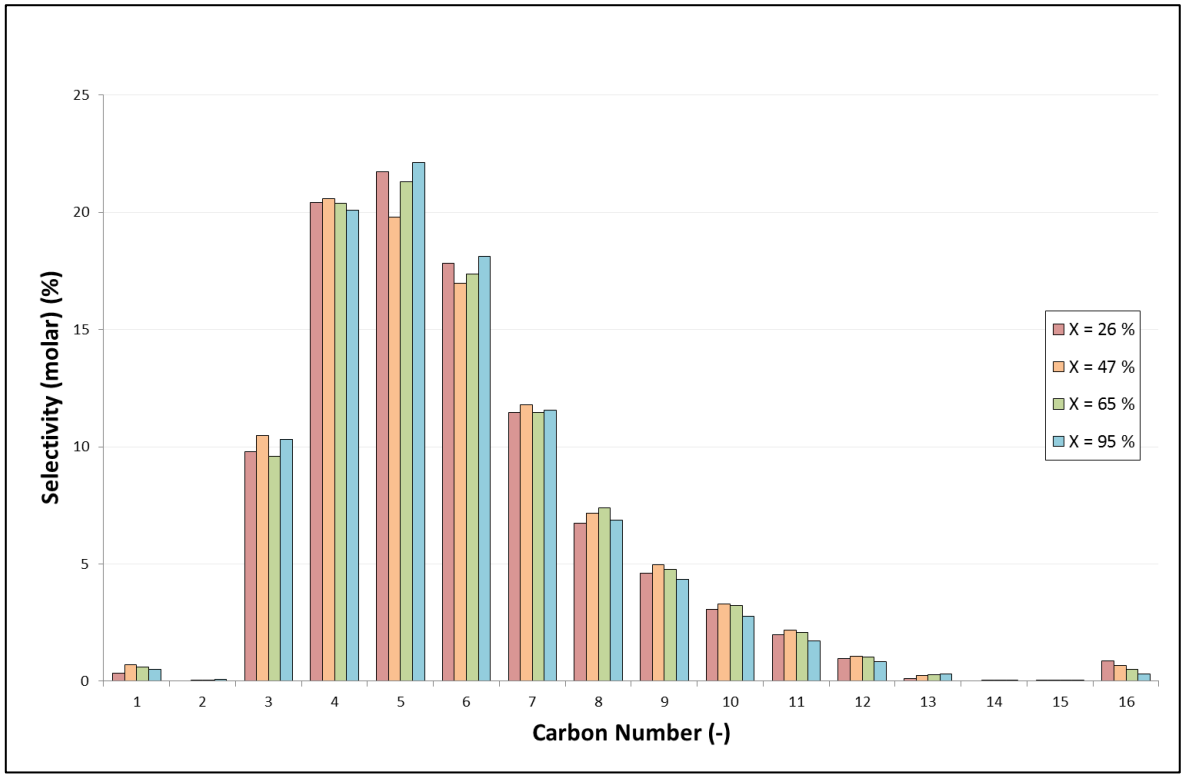

Figure 5.13: Platinum Carbon Number Distribution (n- & iso- combined) at Increasing Conversions (M/A ratio = 0.169)

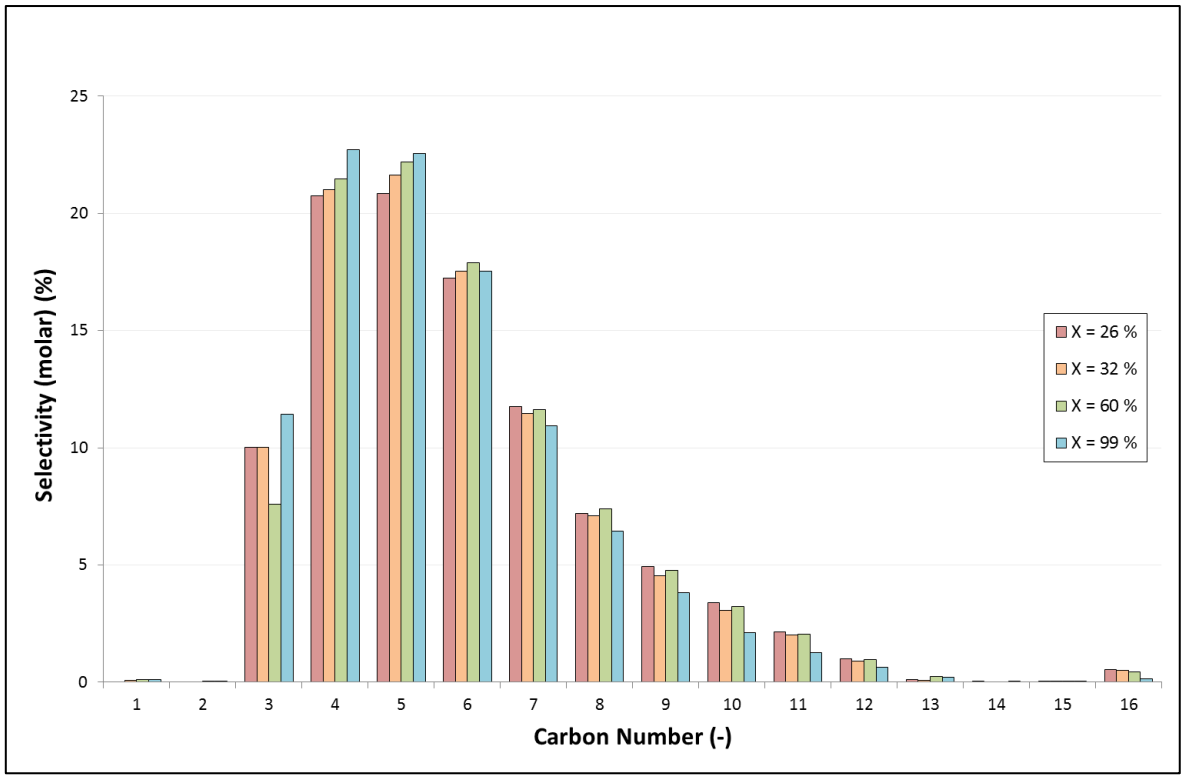

Figure 5.14: Palladium Carbon Number Distribution (n- & iso- combined) Increasing Conversions (M/A ratio = 0.169)

5.3.2 Effect of Metal / Acid Ratios on Selectivities

Figure 5.15 to Figure 5.18 present the product carbon number distributions for each metal (platinum, palladium, nickel and cobalt, respectively) at increasing M/A ratios at approximately constant conversions so comparisons between distributions can be made reliably *(note: the Pd data at M/A = 0.0004 in Figure 5.16 and all the Co data in Figure 5.18 has been normalised to exclude erroneous C1 and C2 data collected during the experiments)*

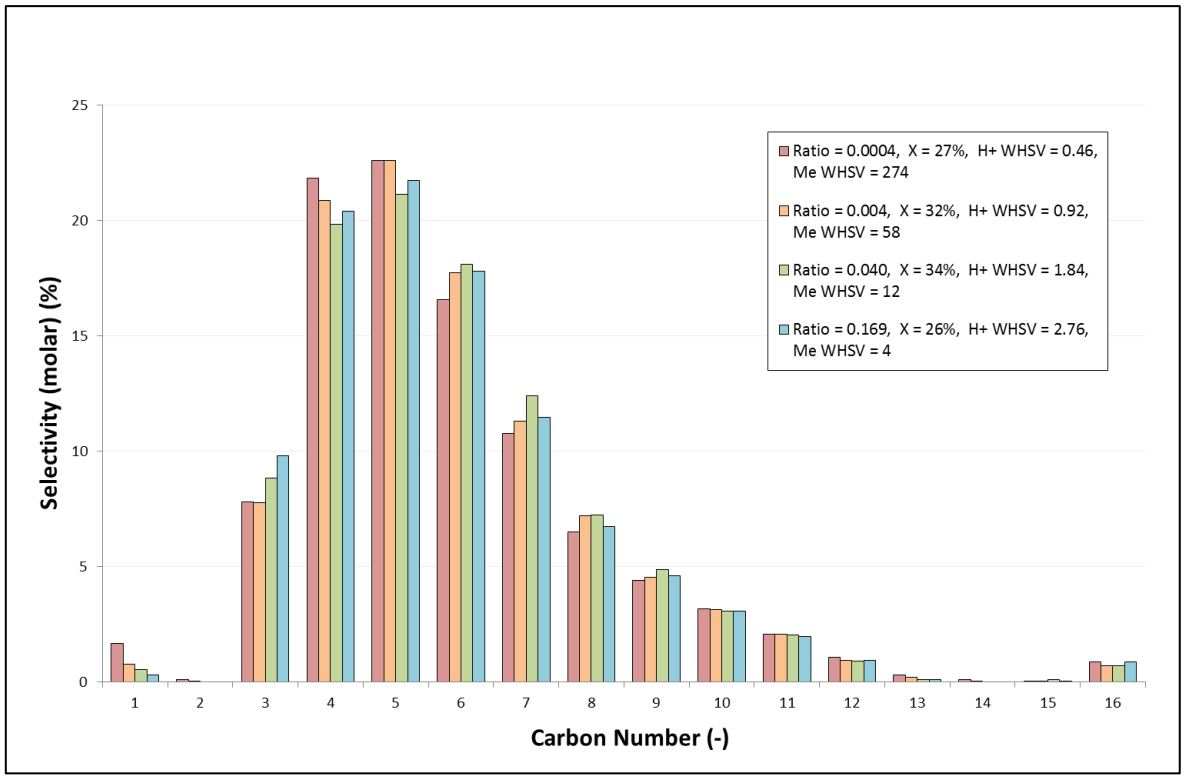

Figure 5.15: Carbon Number Distribution for Increasing Platinum Metal Site / Acid Site Ratios at Approximately Constant Conversions

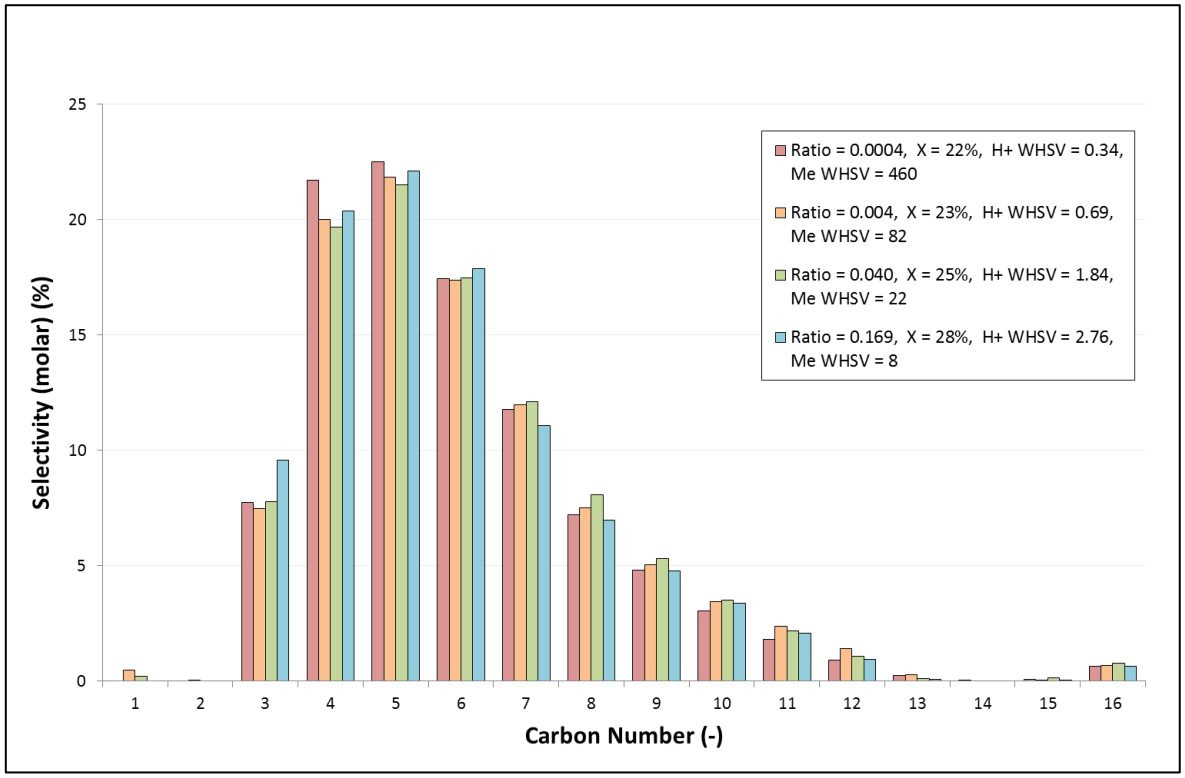

Figure 5.16: Carbon Number Distribution for Increasing Palladium Metal Site / Acid Site Ratios at Approximately Constant Conversions

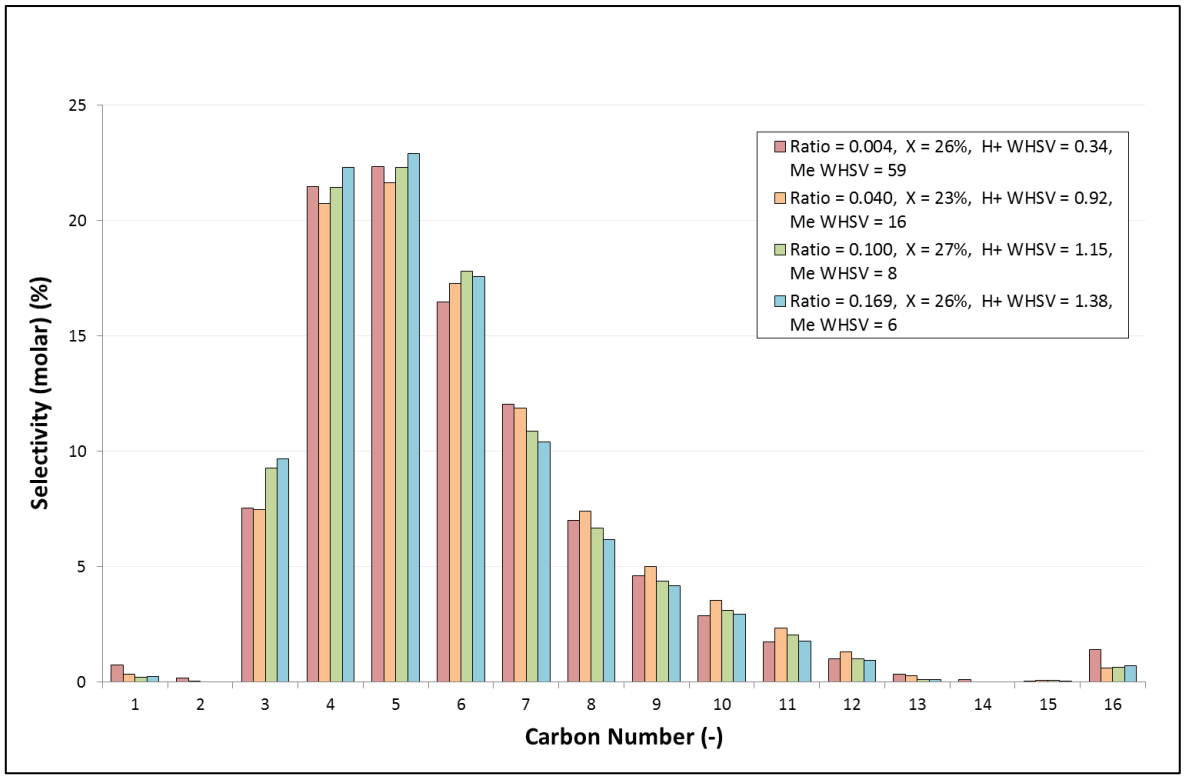

Figure 5.17: Carbon Number Distribution for Increasing Nickel Metal Site / Acid Site Ratios at Approximately Constant Conversions

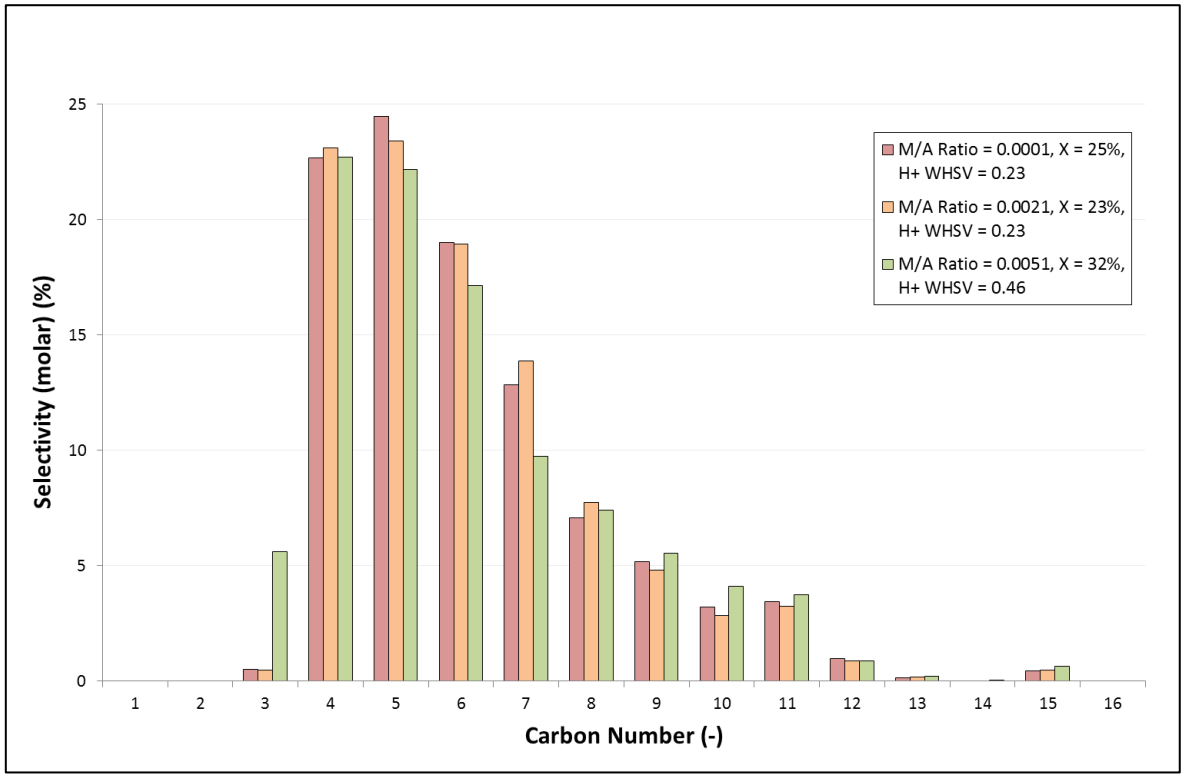

Figure 5.18: Carbon Number Distribution for Increasing Cobalt Metal Site / Acid Site Ratios at Approximately Constant Conversions

6 DISCUSSION

6.1 General Time-on-Stream Performance and Deactivation

Over the duration of each catalyst loading experiment (platinum and palladium ~ 10 days, nickel ~ 13 days and cobalt ~ 8 days) there was limited deactivation of the platinum and palladium catalysts. However, the two base metal catalysts showed greater deactivation with nickel showing the highest loss of activity with time-on-stream. In the absence of detailed experiments at constant WHSV, de-activation could not be determined quantitatively.

Figure 5.5 indirectly provides evidence for deactivation in the case of the supported nickel catalyst during the course of this 10 day experiment. While deactivation may not be immediately obvious from the figure the shape of the curves, particularly those at M/A ratios of 0.040 and 0.100, are related to the order in which different WHSV where tested. For the nickel catalyst, the tests were conducted in the order presented Table 6.1.

Table 6.1: Weight Hourly Space Velocity Testing Order for the Supported Nickel Catalyst

Metal/Acid Ratio	Weight Hourly Space Velocity $g_{feed}/g_{acid.cat}.hr$					
0.040	0.92	0.46	0.23	0.69	1.15	
0.100	0.92	0.46	0.69	1.15	1.61	1.38

From Figure 5.5 and Table 6.1 it can be seen that when the set WHSV were increased to values between those already tested the conversion level observed was lower than that expected from the general shape of the curve. This occurred at 0.69 $g_{feed}/g_{acid.cat}.hr$ in both cases as highlighted and is indicative of deactivation which is most prominent at the start of the experiment (during the first 3 – 5 days on-stream).

Figure 5.1 presents time-on-stream data for the supported Pt/H-MFI-90 catalyst with a ratio of 0.100. It can be seen that at each WHSV no deactivation is discernible and this holds true for all Pt metal loadings. Also, for both Pt (Figure 5.3) and Pd (Figure 5.4) the curves for each M/A ratio are smooth despite the sequence of the tests. Consequently, for the time periods and operating conditions involved in this study, the noble metals are considered to exhibit negligible deactivation. It was not easily possible to observe colour changes in the spent catalyst (a darker colour would suggest coking and thus de-activation). This is due to the fact

that during unloading the spent catalyst is mixed up with the significantly larger volume of silicon carbibde used to hold the catalyst bed in place in the reactor.

The cobalt catalyst experiments were shorter because it was not possible to reduce the WHSV sufficiently (due to the limitations of the C_{16} feed pump) to obtain measureable conversion levels and hence the overall experiment was completed earlier than those of the other supported metal catalysts. The significantly lower metal dispersion for the cobalt catalysts contributed to the fact that it was not possible to load the same metal site to acid site ratios as for the other supported metals. Instead, the same percentage metal mass was loaded, resulting in greatly reduced conversion as the same metal mass had far fewer active (exposed) metal sites for the de-hydrogenation/hydrogenation reactions to take place. Consequently, little specific information can be claimed on the stability of the Co catalysts.

6.2 Catalyst Activity as a Function of Metal Type and Loading

6.2.1 Effects of Metal Loading

For all the metal tested (Pt - Figure 5.3; Pd - Figure 5.4; Ni - Figure 5.5; Co - Figure 5.6), as the metal loading increases (M/A ratio rises) activity increases but that at a certain loading additional metal effects a lesser and lesser extent in the conversions recorded. The curves for M/A ratios of 0.100 and 0.169 start to merge, indicating a limiting level of metal addition (no data provided for Co in Figure 5.6), beyond which additional metal has no further effect on catalyst activity (conversion). The effect is perhaps even clearer when considering the observed reaction rates as a function of M/A ratio for the Pt, Pd and Ni (Figure 5.3, Figure 5.4 and Figure 5.5, respectively) where the rates stabilise at M/A ratios of 0.1, 0.17 and somewhat above 0.17 respectively. There are two possibilities for this, viz. (i) the acid function becomes rate limiting or, (ii) diffusion of intermediate species becomes rate limiting.

Given the experimental conditions (particularly the high temperature) as well as the strength of the acid zeolite (H-MFI-90) it is unlikely that the acid function is limiting the reaction but rather these findings suggest the possibility of a limitation in the transport of intermediate species between the metal and acid sites of the bi-functional catalyst. The nature of the intermediate in question depends on the theory used to describe the hydrocracking reaction, i.e. the classical mechanism or the hydrogen spill over mechanism. Whereas for the classical mechanism the rate limiting step would be the diffusion of olefins between the metal sites and the acid sites (Section 2.3.1.3), in the case of the hydrogen spill over mechanism, the diffusion limited intermediates in question would be activated hydrogen species

(Section 2.3.1.2). This possible transport limitation would be affected by the distance between the active sites involved in the reactions (including the relative dispersion of the various metals) as well as the intrinsic activity of the metal function (individual active metal centres) for olefin or activated hydrogen species generation.

At the lower end of the M/A ratio scale i.e. where less and less metal is added to the zeolite, the successive conversion curves (Figure 5.3, Figure 5.4, Figure 5.5 and Figure 5.6) again start to lie on top of each other. The best example of this may be seen for palladium M/A ratios of 0.0004 and 0.0013 as shown in Figure 5.4, although same is readily apparent for Pt (Figure 5.3) and Co (Figure 5.6). It may be expected that as the M/A ratio decreases so would the conversion until there is no reaction measureable when no metal was loaded.

This is not the case and when the rate data is plotted on a logarithmic scale, as shown in Figure 6.1 for the case of Pd, it becomes clear that the rate approaches a constant value at the very low loadings (within a certain WHSV data set) and, indeed, this „background" rate of reaction is consistent with that observed for the zeolite-only experiments (Figure 5.2). In both cases, zeolite-only, and very low Pd/zeolite (Figure 6.1) the rate approaches a value of 0.1 g_{feed}converted / $g_{acid.cat}$·hr at the conditions of the study.

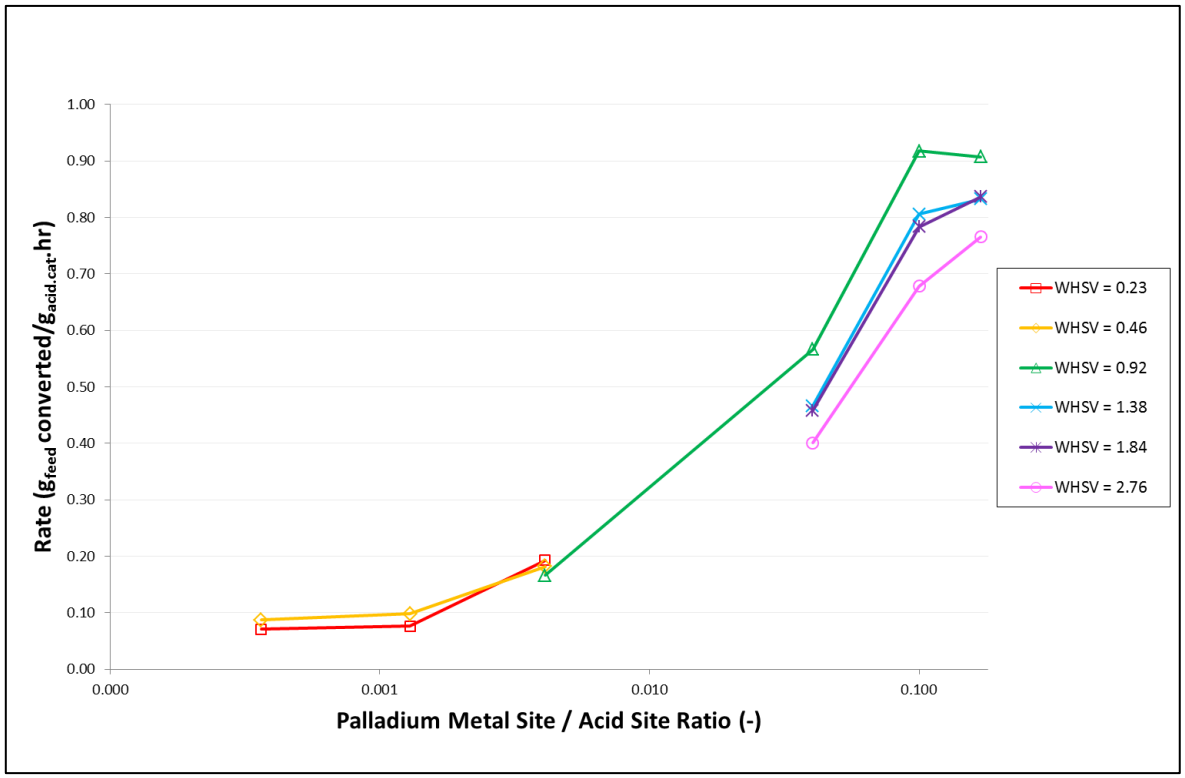

Figure 6.1: The Effect of Palladium Metal Site / Acid Site Ratios on Reaction Rates with increasing Weight Hourly Space Velocity (plotted using a logarithmic scale)

6.2.2 Effects of Metal Type

Figure 5.7 and Figure 5.8 show the effect of the different metals on overall conversion at two different metal loading levels. Figure 5.7 (M/A ratio of 0.004) shows that at low loadings the supported platinum catalyst is significantly more active towards activating hydrogen or de-hydrogenating C_{16} (depending on the reaction mechanism chosen) than the other supported metals but, furthermore, that both noble metals are noticeably more active than the two base metals tested. This was expected according to the hypothesis proposed at the start of the work.

At a higher M/A ratio – in this case 0.169 (Figure 5.8) - the two noble metal curves fall nearly on top of each other (this also held for M/A ratios of 0.100), showing they were approximately equally as active, while the nickel was considerably less active.

It may be noted at these high metal loadings, both the Pt and Pd catalysts are reaching a „saturation" level in terms of the effect of metal loading on activity and interestingly, that at these levels the overall catalyst activity (conversion level) is „independent" of the metal type – further clear evidence for the rate limiting step being intrinsic to some other aspect of the combined catalyst. Much the same observation can be drawn for Figure 5.12 were, at a WHSV of 1.38 $g_{feed}/g_{acid.cat}$.hr, it can be seen at the higher M/A ratios that the palladium and platinum catalysts" performance start to approximate each other, meanwhile the rates resultant from the nickel catalysts remain lower highlighting the inherent lower activity of the base metal.

Potentially, at the higher M/A ratios both noble metals could be activating hydrogen (or de-hydrogenating paraffins) at a rate greater than that which these intermediates can diffuse to the acid sites – however, possibly with differing diffusion resistances (due to the metals being loaded onto a different support other than directly onto the acid zeolite).

6.3 Product Selectivity as a Function of Metal-Type and Loading

Figure 5.13 and Figure 5.14 present the product carbon number distributions for the platinum and palladium catalysts, respectively, at different conversion levels, from which it can be seen that the product distributions are very similar for both catalysts.

Whereas it is generally expected that as the conversion increases the product selectivity should shift to lighter products for reason of the greater concentration of primary products which subsequently undergo secondary cracking thereby decreasing the average product chain length, no such pattern is seen with increasing conversion on the platinum catalyst (Figure 5.13) and, whereas some such trend may be seen for palladium (Figure 5.14) it is slight at best with some increase below C_6 and the opposite above C_6. It should, however, be clear from Figure 5.13 and Figure 5.14 that in all cases the product spectrum represents a notably over-cracked distribution, even at conversions as low as 26%. Coupled with the findings presented in Figure 5.3 and Figure 5.4, from which it can be seen that ever higher metal contents are unlikely to increase cracking activity, the results of Figure 5.13 and Figure 5.14 suggest an „intrinsic" over-cracking even though these catalysts have the highest M/A ratios of the study and represent, from an industrial perspective, catalysts of relatively high metal loading, 1.39 wt% (Pd) and 2 wt% (Pt), respectively. This „intrinsic" (over-cracked) selectivity is also observed for differing M/A ratios at roughly constant conversion for all four metals (Figure 5.15 to Figure 5.18), i.e. even when the catalyst metal contents are well below their „saturation" values in terms of catalyst activity. Moreover, Figure 5.15 to Figure 5.18 show no change in product distribution with increasing M/A ratio, except perhaps in the case on Ni where a slight change may be discerned.

One possible explanation is the diffusion resistance unintentionally introduced by removing the supported metal from being in the zeolite itself to being loaded onto an inert support which is physically separated from the acid function. This increases the diffusion distance considerably and, as a result, once the $C_{16}H_{34}$ feed has been activated by either activated hydrogen or by dehydrogenation to an olefin at the metal site (depending on the mechanism), it migrates to the acid site where the cracking reactions take place but, due to increased diffusion limitations, extensive over-cracking takes place before the product compounds „see" another metal site where they are re-hydrogenated and cracking reactions cease. Thus once the feed is activated it is cracked „to completion" before the reaction can be quenched and, therefore, changing M/A ratio or conversion has little effect on the overall product distribution.

Another possible consideration is that the H-MFI-90 is intrinsically more reactive (Kukard, 2008) – than the larger pore zeolite Y that was used in the work by Alverez *et al.* (1996).

Consequently, as soon as the feed is activated and has diffused into the smaller MFI zeolite pores, it is subsequently cracking many times, thus bringing about the over-cracking observed.

Moreover, the excessive over-cracking of the C_{16} feed may also be attributed to the intrinsic activity of the H-MFI-90 catalyst towards this reaction since the zeolite acts as a strong acid due the high silica-alumina ratio of the H-MFI-90 (ratio of 90:1). Zeolite catalysts with a lower overall acidic strength would result in less over-cracking of the feed compounds as discussed by Kukard (2008) who showed H-MFI-90 to be the most active catalyst (when compared to different types of zeolites with lower acidic strength) under slightly varied conditions (temperature – 250°C, pressure – 40 bar), where the effect of the higher pressures was shown to cause an insignificant change in activity towards hydrocracking reactions (Böhringer *et al*., 2006b).

Thus, it is observed that the product distribution is insensitive to metal type or loading, even for metal loadings above the metal saturation threshold for overall catalyst activity. Moreover, the product distribution is highly over-cracked. These findings point to a rate controlling step independent of the metal function and rather to one solely constrained by either the zeolite (acidity and pore geometry) or an extended metal-acid diffusion path relating to the physically mixed catalyst formulations of this study (or a combination of these effects).

7 CONCLUSIONS AND RECOMMENDATIONS

A suitable test unit has been developed for n-hexadecane hydrocracking studies with online analysis of the entire reaction effluent stream. Several issues, in particular the proper design of the post reactor flow path and vaporiser configuration, are essential to achieving analytical data of good quality and integrity. The final apparatus allows for four catalytic tests to be conducted simultaneously.

Increasing metal loadings and, consequently, the metal / acid site ratio (M/A ratio) of the catalyst increases catalyst activity (as determined by n-hexadecane conversion level) up to a certain M/A ratio, after which no further increase in activity / conversion is observed. At this M/A ratio, different for each of the Pt, Pd, Ni and Co metals evaluated, the (de-)hydrogenation function of the catalyst is no longer rate limiting and the further addition of metal to the catalyst formulation brings no further benefit. The relative activities of the metals tested for promoting hydrocracking activity is found to decrease in the order Pt > Pd >> Ni > Co at conditions of 225°C and 20 bar and molar H_2 : n-$C_{16}H_{34}$ ratio of 10.

For all catalysts evaluated in this study, the product carbon number distributions (selectivities) are essentially invariant with metal type, metal loading and conversion level. Moreover, carbon number distributions are representative of a highly over-cracked product. Despite metal loadings sufficient to „saturate" catalyst activity (i.e. at levels where additional metal content no longer improves activity), the product remains over-cracked such that it has not been possible to determine the M/A ratios required for ideal hydrocracking under the conditions and catalyst configurations of this study. That this is the case suggests that, in all experiments of this study, the „mechanism" controlling hydrocracking performance is either related directly to the specific nature of the H-MFI-90 acid catalyst (both its high acid strength and its micro-porous channel structure) or to the extended separation between metal and acid sites imposed by the physically mixed co-catalyst formulations applied, the latter, which introduces a substantial diffusional resistance to intermediate olefins or activated hydrogen transport, is considered the more likely explanation and it is recommended that further work explores this hypothesis via studies with metal-on-zeolite catalyst configurations.

In respect of metal-induced methanolysis, very low molar methane selectivities were observed throughout the study, in particular when considered in terms of carbon or mass selectivities, and consequently, all the metals evaluated are considered acceptable in terms of methane yield under the conditions evaluated.

Finally, although not directly proven in this study, it is considered highly likely that the poor product distributions observed are due to the physically mixed (separated) mature of the dual co-catalyst formulations employed. Whereas this embodiment was intellectually chosen for purposes of a clear separation of metal and acid functions and specifically so as to independently compare metal functions, the arrangement leads to an unrealistic configuration for the study of bi-functional hydrocracking reactions and the should be abandoned in future studies.

REFERENCES

Aboul-Gheit A.K., Aboul-Fotouh S.M., Aboul-Gheit N.A.K, 2005. Hydroconversion of cyclohexene using catalysts containing Pt, Pd, Ir and Re supported on H-ZSM-5 zeolite, *Applied Catalysis A. General*, **283** 157 - 164

Alvarez F., Ribeiro F.R., Perot G., Thomazeau C., Guisnety M., 1996. Hydroisomerisation and Hydrocracking of Alkanes: 7. Influence of the Balance between Acid and Hydrogenating Functions on the Transformation of n-Decane on PtHY Catalysts, *Journal of Catalysis*, **162** 179 - 189

Blomsma, E., Martens, J.A., Jacobs, P.A., 1997. Isomerisation and Hydrocracking of Heptane over Bimetallic Bifunctional PtPd/H-Beta and PtPd/USY Zeolite Catalysts, *Journal of Catalysis*, **165** 241 - 248

Böhringer, W., University of Cape Town (UCT), *Personal Communication*, 2006.

Böhringer, W., Kotsiopoulos, A., de Boer, M., Knottenbelt, C., Fletcher, J.C.Q., 2006a. Selective Fischer-Tropsch wax hydrocracking – opportunity for improvement of overall gas-to-liquids processing, in "Fischer-Tropsch Synthesis, Catalysts and Catalysis", Davis B. H., Occelli M. (eds), Elsevier, Amsterdam, *Studies in Surface Science and Catalysis*, **163**

Böhringer, W., Kotsiopoulos, A., de Boer, M., Knottenbelt, C. and Fletcher, J.C.Q., 2006b. On the Application of Non-Sulphided Base Metal Catalyst for Normal Paraffin Hydrocracking, *SACEC 2006*, Durban

Calemma V., Peratello S., Perego C., 2000. Hydroisomerisation and hydrocracking of long chain n-alkanes on Pt/amorphous SiO2–Al2O3 catalyst, *Applied Catalysis A: General*, **190** 207 - 218

Collins J.P., Font Freide J.J.H.M., Nay B., 2006. Review: A History of Fischer-Tropsch Wax Upgrading at BP from Catalyst Screening Studies to full Scale Demonstration in Alaska, *Journal of Natural Chemistry*, **15** 1 - 10

Conner, W.C. and Falconer, J.L., 1995. Spillover in Heterogeneous Catalysis, *Chemical Reviews*, **95** 759 – 788

Dry, M., 2001. High Quality Diesel via the Fischer-Tropsch Process - A Review. *Journal of Chemical Technology and Biotechnology*, **77** 43–50

Dry, M.E., 2003. Fischer-Tropsch Synthesis - Industrial, in: *Encyclopaedia of Catalysis. I.T. Horvath (eds.)*, **3** 347, Wiley, New York

Ebenhack, B. referred in: University of Rochester, Researchers Predict Oil Crisis
Available: http://www.rochester.edu/currents/V29/V29N12/story12.html
Accessed: 03/06/2007

Eilers, J., Posthuma, S.A., Sie, S.T., 1990. The Shell Middle Distillate Synthesis Process (SMDS), *Catal. Letters*, **7** 253

Gates, B.C., Katzer, J.R., Schuit, G.C.A., 1979. Chemistry of Catalytic Processes, *Chemical Engineering Series*, McGraw-Hill, New York

Kukard, R.S., Wynne, P.D.T., Böhringer, W., Brosius, R., Fletcher, J.C.Q., 2006. Zeolite Testing Methodology - Verification of the Suitability of Separation of Supported Metal and Zeolite for the Purposes of Zeolite Testing, Unpublished results, Honours Thesis, University of Cape Town

Kukard, R.S., 2008. The Effect of Zeolite Type on the Hydrocracking of Long n-Paraffins, Masters Thesis, University of Cape Town.

Leckel, D., 2005. Hydrocracking of Iron-Catalyzed Fischer-Tropsch Waxes, *Energy & Fuels*, **19** 1795 - 1803

Leckel, D., Liwanga-Ehumbu, M., 2006. Diesel-Selective Hydrocracking of an Iron-Based Fischer-Tropsch Wax Fraction (C_{15}-C_{45}) Using a MoO3-Modified Noble Metal Catalyst, *Energy & Fuels*, **20** 2330 - 2336

Martens, J.A. and Jacobs, P.A., 1990. Conceptual Background for the Conversion of Hydrocarbons on Heterogeneous Acid Catalysts, *Theoretical Aspects of Heterogeneous Catalysis*, 52 - 109

Martens, J.A. and Jacobs, P.A., 1997. Reaction Mechanisms of Acid-Catalysed Hydrocarbon Conversions in Zeolites, in: Ertl, G., Knözinger, H. and Weitkamp, J., 1997, *Handbook of Heterogeneous Catalysis*, Wiley-VCH, Weinheim, **3**

Martens, J.A. and Jacobs, P.A., 2001. Introduction to Acid Catalysis with Zeolites in Hydrocarbon Reactions, *Studies in Surface Science and Catalysis*, **137** 633 - 671

Maxwell, I.E., 1987. Zeolite Catalysis in Hydroprocessing Technology, *Catalysis Today*, **1** 385 - 413

Mills, G.A., Heinemann, H., Milliken, T.H. and Oblad, A.G., 1953. (Houdriforming Reactions) Catalytic Mechanism, *Journal of Industrial and Engineering Chemistry*, **45** 134 - 137

Nakamura, I., Sunada, K. and Fujimoto, K., 1997. Low Temperature Hydrocracking of Paraffinic over Hybrid Catalysts, *Journal of Studies in Surface Science and Catalysis*, **105** 1005 - 1012

Ndimande, C., 2014. Ideal Hydrocracking Catalysts for Conversion of FT wax to Diesel, Masters Thesis, University of Cape Town.

Oak Ridge National Laboratory (ORNL), 2000. An Emissions Mission: Solving the Sulfur Problem, Oak Ridge National Laboratory Review, **33**
Available: http://www.ornl.gov/info/ornlreview/v33_3_00/emissions.htm
Accessed: 01/06/2007

Park, K.C. and Ihm, S.K., 2000. Comparison of Pt/zeolite Catalysts for n-Hexadecane Hydroisomerization, *Applied Catalysis A: General*, **203** 201 - 209

Rezgui Y., Guemini M., 2005. Effect of acidity and metal content on the activity and product selectivity for n-decane hydroisomerisation and hydrocracking over nickel–tungsten supported on silica–alumina catalysts, *Applied Catalysis A. General*, **282** 45 - 53

Roessner, F. and Roland, U., 1996. Hydrogen Spillover in Bifunctional Catalysis, *Journal of Molecular Catalysis A: Chemical*, **112** 401 - 412

Scherzer, J., Gruia, A.J., 1996. Hydrocracking Science and Technology, 1st Edition, Chapter 3, Marcel Dekker Inc., New York

Shah, P.P., Sturtevant, G.C., Gregor, J.H., Humbach, M.J., Padrta, F.G., Steigleder, K.Z.,1988. Fischer-Tropsch Wax Characterization and Upgrading, Final Report for the *U.S. Department of Energy, DOE/PC/80017-T1 (DE88014638)*

Sie, S.T., Senden, M.M.G., van Wechem, H.M.H., 1991. Conversion of Natural Gas to Transportation Fuels via the Shell Middle Distillate Synthesis Process, *Catal. Today*, **8** 371

Sinfelt, J.H., 1973. Specificity in Catalytic Hydrogenolysis by Metals, *Advances in Catalysis*, **23** 91 – 119

Sinnot, R., 2005. Coulson and Richardson"s Chemical Engineering Series: Chemical Engineering Design, Vol. 6. Elsevier Butterworth-Heinemann, 4th edition

Steinberg, K.H., Mroczek, U. and Roessner, F., 1990. Aromatization of Ethane on Platinum Containing ZSM-5 Zeolites, *Applied Catalysis*, **66** 37 - 44

Weisz, P.B. and Swegler, E.W., 1957. Stepwise Reaction on Separate Catalytic Centres: Isomerisation of Saturated Hydrocarbons, *Science*, **126** 31 – 32

Welters W.J.J., van der Waerden O.H., Zandbergen H.W., de Beer J.V.H.J., van Santen R.A, 1995. Hydrocracking of n-Decane over Zeolite-Supported Metal Sulphide Catalysts. 1. CaY-Supported Transition Metal Sulphides, *Ind. Eng. Chem. Res.*, **34** 1156 – 1165

APPENDIX A – TEST UNIT DEVELOPMENT

A.1 Original Hydrocracking Test Unit Design

The final test unit design that was used to carry out the experiments (and as described in Section 4) came about through a long process of modifications to the initial design and after the primary test unit construction. A detailed discussion of the issues, concerns and steps taken in terms of the initial construction of the apparatus has been covered extensively in work by Kukard (2008) and will not be repeated here. Both the original test unit of Kukard (2008) and a second test unit were employed in this study – the two dual-tube units being connected via a multi-port switching valve to a single gas chromatograph for product analysis (and shown in Figure A.1 and Figure A.4).

A process flow diagram of the original design is shown in Figure A.2 and Figure A.3, for a single dual-tube test unit, so it can be compared to the final design of the unit once all further modification had been completed.

Figure A.1: Photograph of Original Experimental Apparatus (both test units shown)

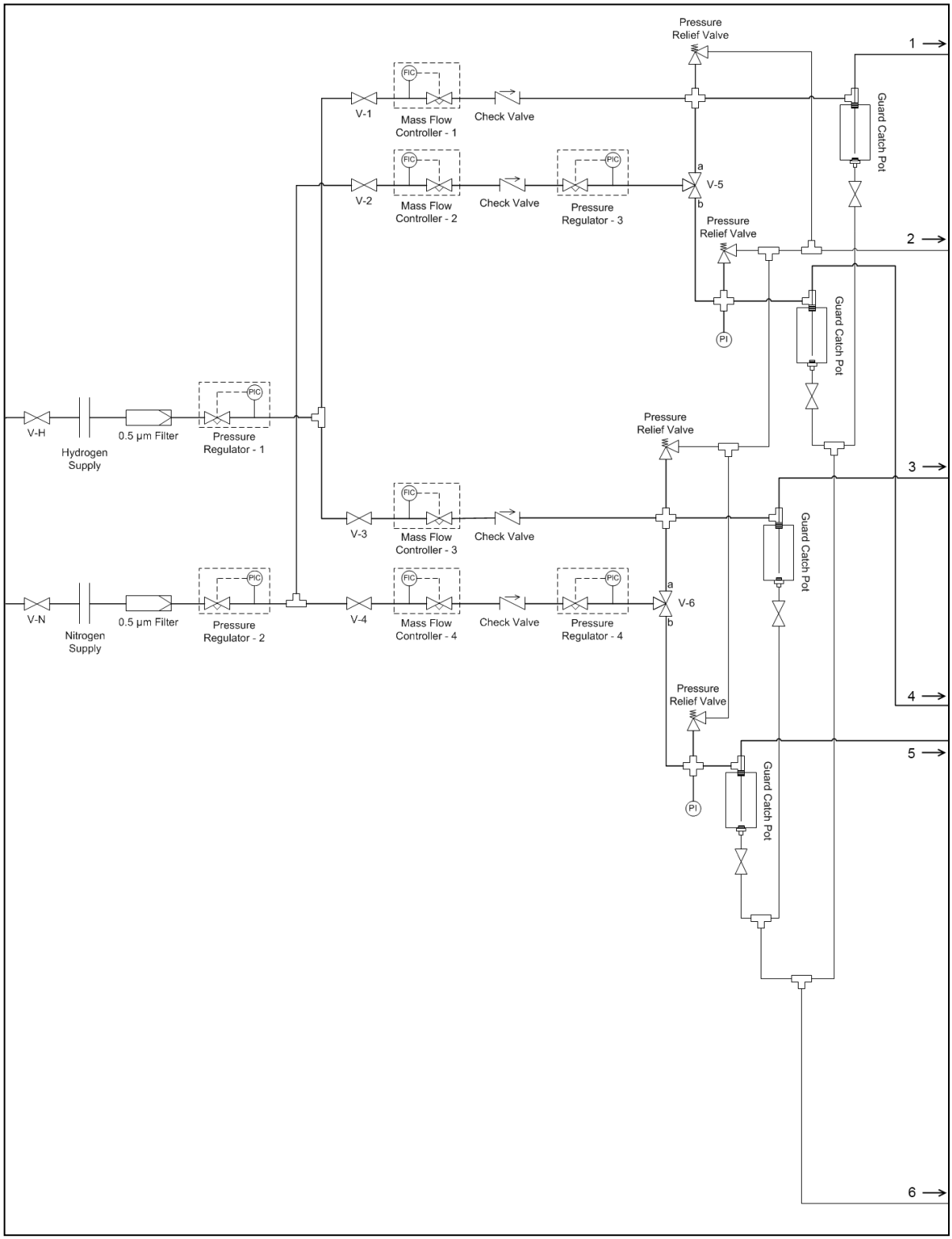

Figure A.2: Original Experimental Apparatus Flow Diagram – Gaseous Feed Section

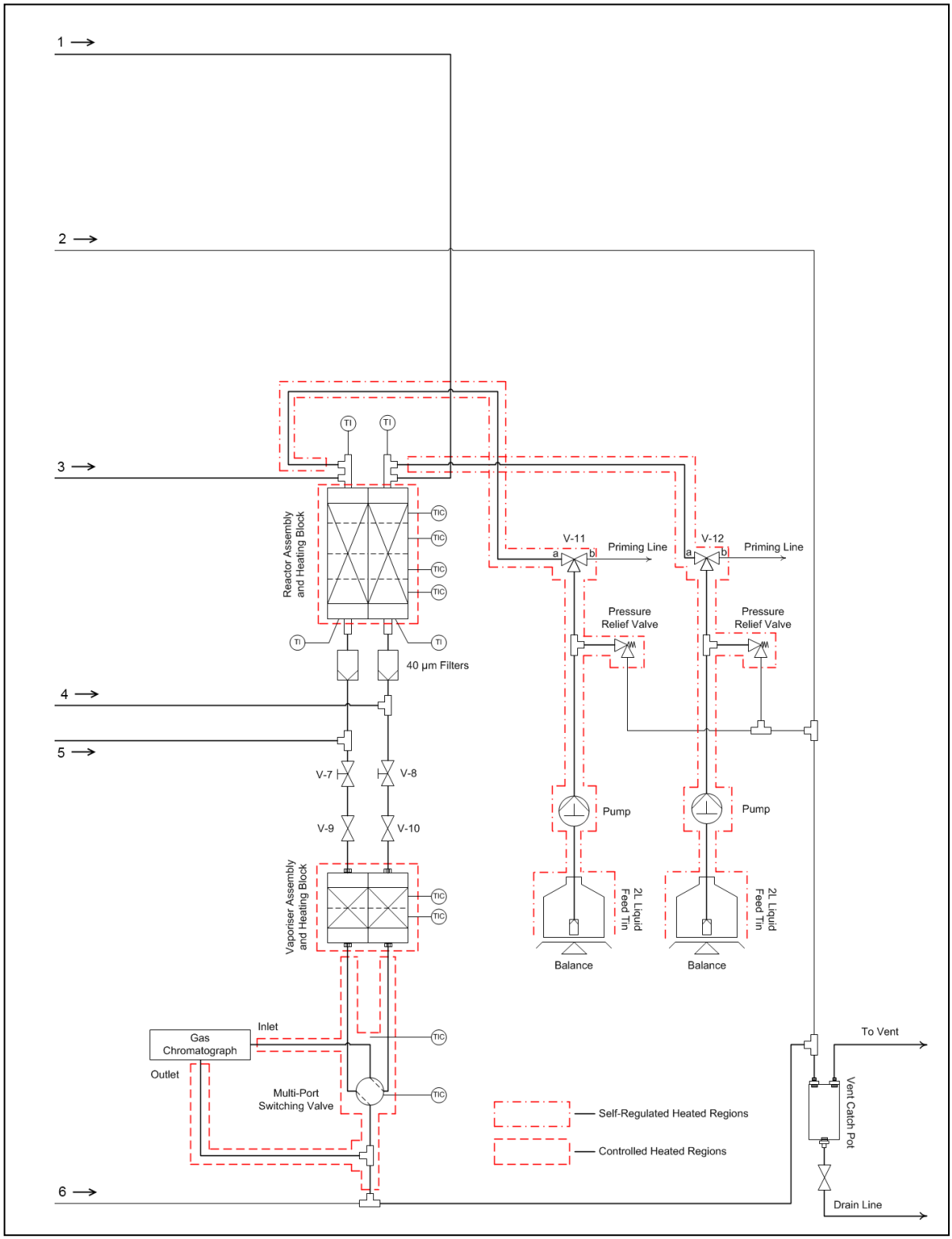

Figure A.3: Original Experimental Apparatus Flow Diagram - Liquid feed, Reactor and Vaporiser Section

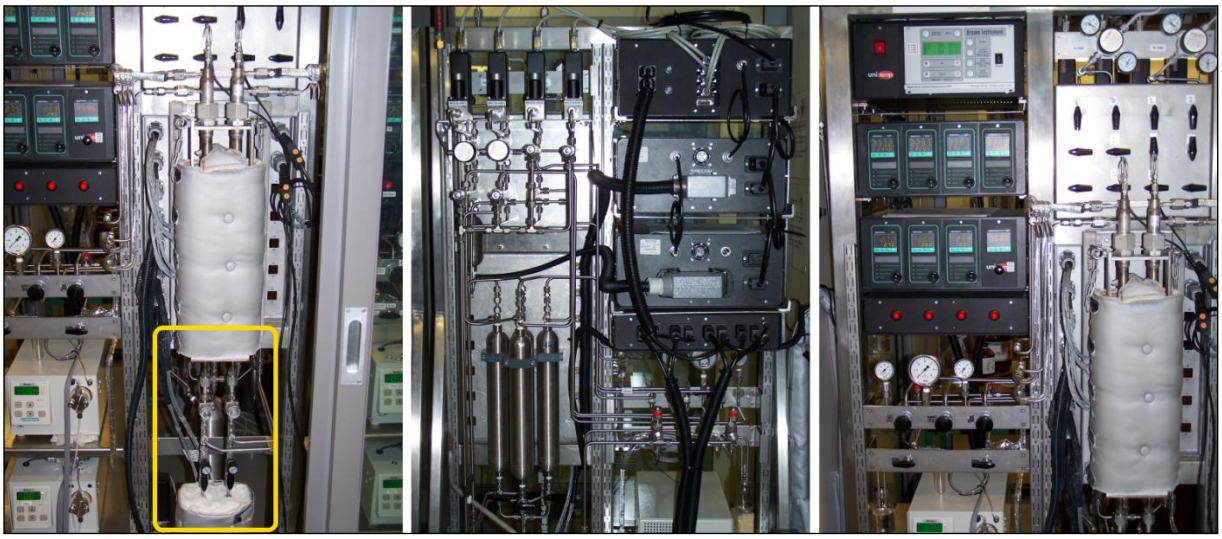

Figure A.4: Three Photographs Highlighting Specific Features of the Unmodified Design

Left: Old Vaporiser Design (shown in the yellow highlighted area);

Centre: Example of Tubing Design;

Right: Control Boxes and Valve Panels

(Only the vaporiser was adjusted in the new design)

A.2 Modifications to the Original Design

The major problem was the inability to obtain stable chromatographic results throughout the period of an experimental run- see Figure A.6 – and this was ascribed to three possible causes, viz. cold-spots in post-reactor lines, general tubing design faults and the product vaporiser temperature profile, respectively.

A.2.1 Suspected Cold-Spots in Post-Reactor Lines

Several attempts were made to improve control over the post-reactor tubing temperature as it was believed that cold spots causing condensation of product droplets and their erratic transport to the chromatographic injection point was causing a large variability in the amount of product that is injected onto the GC column. The droplets would also contain a greater percentage of heavy products and thus affect both conversion and selectivity data.

A general attempt to solve the cold spot(s) problems was to wrap additional heating cord and insulation around the tubes between the reactor and the vaporiser and from the vaporiser outlet to the multiport switching valve. However, all such attempts did not solve the problem of the inconsistent total chromatographic signal. The vaporiser temperature was also increased with limited affect, such

that, after numerous endeavours, it was concluded that cold spots in the main lines were not the cause of the erratic chromatographic data.

A.2.2 Suspected Tubing Design Issues

Once cold spots had been eliminated as the cause of the chromatographic variability, the general configuration of the tubing was brought into question.

Below the reactor and before the diluent entry point a T-piece micro-filter was installed to trap any particulate matter which may have eluted from the reactor contaminating the vaporizer where the higher temperature may lead to a further conversion of the reactor effluent. The filter resulted in a potentially large „cold spot" and a region in which product effluent could pool before being „released" to the general product stream before reaching the chromatographic injection point. In particular, the entry point of the nitrogen diluent line was perpendicular to the reactor effluent line, potentially allowing for reactor effluent to travel down this line, cool and condense to form larger droplets which could be carried back into the main product stream via the flow of diluent nitrogen, with the effect of an erratic total chromatographic reading.

Consequently, the T-piece micro-filter was removed entirely (with additional glass wool inserted at the bottom of the reactor for this filtration purpose) and the diluent nitrogen entry point was angled at 45°, as shown in Figure A.5, so as to inhibit flow of reactor effluent up the cool diluent line.

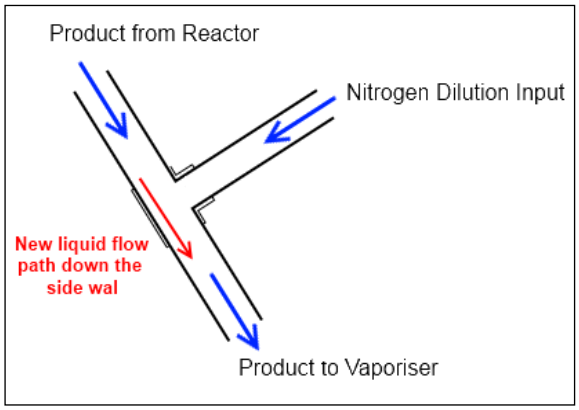

Figure A.5: New Piping Diagram at the Diluent Entry Point

(highlighted in red)

A.2.3 Vaporiser Temperature Profile

Originally, once the product left the reactor, the tubing was not heated until the start of the vaporiser. This meant the product was allowed to cool in the section between these two major components while

the dilution gas was added, even though from the vaporiser all the way to the GC the lines were heated to 200°C to prevent subsequent condensation. No attempt was made to heat the lines between reactor and vaporiser as the system was designed such that the vaporiser would provide sufficient heating (along with the dilution) to ensure complete vaporisation of the reactor effluent.

Two main variations to this arrangement were investigated, viz. changing the vaporiser temperature and a totally revised physical embodiment of the product vaporisation section of the test unit. The effect of increasing the vaporiser temperature from 250°C to 275°C did not improve chromatographic consistency but rather it had the reverse effect with more outliers to the general trends and a greater randomness to the results, contrary to the hypothesis that a temperature increase would ensure the products were all in the vapour phase. Consequently, the reverse was tried; the temperature was reduced and the insulation at the top of the vaporiser was removed. This, while not solving the problem, resulted in a definite improvement in chromatographic stability, raising the possibility of „flash-vaporisation" in an excessively hot vaporiser resulting in a „slug" of vaporised product transferring to the chromatographic injection point as successive liquid droplets entered the vaporiser. As a consequence there was not a steady flow of product to the GC, and this resulted in the inconsistent results. Thus, the problem was determined to be „hot-spots" rather than the cold spots that were originally suspected.

Given the largely uniform temperature afforded by the large brass block of the vaporiser, the brass blocks were discarded completely. Instead a metal conduit of 2.5 cm diameter was installed around the vaporizer tube and all the connecting tubes extending from the reactor exit, along the nitrogen dilution point, all the way to the back pressure regulator below the vaporiser tube (which was about 10 cm beyond the point at which the sample tee-off point was located). Resistive heating wire was wound in a spiral groove around the metal conduit, with an increasing coil density so as to impose a suitable temperature gradient (which increased slowly) along the vaporiser tube which was suitably insulated. With a temperature gradient of no more than 2 °C/cm along any part of the vaporiser, the temperature gradually decreases from the reactor exit temperature of approximately 200°C to the lowest temperature at the point where the nitrogen dilution flow is introduced (as the nitrogen diluent is not pre-heated before addition) from where it steadily increases to the hottest point at which the sample line branches off as shown in Figure A.7. Chromatographic stability was excellent with this configuration as shown for all the four reactor tubes in Figure A.8 to Figure A.11. The temperature of the heating zone is controlled by a thermocouple inside the conduit at the height of the sampling tee-off point.

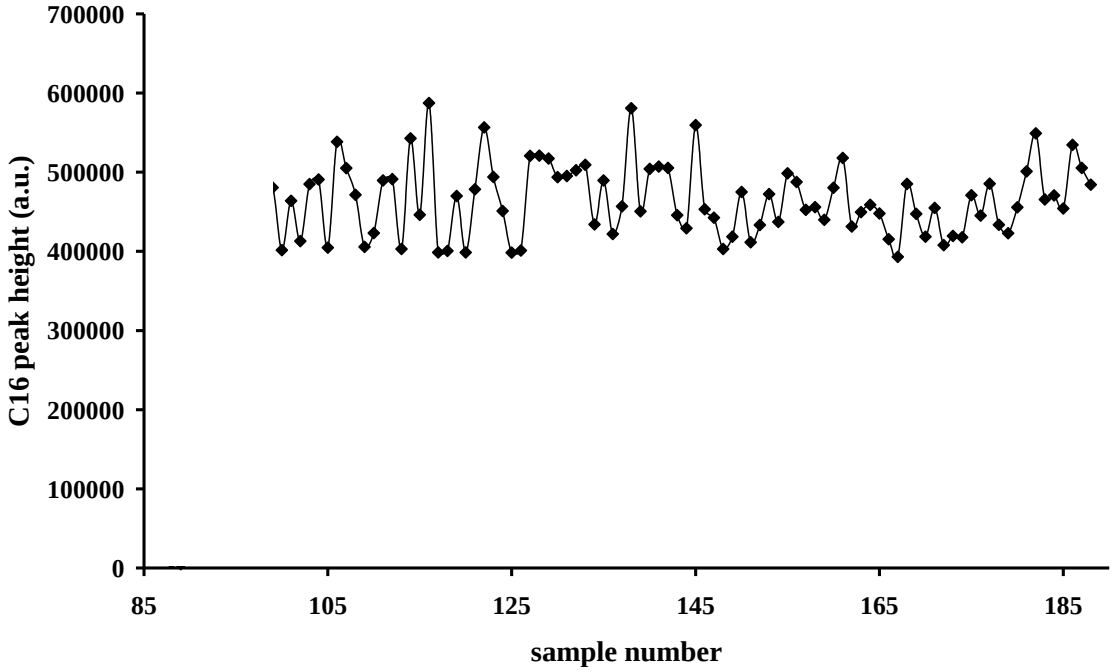

Figure A.6: A Plot Showing the Wide Scatter in Chromatographic Data from the Original Test Unit Design (Pure C_{16} feed with reactor packed with only SiC)

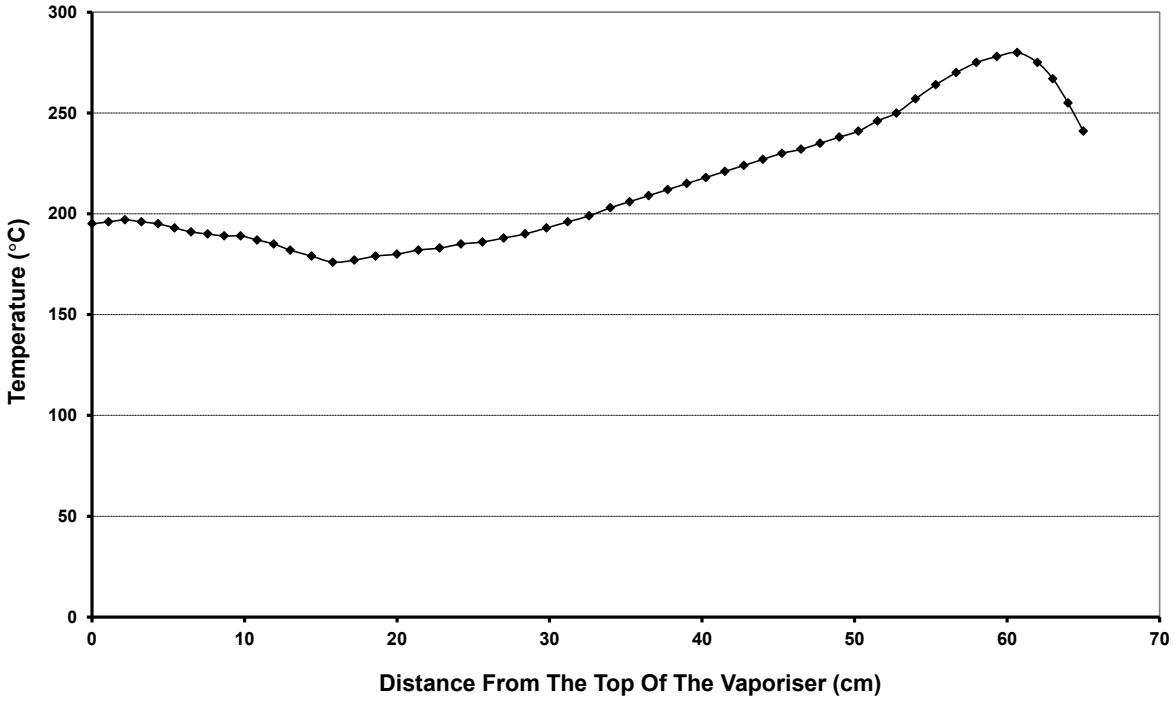

Figure A.7: Vaporiser Temperature Profile for First Unit's Reactor Two (Pure C_{16} feed with reactor packed with only SiC)

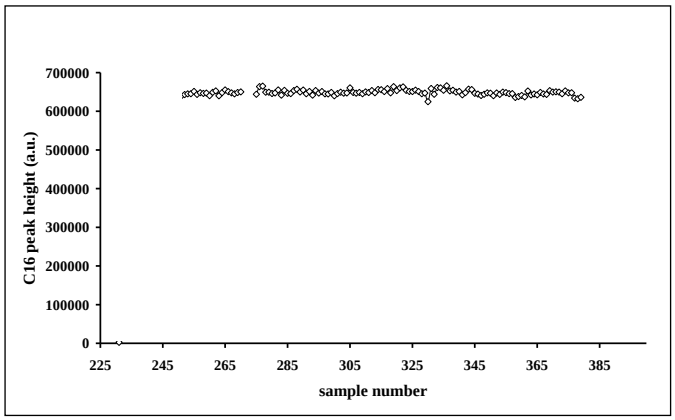

Figure A.8: Stable GC Results Obtained from First Test Unit Reactor 1 (Pure C_{16} feed with reactor packed with only SiC)

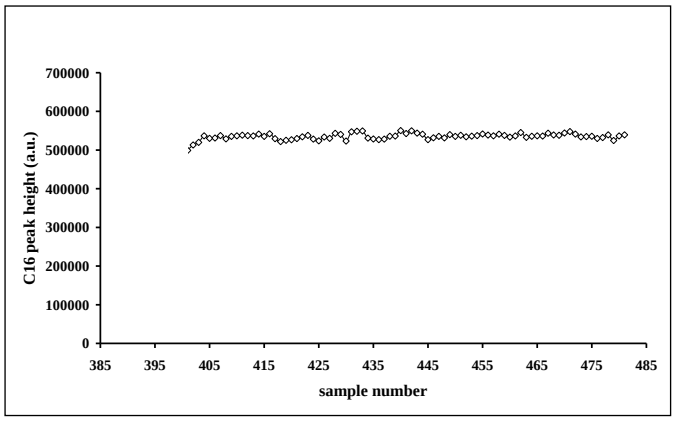

Figure A.9: Stable GC Results Obtained from First Test Unit Reactor 2 (Pure C_{16} feed with reactor packed with only SiC)

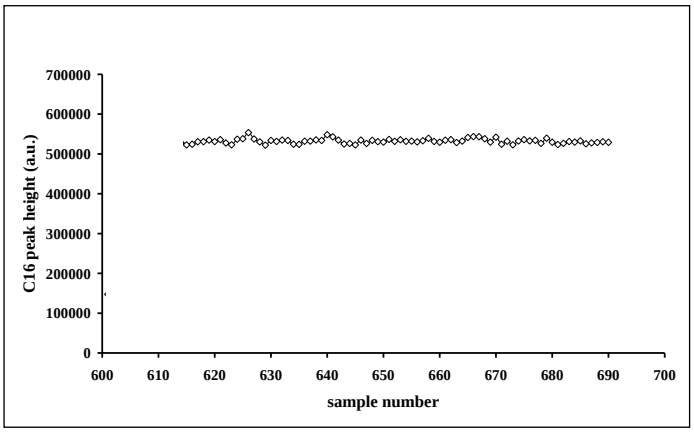

Figure A.10: Stable GC Results Obtained from Second Test Unit Reactor 1 (Pure C_{16} feed with reactor packed with only SiC)

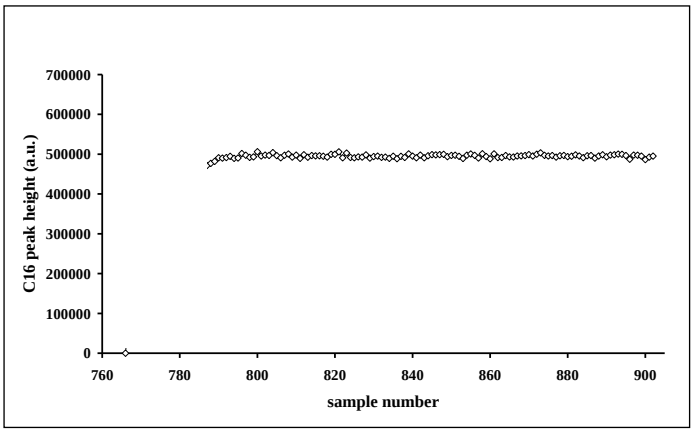

Figure A.11: Stable GC Results Obtained from Second Test Unit Reactor 2 (Pure C_{16} feed with reactor packed with only SiC)

In summary, therefore, it is thought that the following criteria are important to stable product vaporisation;

i. the partial pressure of hexadecane must increase incrementally and slowly along the length of the vaporizer and,

ii. that deleterious step changes include either a drastic increase in temperature and C_{16} vapour pressure or a significant lowering of the partial pressure due to dilution via nitrogen. If a step change is introduced the effect of such a change can be moderated by increasing the surface area on which C_{16} is evaporated – in other words adding silicon carbide in the vaporiser unit at the point where the dilution gas is introduced into the partly liquid reactor effluent.

APPENDIX B - TEMPERATURE PROGRAMMED REDUCTION (TPR) DATA

TPR experiments were carried out on the nickel and cobalt catalyst to determine the temperature at which the reduction needed to be done. Within the department it is common practice to reduce platinum and palladium catalysts at 350°C so TPR was not carried out on these catalysts.

For the nickel catalyst the reduction of the metal was not complete until over 500°C was reached (Figure B.1) – however, as the reactor furnaces cannot be operated at over 450°C, the reduction could only be done at that temperature.

By the time the temperature had passed 250°C the cobalt was fully reduced (Figure B.2). The reason for reducing the cobalt catalyst at only 250°C was to minimise the sintering of the catalyst. The CO chemisorption data showed that the dispersion was decreased by approximately 0.5% for every 100°C increase in the reduction temperature and given the very low dispersion numbers for the cobalt it was decided to reduce it as low as possible to retain the largest dispersion possible.

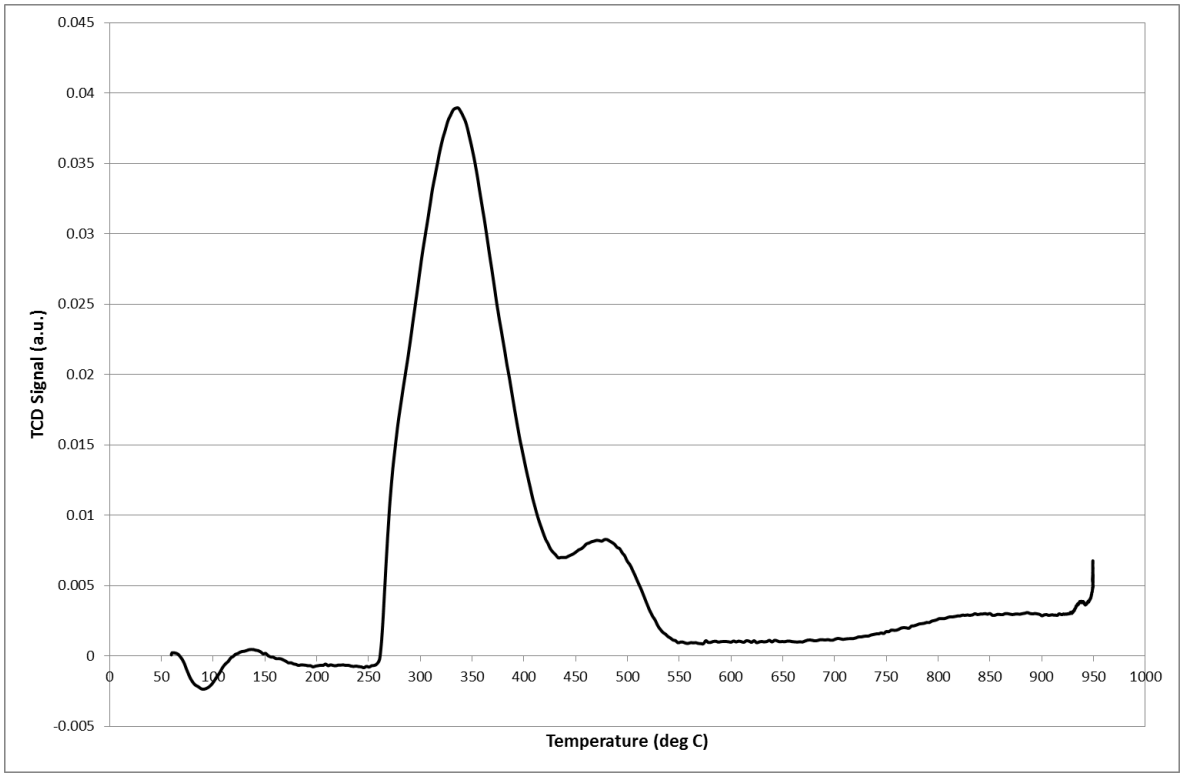

Figure B.1: The Temperature Programmed Reduction Profile of Supported Nickel Catalyst

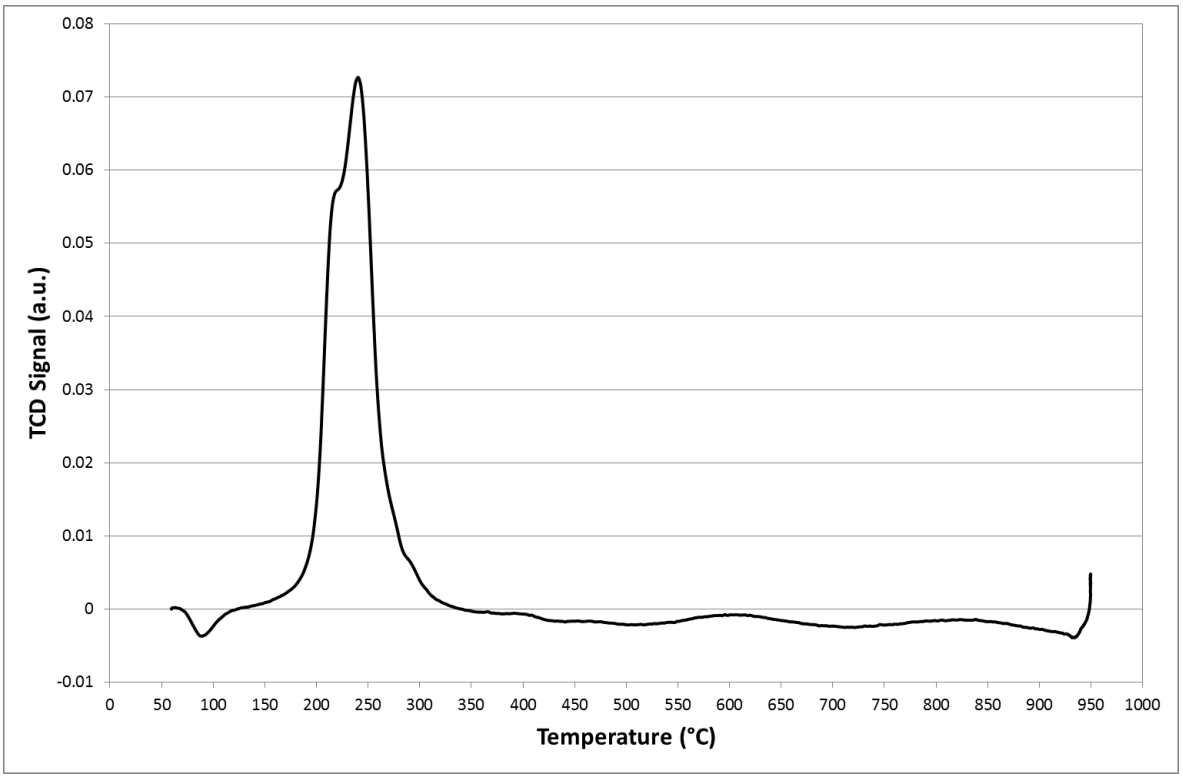

Figure B.2: The Temperature Programmed Reduction Profile of Supported Cobalt Catalyst

In all cases the reduction temperatures used were above the reaction temperature thus ensuring the nature of the supported metal was not altered thermally during the reaction.

APPENDIX C - DETAILED CATALYST LOADINGS CALCULATIONS AND DATA

In this section the detailed catalyst calculations are presented in table form for each of the four tested metals – this includes the acid and metal site numbers and calculations and weight percentage metal in the final combined catalyst formulation. Microsoft Excel ® Goal Seek was used to calculate the supported metal catalyst charges that were needed to get the desired M/A ratio. These are highlighted in Table C.1 to Table C.4.

Table C.1: Complete Detailed Platinum Catalyst Loading Calculations and Data

Supported Platinum Co-Catalyst and Zeolite Co-Catalyst Loading Calculations							
Desired Metal (Pt) / Acid site ratio	**site/site**	0.0004	0.0013	0.004	0.040	0.100	0.169
% Pt loading on inert support	**wt %**	5	5	5	5	5	5
Pt dispersion *	**%**	17.9	17.9	17.9	17.9	17.9	17.9
Pt crystalite size *	**nm**	6.3	6.3	6.3	6.3	6.3	6.3
Pt mass per gram SMC **	$g_{(platinum)}/g_{(SMC)}$ **	0.05	0.05	0.05	0.05	0.05	0.05
Pt moles per gram SMC	$mol_{(platinum)}/g_{(SMC)}$	0.00026	0.00026	0.00026	0.00026	0.00026	0.00026
Pt atoms per gram SMC	$atoms_{(platinum)}/g_{(SMC)}$	1.5E+20	1.5E+20	1.5E+20	1.5E+20	1.5E+20	1.5E+20
Number of Pt sites per gram SMC	$sites_{(platinum)}/g_{(SMC)}$	2.8E+19	2.8E+19	2.8E+19	2.8E+19	2.8E+19	2.8E+19
Calculations to determine required co-catalyst formultion loadings							
Required ratio of zeolite mass / SMC mass	$g_{(zeolite)}/g_{(SMC)}$	628.29	193.32	62.83	6.28	2.51	1.49
Desired mass of zeolite	$g_{(zeolite)}$	4.00	4.00	1.00	1.00	1.00	1.00
Desired mass of SMC	$g_{(SMC)}$	0.0064	0.0207	0.0159	0.1592	0.3980	0.6724
Desired total catalyst formulation mass	$g_{(combined\ formulation)}$	4.01	4.02	1.02	1.16	1.40	1.67
Supported platinum co-catalyt & zeolite (H-MFI-90) co-catalyst loadings USED							
Mass of zeolite co-catalyst used	$g_{(zeolite)}$	4.0006	4.0004	0.9998	0.9999	1.0005	0.9997
Mass of supported platinum co-catalyst used	$g_{(SMC)}$	0.0067	0.0214	0.0159	0.1596	0.3978	0.6722
Mass of total combined catalyst	$g_{(combined\ formulation)}$	4.01	4.02	1.02	1.16	1.40	1.67
Actual Acid Sites	$Site_{(Acid)}$	4.41E+20	4.41E+20	1.10E+20	1.10E+20	1.10E+20	1.10E+20
Actual Metal Sites	$Site_{(platinum)}$	1.85E+17	5.92E+17	4.40E+17	4.42E+18	1.10E+19	1.86E+19
Actually Metal / Acid site ratio		**0.0004**	**0.0013**	**0.004**	**0.040**	**0.100**	**0.169**
Mass of 'pure' platinum on combined catalyst	$g_{(platinum)}$	0.00034	0.00107	0.00080	0.00798	0.01989	0.03361
% Platinum in combined catalyst	**wt %**	0.01	0.03	0.08	0.69	1.42	2.01

* Pt Dispersion & Pt Crystalite size was determined using CO Chemisoption (350°C)

** SMC - Supported Metal Co-catalyst (Platinum)

Table C.2: Complete Detailed Palladium Catalyst Loading Calculations and Data

Supported Palladium Co-Catalyst and Zeolite Co-Catalyst Loading Calculations							
Desired Metal (Pd) / Acid site ratio	**site/site**	0.0004	0.0013	0.004	0.040	0.100	0.169
% Pd loading on inert support	**wt %**	5	5	5	5	5	5
Pd dispersion *	**%**	18.9	18.9	18.9	18.9	18.9	18.9
Pd crystalite size *	**nm**	5.9	5.9	5.9	5.9	5.9	5.9
Pd mass per gram SMC **	**$g_{(palladium)}/g_{(SMC)}$ ****	0.05	0.05	0.05	0.05	0.05	0.05
Pd moles per gram SMC	**$mol_{(palladium)}/g_{(SMC)}$**	0.00047	0.00047	0.00047	0.00047	0.00047	0.00047
Pd atoms per gram SMC	**$atoms_{(palladium)}/g_{(SMC)}$**	2.8E+20	2.8E+20	2.8E+20	2.8E+20	2.8E+20	2.8E+20
Number of Pd sites per gram SMC	**$sites_{(palladium)}/g_{(SMC)}$**	5.3E+19	5.3E+19	5.3E+19	5.3E+19	5.3E+19	5.3E+19
Calculations to determine required co-catalyst formultion loadings							
Required ratio of zeolite mass / SMC mass	**$g_{(zeolite)}/g_{(SMC)}$**	1211.77	372.85	121.18	12.12	4.85	2.87
Desired mass of zeolite	**$g_{(zeolite)}$**	4.00	4.00	2.00	1.00	1.00	1.00
Desired mass of SMC	**$g_{(SMC)}$**	0.0033	0.0107	0.0165	0.0825	0.2063	0.3487
Desired total catalyst formulation mass	**$g_{(combined\ formulation)}$**	4.00	4.01	2.02	1.08	1.21	1.35
Supported palladium co-catalyt & zeolite (H-MFI-90) co-catalyst loadings USED							
Mass of zeolite co-catalyst used	**$g_{(zeolite)}$**	4.0004	4.0009	2.0003	1.0000	0.9995	1.0001
Mass of supported palladium co-catalyst used	**$g_{(SMC)}$**	0.0030	0.0107	0.0169	0.0831	0.2067	0.3490
Mass of total combined catalyst	**$g_{(combined\ formulation)}$**	4.00	4.01	2.02	1.08	1.21	1.35
Actual Acid Sites	**$Site_{(Acid)}$**	4.41E+20	4.41E+20	2.20E+20	1.10E+20	1.10E+20	1.10E+20
Actual Metal Sites	**$Site_{(palladium)}$**	1.60E+17	5.71E+17	9.02E+17	4.44E+18	1.10E+19	1.86E+19
Actually Metal / Acid site ratio		**0.0004**	**0.0013**	**0.004**	**0.040**	**0.100**	**0.169**
Mass of 'pure' palladium on combined catalyst	**$g_{(palladium)}$**	0.00015	0.00054	0.00085	0.00416	0.01034	0.01745
% Palladium in combined catalyst	**wt %**	0.00	0.01	0.04	0.38	0.86	1.29

* Pd Dispersion & Pd Crystalite size was determined using CO Chemisoption (350°C)

** SMC - Supported Metal Co-catalyst (Palladium)

Table C.3: Complete Detailed Nickel Catalyst Loading Calculations and Data

Supported Nickel Co-Catalyst and Zeolite Co-Catalyst Loading Calculations					
Desired Metal (Ni) / Acid site ratio	**site/site**	0.0040	0.0400	0.100	0.169
% Ni loading on inert support	**wt %**	5	5	5	5
Ni dispersion *	**%**	15.0	15.0	15.0	15.0
Ni crystalite size *	**nm**	6.7	6.7	6.7	6.7
Ni mass per gram SMC **	**$g_{(nickel)}/g_{(SMC)}$ ****	0.05	0.05	0.05	0.05
Ni moles per gram SMC	**$mol_{(nickel)}/g_{(SMC)}$**	0.00085	0.00085	0.00085	0.00085
Ni atoms per gram SMC	**$atoms_{(nickel)}/g_{(SMC)}$**	5.1E+20	5.1E+20	5.1E+20	5.1E+20
Number of Ni sites per gram SMC	**$sites_{(nickel)}/g_{(SMC)}$**	7.7E+19	7.7E+19	7.7E+19	7.7E+19
Calculations to determine required co-catalyst formultion loadings					
Required ratio of zeolite mass / SMC mass	**$g_{(zeolite)}/g_{(SMC)}$**	174.87	17.49	6.99	4.14
Desired mass of zeolite	**$g_{(zeolite)}$**	4.00	2.00	2.00	2.00
Desired mass of SMC	**$g_{(SMC)}$**	0.0229	0.1144	0.2859	0.4832
Desired total catalyst formulation mass	**$g_{(combined\ formulation)}$**	4.02	2.11	2.29	2.48
Supported nickel co-catalyt & zeolite (H-MFI-90) co-catalyst loadings USED					
Mass of zeolite co-catalyst used	**$g_{(zeolite)}$**	4.0006	2.0005	2.0006	2.0001
Mass of supported nickel co-catalyst used	**$g_{(SMC)}$**	0.0232	0.1147	0.2860	0.4834
Mass of total combined catalyst	**$g_{(combined\ formulation)}$**	4.02	2.12	2.29	2.48
Actual Acid Sites	**$Site_{(acid)}$**	4.41E+20	2.20E+20	2.20E+20	2.20E+20
Actual Metal Sites	**$Site_{(nickel)}$**	1.79E+18	8.84E+18	2.20E+19	3.72E+19
Actually Metal / Acid site ratio		**0.0041**	**0.0401**	**0.100**	**0.169**
Mass of 'pure' nickel on combined catalyst	**$g_{(nickel)}$**	0.00116	0.00574	0.01430	0.02417
% Nickel in combined catalyst *	**wt % ***	0.03	0.27	0.63	0.97

* Ni Dispersion & Ni Crystalite size was determined using CO Chemisoption (450°C)

** SMC - Supported Metal Co-catalyst (Nickel)

*** Due to the very poor dispersion numbers for the supported cobalt co-catalyst, the wt % metal loading was kept the same as that of nickel (both being base metals)

As the cobalt dispersion numbers were significantly lower than those of the other metals (0.4% compared to >15%) it was not possible to use the same ratios as the resultant catalyst bed would have been too large to fit in the isothermal zone in the reactor tube (Section 4.2.2). It was decided to use the same percent metal in the combined catalyst as that of the nickel – the other base metal tested – so a possible standard could be set, even though this was not the ideal situation. This is highlighted in the last row in Table C.3 and Table C.4. Where possible, the highest cobalt loading (M/A = 0.0051) has been compared to the other metals loadings at a M/A of 0.004 (Section 5)

Table C.4: Complete Detailed Cobalt Catalyst Loading Calculations and Data

Supported Cobalt Co-Catalyst and Zeolite Co-Catalyst Loading Calculations					
Desired Metal (Co) / Acid site ratio	**site/site**	0.0040	0.0400	0.100	0.169
% Co loading on inert support	**wt %**	5	5	5	5
Co dispersion *	**%**	0.5	0.5	0.5	0.5
Co crystalite size *	**nm**	220.2	220.2	220.2	220.2
Co mass per gram SMC **	**$g_{(cobalt)}/g_{(SMC)}$ ****	0.05	0.05	0.05	0.05
Co moles per gram SMC	**$mol_{(cobalt)}/g_{(SMC)}$**	0.00085	0.00085	0.00085	0.00085
Co atoms per gram SMC	**$atoms_{(cobalt)}/g_{(SMC)}$**	5.1E+20	5.1E+20	5.1E+20	5.1E+20
Number of Co sites per gram SMC	**$sites_{(cobaltl)}/g_{(SMC)}$**	2.3E+18	2.3E+18	2.3E+18	2.3E+18
Calculations to determine required co-catalyst formultion loadings					
Desired mass of zeolite	**$g_{(zeolite)}$**	4.00	4.00	4.00	4.00
Desired mass of SMC	**$g_{(SMC)}$**	0.0232	0.2294	0.5720	0.9668
Desired total catalyst formulation mass	**$g_{(combined\ formulation)}$**	4.02	4.23	4.57	4.97
Supported cobaltco-catalyt & zeolite (H-MFI-90) co-catalyst loadings USED					
Mass of zeolite co-catalyst used	**$g_{(zeolite)}$**	4.0005	4.0001	4.0007	4.0005
Mass of supported cobalt co-catalyst used	**$g_{(SMC)}$**	0.0262	0.2302	0.5726	0.9666
Mass of total combined catalyst	**$g_{(combined\ formulation)}$**	4.03	4.23	4.57	4.97
Actual Acid Sites	**$Site_{(acid)}$**	4.41E+20	4.41E+20	4.41E+20	4.41E+20
Actual Metal Sites	**$Site_{(cobalt)}$**	6.08E+16	5.34E+17	1.33E+18	2.24E+18
Actually Metal / Acid site ratio		**0.0001**	**0.0012**	**0.003**	**0.005**
Mass of 'pure' cobaltl on combined catalyst	**$g_{(nickel)}$**	0.00131	0.01151	0.02863	0.04833
% Cobalt in combined catalyst ***	**wt % *****	0.03	0.27	0.63	0.97

* Co Dispersion & Co Crystalite size was determined using CO Chemisoption (250°C)
** SMC - Supported Metal Co-catalyst (Cobalt)
*** Due to the very poor dispersion numbers for the supported cobalt co-catalyst, the wt % metal loading was kept the same as that of nickel (both being base metals)

APPENDIX D - RAW GC DATA AND DATA WORKUP

Table D.1and Table D.2 show a sample of the raw data that was obtained from the GC. Most of the component chromatographic peaks were identified using combined Gas Chromatograph Mass Spectrometry, however not all the peaks (particularly the long chained molecules) could be identified. These peaks have been given „names" based on their retention time and compounds eluting at similar retention times - in some cases they have been allocated a generic title. It has been possible to identify all the normal (straight chain) and lower molecular weight products. Appendix E presents the worked up data for all the hydrocracking experiments.

Table D.1: Sample GC Data from the second GC analysis with Supported Platinum / H-MFI-90

(Supported Metal Mass = 0.6722g, Zeolite Mass = 0.9997g, M/A ratio = 0.169, T = 225°C, P = 20 Bar)

Index	Name	Time	Height	Area
		[Min]	[uV]	[uV.Min]
64	methane	4.36	115.9	7.9
66	ethane	4.48	83.6	4
72	propylene	4.9	12.3	0.1
73	n-propane	4.95	22789.1	589.5
77	isobutane	5.77	16966.6	520.3
0	isobutene	6.28	N.D.	N.D.
80	n-butane	6.47	32281.1	1002.4
82	t-2-butene	6.75	5.5	0.1
85	c-2-butene	7.02	5.3	0
87	3-me-1-butene	8.03	13	0
88	2-me-butane	8.49	29476.4	1032.9
92	1-pentene	8.94	8.2	0
0	2-me-1-butene	9.2	N.D.	N.D.
93	n-pentane	9.29	26561.7	859.9
96	t-2-pentene	9.45	18.2	0.2
0	c-2-pentene	9.81	N.D.	N.D.
97	2-me-2-butene	9.94	7.2	0
99	2,2-dime-butane	10.39	106.5	4.1
108	3-me-1-pentene	10.99	8.3	0
109	4-me-1-pentene	11.13	4.1	0
113	2,3-dime-butane	11.26	3066.5	101.7
114	2-me-pentane	11.38	16633.9	520.9
121	3-me-pentane	11.78	11342	359.6
123	1-hexene	11.97	14.7	0.3
127	n-hexane	12.26	26945.7	785.1
128	t-2-hexene	12.44	16.3	0.2
129	2-me-2-pentene	12.46	4.2	0.1
0	3-me-2-pentene, (Z)-	12.57	N.D.	N.D.
130	c-2-hexene	12.74	3.6	0
0	2-pentene, 3-methyl-, (E)-	12.83	N.D.	N.D.
132	2,2-dime-pentane	12.93	327.3	10.1
135	2,4-dime-pentane	13.08	2237.9	66.5
140	1-hexene, 3-methyl-	13.39	6.4	0
141	1-hexene, 5-methyl-	13.53	3.8	0.2
142	1-hexene, 4-methyl-	13.73	50.6	1.7
143	4-me-t-2-hexene	13.83	5.1	0.1
0	4-me-c-2-hexene	13.86	N.D.	N.D.
144	2-me-hexane	14.02	12040	337.1
145	2,3-dime-pentane	14.07	3453	100.7
147	3-me-hexane	14.23	11812.8	331.3
148	X1	14.36	6.8	0
149	2-me-1-hexene	14.42	58.9	1.8
150	1-heptene	14.49	774.8	22.4
151	XXX	14.55	64.1	2.4
152	3-me-t-3-hexene	14.72	11.7	0.1
153	3-me-c-3-hexene	14.73	16.3	0.1
154	n-heptane	14.8	15074.3	410.3
155	2-hexene, 3-methyl-, (E)-	14.91	7.9	0
0	X2	14.98	N.D.	N.D.
156	2-hexene, 3-methyl-, (Z)-	15.05	8.3	0.1
0	2-pentene, 4,4-dimethyl-	15.15	N.D.	N.D.
157	2,2,4-trime-pentane	15.33	425.5	14.1

Table D.2: Sample GC Data (Continued from Table D.1)

Index	Name	Time [Min]	Height [uV]	Area [uV.Min]
160	2,5-dime-hexane	15.54	2302.2	62.4
161	2,4-dime-hexane	15.59	3076	87.2
162	X3	15.78	186.2	6.3
164	X4	15.86	13	0.2
167	X5	15.93	50.5	1.8
168	X6	15.98	81	2.2
172	2,3-dime-hexane	16.18	1416.7	39.7
174	2-me-heptane	16.28	6583.6	178.7
175	4-me-heptane	16.32	2543.2	66.2
176	2-methyl-3-ethyl-pentane ?	16.39	772.4	24
177	3-me-heptane	16.45	6454.7	202.8
0	3-ethyl-hexane	16.5	N.D.	N.D.
179	X	16.63	145.7	4.2
180	1-hexene, 5,5-dimethyl-	16.69	129	3.8
181	3-ethyl-2-hexene	16.79	74.9	2.4
183	XX	16.87	68	2
185	n-octane	16.98	5916.6	159.6
186	2-hexene, 2,3-dimethyl-	17.08	20	0.7
187	1,4-pentadiene, 2,3,3-trimethyl-	17.16	76	2.5
0	2-hexene, 3,5-dimethyl-	17.11	N.D.	N.D.
190	cyclohexane, 1,3-dimethyl, trans-	17.36	177	4.8
191	2,3,3-trime-hexane	17.41	249.6	6.7
192	2,3,4-trime-hexane	17.48	1143.7	31.2
194	2,6-dime-heptane	17.61	1065.4	32.7
196	2,5-dime-heptane	17.75	2541.4	91.8
197	3,5-dime-heptane	17.82	163.5	5
0	X7	17.84	N.D.	N.D.
198	X8	17.91	25.7	1.1
199	X9	17.95	36.4	1.2
200	X10	18.01	181.1	5.8
201	X11	18.07	63	2.1
202	2.3-dime-heptane	18.16	763.4	21.9
203	2-me-octane	18.23	787.3	32.6
204	4-me-octane	18.29	4653.2	156.5
205	3-heptene, 2,6-dimethyl-	18.35	21	0.5
206	3-me-octane	18.43	3297.2	96.4
207	X12	18.53	71.6	2
209	X13	18.66	11.5	0
211	3-heptene, 4-ethyl-	18.75	155.9	6.2
212	X14	18.83	167.3	4.7
214	n-nonane	18.94	2939.5	78.9
215	X15	19	63.9	2.8
216	X16	19.09	22.8	0.8
217	X17	19.23	304.3	12.2
218	2,4,6-trime-heptane	19.32	920	26.9
220	2,5-dime-octane	19.44	1335.2	44.3
222	2,7-dime-octane	19.56	165	4.1
223	2,6-dime-octane	19.61	1119.8	34.1
225	3,6-dime-octane	19.73	580.6	17.8
226	X18	19.79	180.5	7
228	X19	19.88	78.5	2.1
230	4-ethyl-octane	20	1012	30.7
231	5-me-nonane	20.06	712.5	17.4
232	2-me-nonane	20.1	1380.3	38
233	4-me-nonane	20.14	1491.4	41
234	3-ethyl-octane	20.22	246.3	7.1
235	3-me-nonane	20.27	1490.5	41
237	X20	20.41	177.1	6.4
238	X21	20.49	33.6	0.5
239	X22	20.61	132.6	4.3
242	n-decane	20.77	1363.2	38.9
243	X23	20.83	67.2	2.4
244	X24	20.92	155.5	6.6
247	dime-nonane, a	21.08	536.2	20.3
249	dime-nonane, b	21.17	653.6	21.7
0	2,5-dime-nonane	21.19	N.D.	N.D.
250	2,6-dime-nonane	21.23	483.6	18.8
251	3,7-dime-nonane	21.34	500.4	23.4
252	dime-nonane, c	21.45	554.2	16.7
253	dime-nonane, d	21.5	182.9	5.6
254	dime-nonane, e	21.55	317.6	12.6
256	X25	21.65	31.1	0.6
257	X26	21.71	89.9	2.4
258	X27	21.76	163.8	5.3
259	X42	21.85	552.1	26.2
0	5-me-decane	21.87	N.D.	N.D.
260	4-me-decane	21.91	553	16.8
261	2-me-decane	21.97	561.9	17.1
262	X31	22.04	125	3.7
263	3-me-decane	22.11	648.9	20
265	X32	22.21	62.5	2
266	X33	22.28	84.5	3.8
267	X34	22.32	130.1	4.9
268	X35	22.39	49.1	2
271	X36	22.55	84.6	3.9
272	n-undecane	22.63	490.8	16.9
278	C12, dibranched, a	22.92	148.1	5.2
279	C12, dibranched, b	23	403.3	26.1
280	C12, dibranched, c	23.13	330.1	13.4
281	C12, dibranched, d	23.21	270.8	9.7
282	C12, dibranched, e	23.34	227.7	8.4
283	C12, dibranched, f	23.41	93.7	4.1
284	C12, dibranched, g	23.48	121.7	4.2
285	C12, dibranched, h	23.53	72.6	2.2
286	C12, dibranched, i	23.57	13.6	0.4
287	C12, dibranched, j	23.63	62.6	2.1
288	6-me-undecane	23.73	262.5	12.6
0	5-me-undecane	23.75	N.D.	N.D.
289	4-me-undecane	23.82	209.5	7.5
290	2-me-undecane	23.9	222.4	7.8
291	X28	23.96	50.4	2.4
292	3-me-undecane	24.04	265.4	9.6
294	X29	24.17	62.3	3.4
296	X30	24.29	53.2	3.1
300	n-dodecane	24.6	98.7	4.5
303	C13, dibranched, a	24.82	56.7	2
304	C13, dibranched, b	24.88	65.2	3.4
305	C13, dibranched, c	24.93	116.6	5.4
306	C13, dibranched, d	25	104.5	4.2
0	C13, dibranched, e	25.08	N.D.	N.D.
307	C13, dibranched, f	25.1	123.8	6.6
308	C13, dibranched, g	25.2	20.6	1.1
309	C13, dibranched, h	25.25	73	2.9
310	C13, dibranched, i	25.35	49.5	1.8
312	C13, dibranched, j	25.43	35.7	1.4
313	C13, dibranched, k	25.49	49.3	2
316	6-me-dodecane	25.69	46.3	1.2
0	5-me-dodecane	25.76	N.D.	N.D.
318	4-me-dodecane	25.84	65.8	2.8
319	2-me-dodecane	25.94	68.6	2.9
321	3-me-dodecane	26.09	72.9	2.6
331	n-tridecane	26.65	1.7	0.1
346	6-me-tridecane	27.78	8.7	0.2
347	5-me-tridecane	27.85	12.7	0.5
350	4-me-tridecane	27.96	11.1	0.3
351	2-me-tridecane	28.04	4.5	0
352	3-me-tridecane	28.18	8.4	0
355	n-tetradecane	28.91	12.2	0.1
366	7-me-tetradecane	29.92	31.6	0.8
0	6-me-tetradecane	29.96	N.D.	N.D.
367	5-me-tetradecane	30.03	52.5	2.8
369	4-me-tetradecane	30.15	52.5	3.4
370	2-me-tetradecane	30.26	35.7	1.6
372	3-me-tetradecane	30.42	15.3	0.6
380	n-pentadecane	31	37	1
381	C16, dibranched, a	31.1	55	2.5
382	C16, dibranched, b	31.21	27.8	0.5
383	C16, dibranched, c	31.28	125.9	7
384	C16, dibranched, d	31.39	42.4	1.7
385	C16, dibranched, e	31.45	33.7	1.2
0	C16, dibranched, f	31.47	N.D.	N.D.
0	C16, dibranched, g	31.57	N.D.	N.D.
386	C16, dibranched, h	31.59	31.7	1.4
387	C16, dibranched, i	31.68	15.5	0.7
0	C16, dibranched, j	31.74	N.D.	N.D.
388	C16, dibranched, k	31.84	22.1	0.7
390	7-me-pentadecane	32.08	30.1	1
391	6-me-pentadecane	32.12	19.4	0.7
392	5-me-pentadecane	32.2	27.9	1
393	4-me-pentadecane	32.33	25.8	0.9
394	2-me-pentadecane	32.44	21.9	0.7
397	3-me-pentadecane	32.61	29.8	1.3
399	X37	32.83	7.3	0
400	X38	32.85	13.1	0.1
0	X39	32.94	N.D.	N.D.
0	X40	33	N.D.	N.D.
401	X41	33.06	12.6	0.1
403	n-hexadecane	33.21	1081	43.6
Total	-	-	313728	9551.2

GC data for a given set of experiments, i.e. when all four reactors were loaded and running, was recorded in a single Microsoft Excel document with each GC analysis on an individual sheet (as shown in Table D.1). In order to process this data in a more efficient manner a number of macros were written to assist in data management and calculations.

Firstly, data from the different sheets within the Excel document are combined into one sheet containing all the data. This macro is presented below:

```
Sub retrieveFIDdata()

   Set newbook = Workbooks.Add
      newbook = InputBox("Please enter a filename",
"Create a new workbook", _
      "C:\Documents and Settings\admin\My
Documents\UCT\Macro\")

   ActiveWorkbook.SaveAs newbook

   Workbooks(2).Worksheets(1).Activate

   lastrow = Range("A3").End(xlDown).Row

   MsgBox lastrow
   For x = 1 To Workbooks(2).Worksheets.Count

      For y = 1 To lastrow - 2
      Workbooks(3).Worksheets("sheet1").Activate
      Range("A3").Select
      ActiveCell.Offset(y - 1, x + 2) =
Workbooks(2).Worksheets(x).Cells(y + 2, 5).Value

      Next
   Next
   For y = 1 To lastrow - 2
      Workbooks(3).Worksheets("sheet1").Activate
      Range("A3").Select
      ActiveCell.Offset(y - 1, 0) =
Workbooks(2).Worksheets(1).Cells(y + 2, 2).Value
   Next
   Sheets.Add
   Sheets("Sheet4").Move After:=Sheets(4)
   Sheets.Add
   Sheets("Sheet5").Move After:=Sheets(5)
   Sheets.Add
   Sheets("Sheet6").Move After:=Sheets(6)
   Sheets.Add
   Sheets("Sheet7").Move After:=Sheets(7)
   Sheets.Add
   Sheets("Sheet8").Move After:=Sheets(8)
   Sheets.Add
   Sheets("Sheet9").Move After:=Sheets(9)
   Sheets.Add
   Sheets("Sheet10").Move After:=Sheets(10)
   Workbooks(3).Worksheets("sheet1").Select
   Columns("A:A").ColumnWidth = 35.86
   Sheets("Sheet1").Name = "PeakArea"

End Sub
```

The second step removes all cells that contained N.D. (No Data) from the sheet – the chromatography data system inserts N.D. values where no peaks are measures for a specific retention time. These are replaced with zeros so they can be processed as numbers. This macro is presented below:

```
Sub MissingPeaks()

   Columns("A:A").Select
   Selection.Copy
   Sheets("Sheet2").Select
   Columns("A:A").Select
   ActiveSheet.Paste
   Columns("A:A").ColumnWidth = 35.86
   Sheets("PeakArea").Select

   lastrow = Range("D3").End(xlDown).Row
   lastcolumn = Range("D3").End(xlToRight).Column

   MsgBox lastrow
   MsgBox lastcolumn

   For x = 0 To lastcolumn
      For y = 0 To lastrow
      Range("D3").Activate
      If ActiveCell.Offset(y, x).Value = "N.D." Then
      ActiveCell.Offset(y, x).Value = 0
      End If
      Next
   Next
   Sheets("Sheet2").Name = "CarbonPercentage"
End Sub
```

Once all the data is in the same sheet and in number form, it is split into different documents depending on which reactor the raw data came from, one for each reactor. The macro for splitting the data into four files is presented below:

```
Sub splitdatafrom4reactors()

   Dim reactor As Double
   reactor = 1
   For reactor = 1 To 4

      Set newbook = Workbooks.Add
         newbook = InputBox("Please enter a filename",
"Create a new workbook", _
         "C:\Documents and Settings\admin\My
Documents\UCT\Macro\")

      ActiveWorkbook.SaveAs newbook


      Workbooks(2).Worksheets("PeakArea").Activate

      lastrow = Range("A3").End(xlDown).Row
      lastcolumn = Range("D3").End(xlToRight).Column
      Dim col As Double
      col = 3
      MsgBox lastrow
      MsgBox lastcolumn

      For x = 1 To lastcolumn - 3
         For y = 1 To lastrow - 2
         Workbooks(3).Worksheets("sheet1").Activate
         Range("A3").Select
         ActiveCell.Offset(y - 1, col) =
Workbooks(2).Worksheets("PeakArea").Cells(y + 2, x + 2
+ reactor).Value
         Next
         x = x + 3
         col = col + 1
      Next

      For y = 1 To lastrow - 2
         Workbooks(3).Worksheets("sheet1").Activate
         Range("A3").Select
         ActiveCell.Offset(y - 1, 0) =
Workbooks(2).Worksheets("PeakArea").Cells(y + 2,
1).Value
      Next
      Columns("A:A").ColumnWidth = 35.86
      Sheets("Sheet1").Name = "PeakArea"
      ActiveWorkbook.Close

   Next

End Sub
```

With the data in the respective files for each reactor (i.e. each experiment) the main calculations are performed on the data, namely determination of conversions and selectivities. This macro is presented below:

```
Sub ConversionandSelectivity()

   MsgBox ("Make sure to assign the carbon number to
every peak in column B!")
   Sheets("CarbonPercentage").Name =
"ConversionandSelectivity"
   Columns("A:A").ColumnWidth = 35.86
   Worksheets("PeakArea").Select
   Range("D3").Activate
   lastrow = Range("D3").End(xlDown).Row
   lastcolumn = Range("D3").End(xlToRight).Column
   Sheets("PeakArea").Select

   Dim total As Double
   Dim sumproducts As Double
   Dim conversion As Double

   For x = 4 To lastcolumn
      total =
Application.WorksheetFunction.sum(Range(Cells(3, x),
Cells(lastrow, x)))
      sumproducts =
Application.WorksheetFunction.sum(Range(Cells(3, x),
Cells(lastrow - 1, x)))
      conversion = (sumproducts / total) * 100
      Sheets("ConversionandSelectivity").Cells(2, x).Value
= conversion
   Next x

   Sheets("ConversionandSelectivity").Select
   Range("D3").Activate
   ActiveCell.FormulaR1C1 = "=PeakArea!RC"
   'Selectivities on carbon basis
   'Molar selectivities
   ActiveCell.FormulaR1C1 =
"=PeakArea!RC/PeakArea!RC2"
   Range("D3").Select
   Selection.Copy
   Range(Cells(3, 4), Cells(lastrow - 1, lastcolumn)).Select
   ActiveSheet.Paste
   Selection.NumberFormat = "0.00"

   Dim testarray() As Double

   lastrow = Range("D3").End(xlDown).Row
   lastcolumn = Range("D3").End(xlToRight).Column
   ncellsincolumn = lastrow - 2
   ncellsinrow = lastcolumn - 3

   ReDim testarray(ncellsincolumn, ncellsinrow)

   For x = 4 To lastcolumn
      For y = 3 To lastrow
      testarray(y - 2, x - 3) = Cells(y, x)
      Next y
   Next x

   For x = 4 To lastcolumn
      sumcolumn =
Application.WorksheetFunction.sum(Range(Cells(3, x),
Cells(lastrow, x)))
      For y = 3 To lastrow
      testarray(y - 2, x - 3) = (testarray(y - 2, x - 3) /
sumcolumn) * 100
      Cells(y, x).Value = testarray(y - 2, x - 3)
      Next
   Next
End Sub
```

Finally, the last step is to sum the normal and isomer compounds for each carbon number so the carbon number distributions can be plotted. The macro to do this is presented below:

```
Sub Hydrocracking_lumped_E_F()
'
' Hydrocracking_lumped_E_F Macro
' Macro recorded 7/11/2009 by
'
    Range("D2").Select
    ActiveCell.FormulaR1C1 =
"=ConversionandSelectivity!R[1]C"
    Range("D3").Select
    ActiveCell.FormulaR1C1 =
"=ConversionandSelectivity!R[1]C"
    Range("D4").Select
    ActiveCell.FormulaR1C1 =
"=SUM(ConversionandSelectivity!R[1]C:R[2]C)"
    Range("D5").Select
    ActiveCell.FormulaR1C1 = _
        "=SUM(ConversionandSelectivity!R[2]C:R[6]C)-
ConversionandSelectivity!R[4]C"
    Range("D6").Select
    ActiveCell.FormulaR1C1 =
"=ConversionandSelectivity!R[3]C"
    Range("D7").Select
    ActiveCell.FormulaR1C1 = _
        "=SUM(ConversionandSelectivity!R[5]C:R[12]C)-
ConversionandSelectivity!R[9]C"
    Range("D8").Select
    ActiveCell.FormulaR1C1 =
"=ConversionandSelectivity!R[8]C"
    Range("D9").Select
    ActiveCell.FormulaR1C1 = _
        "=SUM(ConversionandSelectivity!R[11]C:R[23]C)-
ConversionandSelectivity!R[18]C"
    Range("D10").Select
    ActiveCell.FormulaR1C1 =
"=ConversionandSelectivity!R[17]C"
    Range("D11").Select
    ActiveCell.FormulaR1C1 = _
        "=SUM(ConversionandSelectivity!R[22]C:R[42]C)-
ConversionandSelectivity!R[38]C"
    Range("D12").Select
    ActiveCell.FormulaR1C1 =
"=ConversionandSelectivity!R[37]C"
    Range("D13").Select
    ActiveCell.FormulaR1C1 = _
        "=SUM(ConversionandSelectivity!R[41]C:R[62]C)-
ConversionandSelectivity!R[58]C"
    Range("D14").Select
    ActiveCell.FormulaR1C1 =
"=ConversionandSelectivity!R[57]C"
    Range("D15").Select
    ActiveCell.FormulaR1C1 =
"=SUM(ConversionandSelectivity!R[61]C:R[79]C)"
    Range("D16").Select
    ActiveCell.FormulaR1C1 =
"=ConversionandSelectivity!R[79]C"
    Range("D17").Select
    ActiveCell.FormulaR1C1 =
"=SUM(ConversionandSelectivity!R[79]C:R[97]C)"
    Range("D18").Select
    ActiveCell.FormulaR1C1 =
"=ConversionandSelectivity!R[97]C"
    Range("D19").Select
    ActiveCell.FormulaR1C1 =
"=SUM(ConversionandSelectivity!R[97]C:R[120]C)"
    Range("D20").Select
    ActiveCell.FormulaR1C1 =
"=ConversionandSelectivity!R[120]C"
    Range("D21").Select
    ActiveCell.FormulaR1C1 =
"=SUM(ConversionandSelectivity!R[120]C:R[137]C)"
    Range("D22").Select
    ActiveCell.FormulaR1C1 =
"=ConversionandSelectivity!R[137]C"
    Range("D23").Select
    ActiveCell.FormulaR1C1 =
"=SUM(ConversionandSelectivity!R[137]C:R[152]C)"
    Range("D24").Select
    ActiveCell.FormulaR1C1 =
"=ConversionandSelectivity!R[152]C"
    Range("D25").Select
    ActiveCell.FormulaR1C1 =
"=SUM(ConversionandSelectivity!R[152]C:R[156]C)"
    Range("D26").Select
    ActiveCell.FormulaR1C1 =
"=ConversionandSelectivity!R[156]C"
    Range("D27").Select
    ActiveCell.FormulaR1C1 =
"=SUM(ConversionandSelectivity!R[156]C:R[161]C)"
    Range("D28").Select
    ActiveCell.FormulaR1C1 =
"=ConversionandSelectivity!R[161]C"
    Range("D29").Select
    ActiveCell.FormulaR1C1 =
"=SUM(ConversionandSelectivity!R[161]C:R[182]C)"
    Range("D33").Select
    ActiveCell.FormulaR1C1 = "=SUM(R[-31]C:R[-4]C)"
    Range("D34").Select
End Sub
```

APPENDIX E - CONVERSION AND SELECTIVITY DATA

This section presents a full set of conversion and selectivity data for all the tested metals and loadings. As a number of points are averaged to determine the conversion and selectivity data, it is possible to determine the statistical error in the data – these error values are also presented.

Table E.1: Detailed Conversion, Error and Rate Data for all Supported Platinum Loadings

Conversion Data (%)										
Reactor Number	WHSV ($g_{feed}/g_{acid.cat}.hr$)									Metal/Acid Ratio
	0.11	0.23	0.34	0.46	0.69	0.92	1.38	1.84	2.76	
1	97.64	37.39	29.61	26.94	15.64					0.0004
4	99.87	52.27	40.86	31.31	20.53					0.0013
2				92.38		32.38	17.32			0.0040
3						95.62	45.22	34.02	21.52	0.0401
1						95.79	61.25	44.95	25.88	0.0999
4						95.06	65.14	46.87	26.04	0.1690

Statistical Analysis - Percentage Error Values (for each conversion) (% error)										
Reactor Number	WHSV ($g_{feed}/g_{acid.cat}.hr$)									Metal/Acid Ratio
	0.11	0.23	0.34	0.46	0.69	0.92	1.38	1.84	2.76	
1	0.90	0.40	1.30	0.64	0.50					0.0004
4	0.33	0.68	1.39	1.94	2.74					0.0013
2				2.16		2.69	1.59			0.0040
3						1.20	2.76	0.71	1.07	0.0401
1						1.75	0.82	0.99	1.51	0.0999
4						1.09	3.98	2.68	1.86	0.1690

Rate Data (g_{feed} converted/$g_{acid.cat}.hr$)										
Reactor Number	WHSV ($g_{feed}/g_{acid.cat}.hr$)									Metal/Acid Ratio
	0.11	0.23	0.34	0.46	0.69	0.92	1.38	1.84	2.76	
1	11.22	8.59	10.21	12.38	10.78					0.0004
4	11.47	12.01	14.08	14.39	14.15					0.0013
2				42.46		29.76	23.89			0.0040
3						87.90	62.35	62.55	59.35	0.0401
1						88.05	84.45	82.64	71.36	0.0999
4						87.38	89.81	86.17	71.79	0.1690

Table E.2: Detailed Selectivity Data for the Three Lowest Platinum Metal Site / Acid Site Ratios

	Platinum metal/acid: 0.0004					Platinum metal/acid: 0.0013					Platinum metal/acid: 0,004		
Acid WHSV ($g_{feed}/g_{acid.cat}.hr$)	0.11	0.23	0.34	0.46	0.69	0.11	0.23	0.34	0.46	0.69	0.46	0.92	1.38
Metal WHSV ($g_{feed}/g_{metal.cat}.hr$)	69	137	206	274	412	21	43	64	86	129	29	58	87
Conversion (%)	97.64	37.39	29.61	26.94	15.64	99.87	52.27	40.86	31.31	20.53	92.38	32.70	17.40
C1	0.30	0.55	1.79	1.67	1.64	0.06	0.41	1.72	1.96	1.92	0.96	0.77	0.63
C2	0.25	0.16	0.10	0.10	0.00	1.05	0.16	0.11	0.07	0.00	0.13	0.02	0.00
C3	8.16	7.09	6.93	6.87	7.33	11.03	7.43	7.35	7.08	7.32	8.26	7.78	8.86
iso-C4	9.01	8.80	8.92	8.88	9.56	11.48	8.42	8.57	8.02	8.39	8.42	8.53	9.30
n-C4	12.81	11.37	11.01	11.00	11.19	15.60	12.09	11.77	10.87	11.28	12.51	12.35	13.35
iso-C5	11.04	10.93	11.07	11.10	11.96	12.87	11.81	11.76	10.45	11.64	11.75	11.88	12.57
n-C5	11.19	10.94	10.89	11.07	11.01	11.74	11.17	10.91	10.11	10.82	10.38	10.74	10.76
iso-C6	9.30	9.09	8.85	8.53	8.70	9.79	9.83	9.49	9.19	9.60	9.96	9.67	9.50
n-C6	7.97	8.37	8.50	8.72	8.68	6.32	8.33	8.07	8.37	8.69	8.01	8.07	7.98
iso-C7	7.34	7.75	7.79	7.73	7.94	6.78	7.67	7.47	8.07	7.95	8.02	7.58	7.56
n-C7	3.45	3.97	3.98	4.03	3.97	2.10	3.67	3.59	4.13	3.93	3.76	3.74	3.71
iso-C8	5.84	5.78	5.46	5.23	4.93	4.86	5.77	5.62	6.23	5.40	6.10	5.64	4.82
n-C8	1.59	1.87	1.88	1.93	1.89	0.55	1.55	1.58	1.83	1.65	1.69	1.57	1.54
iso-C9	4.13	4.00	3.70	3.71	3.16	2.89	3.68	3.69	4.17	3.48	3.88	3.65	2.87
n-C9	0.88	1.11	1.07	1.10	1.07	0.13	0.92	0.94	1.09	0.99	0.85	0.89	0.85
iso-C10	2.67	2.80	2.69	2.57	1.93	1.58	2.70	2.58	2.74	2.26	2.31	2.47	1.86
n-C10	0.55	0.83	0.83	0.88	0.89	0.02	0.61	0.70	0.80	0.78	0.45	0.66	0.69
iso-C11	1.75	1.91	1.67	1.70	0.98	0.79	1.67	1.73	1.97	1.29	1.26	1.68	1.04
n-C11	0.16	0.51	0.53	0.59	0.59	0.02	0.38	0.46	0.53	0.52	0.18	0.41	0.45
iso-C12	0.93	0.94	0.89	0.89	0.61	0.27	0.84	0.85	0.95	0.66	0.55	0.75	0.44
n-C12	0.03	0.25	0.27	0.31	0.31	0.00	0.12	0.22	0.27	0.27	0.06	0.19	0.23
iso-C13	0.29	0.20	0.18	0.19	0.05	0.04	0.21	0.15	0.19	0.07	0.19	0.14	0.02
n-C13	0.02	0.11	0.12	0.14	0.14	0.00	0.09	0.09	0.12	0.13	0.02	0.08	0.09
iso-C14	0.05	0.04	0.05	0.05	0.00	0.00	0.02	0.02	0.04	0.01	0.03	0.00	0.00
n-C14	0.01	0.04	0.04	0.05	0.00	0.00	0.02	0.03	0.04	0.01	0.00	0.01	0.00
iso-C15	0.05	0.00	0.00	0.00	0.00	0.01	0.02	0.00	0.00	0.00	0.03	0.00	0.00
n-C15	0.02	0.02	0.03	0.04	0.05	0.00	0.02	0.04	0.05	0.08	0.00	0.02	0.03
iso-C16	0.22	0.57	0.74	0.92	1.41	0.00	0.39	0.50	0.68	0.86	0.23	0.71	0.85
n-C16													
n- / iso- C4	1.42	1.29	1.24	1.24	1.17	1.36	1.44	1.37	1.35	1.37	1.49	1.45	1.44
n- / iso- C5	1.01	1.00	0.98	1.04	0.92	0.91	0.95	0.64	0.97	0.94	0.88	0.90	0.86
n- / iso- C6	0.86	0.92	0.96	1.02	1.00	0.65	0.85	0.88	0.91	0.90	0.80	0.83	0.84
n- / iso- C7	0.47	0.51	0.51	0.52	0.50	0.31	0.48	0.48	0.51	0.49	0.47	0.49	0.49
C3 - Parafins	10.99	7.24	7.05	6.80	6.94	7.99	6.74	6.49	6.37	6.62	8.10	7.56	8.48
C3 - Olefins	0.04	0.19	0.30	0.28	0.38	0.17	0.35	0.44	0.50	0.71	0.15	0.22	0.38
C4 - Parafins	26.98	19.62	19.07	17.72	18.00	21.05	18.58	17.92	17.53	17.46	20.37	19.91	21.04
C4 - Olefins	0.10	0.90	1.27	1.17	1.66	0.77	1.59	2.01	2.34	3.30	0.56	0.97	1.62
C5 - Parafins	24.52	21.70	20.93	18.87	19.98	21.17	19.53	18.99	18.65	18.08	21.43	21.32	21.16
C5 - Olefins	0.10	1.29	1.75	1.69	2.48	1.06	2.34	2.97	3.52	4.90	0.70	1.30	2.17
C6 - Parafins	16.07	17.46	16.65	16.61	16.93	16.69	16.24	15.77	15.36	14.86	17.49	17.05	16.39
C6 - Olefins	0.04	0.70	0.91	0.94	1.35	0.58	1.23	1.58	1.89	2.52	0.47	0.69	1.09
C7 - Parafins	8.47	10.64	10.22	11.31	10.84	10.15	10.50	10.25	10.02	9.70	11.15	10.73	10.49
C7 - Parafins	0.41	0.70	0.84	0.89	1.04	0.64	1.23	1.52	1.74	2.20	0.64	0.59	0.78

Table E.3: Detailed Selectivity Data for the Three Highest Platinum Metal Site / Acid Site Ratios

	Platinum metal/acid: 0,040				Platinum metal/acid: 0,100				Platinum metal/acid: 0,169			
Acid WHSV ($g_{feed}/g_{acid.cat}.hr$)	0.92	1.38	1.84	2.76	0.92	1.38	1.84	2.76	0.92	1.38	1.84	2.76
Metal WHSV ($g_{feed}/g_{metal.cat}.hr$)	6	9	12	17	2	3	5	7	1	2	3	4
Conversion (%)	95.89	45.22	34.02	21.52	96.36	61.25	44.95	25.88	95.24	65.14	46.87	26.34
C1	0.24	0.64	0.54	0.28	0.37	0.55	0.47	0.27	0.52	0.59	0.70	0.33
C2	0.07	0.00	0.00	0.00	0.05	0.00	0.00	0.00	0.07	0.02	0.01	0.00
C3	10.03	8.27	8.85	7.55	10.66	8.85	9.38	9.72	10.30	9.58	10.47	9.80
iso-C4	8.43	6.65	6.72	6.24	7.58	6.54	6.57	6.41	6.06	6.46	6.62	6.29
n-C4	12.63	13.25	13.13	13.02	14.57	13.77	13.81	13.66	14.03	13.91	13.98	14.13
iso-C5	13.09	12.39	11.46	12.15	12.31	11.97	11.72	11.66	11.80	11.49	10.69	11.73
n-C5	9.61	10.51	9.69	10.47	10.06	10.14	10.04	10.04	10.32	9.83	9.12	10.00
iso-C6	10.10	10.56	10.11	10.26	9.98	10.11	10.11	10.39	10.04	9.81	9.43	10.08
n-C6	8.04	8.03	8.02	8.16	7.58	7.73	7.90	8.02	8.10	7.56	7.55	7.74
iso-C7	8.01	7.96	8.60	9.13	7.69	8.00	8.06	8.16	7.91	7.97	8.17	7.98
n-C7	3.55	3.46	3.82	3.18	3.36	3.49	3.53	3.56	3.64	3.49	3.62	3.48
iso-C8	5.52	5.79	5.80	5.49	5.39	5.93	5.51	5.41	5.57	6.04	5.79	5.41
n-C8	1.29	1.36	1.46	1.62	1.18	1.32	1.34	1.35	1.29	1.34	1.39	1.34
iso-C9	3.60	3.93	4.09	4.10	3.51	3.97	4.00	3.77	3.72	4.08	4.22	3.87
n-C9	0.61	0.72	0.79	0.89	0.55	0.69	0.74	0.75	0.63	0.70	0.76	0.75
iso-C10	2.26	2.50	2.51	2.57	2.22	2.71	2.58	2.40	2.42	2.78	2.79	2.54
n-C10	0.32	0.48	0.56	0.66	0.27	0.43	0.49	0.55	0.35	0.44	0.51	0.54
iso-C11	1.40	1.63	1.71	1.59	1.37	1.81	1.67	1.64	1.57	1.85	1.88	1.66
n-C11	0.14	0.28	0.34	0.42	0.12	0.25	0.28	0.34	0.16	0.24	0.30	0.33
iso-C12	0.62	0.69	0.75	0.77	0.64	0.91	0.80	0.73	0.78	0.93	0.92	0.78
n-C12	0.05	0.12	0.15	0.21	0.04	0.10	0.13	0.17	0.06	0.10	0.14	0.17
iso-C13	0.20	0.13	0.05	0.03	0.23	0.21	0.15	0.03	0.28	0.23	0.20	0.04
n-C13	0.01	0.04	0.06	0.08	0.01	0.03	0.05	0.06	0.01	0.03	0.05	0.06
iso-C14	0.01	0.00	0.00	0.00	0.01	0.00	0.00	0.00	0.01	0.00	0.00	0.00
n-C14	0.00	0.00	0.00	0.00	0.00	0.00	0.00	0.00	0.00	0.00	0.00	0.00
iso-C15	0.03	0.00	0.00	0.00	0.03	0.02	0.00	0.00	0.04	0.02	0.00	0.00
n-C15	0.01	0.06	0.10	0.18	0.01	0.03	0.06	0.15	0.01	0.01	0.02	0.05
iso-C16	0.14	0.56	0.70	0.95	0.19	0.45	0.61	0.77	0.31	0.50	0.68	0.88
n-C16												
n- / iso- C4	1.50	1.99	1.96	2.09	1.92	2.11	2.10	2.13	2.32	2.15	2.11	2.25
n- / iso- C5	0.73	0.85	0.85	0.86	0.82	0.85	0.86	0.86	0.88	0.86	0.85	0.85
n- / iso- C6	0.80	0.76	0.79	0.80	0.76	0.76	0.78	0.77	0.81	0.77	0.80	0.77
n- / iso- C7	0.44	0.43	0.44	0.35	0.44	0.44	0.44	0.44	0.46	0.44	0.44	0.44
C3 - Parafins	10.00	8.25	8.83	7.55	10.65	8.85	9.38	9.72	10.30	9.58	10.45	9.80
C3 - Olefins	0.02	0.02	0.02	0.00	0.01	0.00	0.00	0.00	0.00	0.00	0.02	0.00
C4 - Parafins	20.99	19.83	19.81	19.15	22.13	20.29	20.38	20.07	20.05	20.37	20.59	20.42
C4 - Olefins	0.07	0.07	0.04	0.11	0.02	0.01	0.01	0.00	0.03	0.01	0.01	0.00
C5 - Parafins	22.60	22.78	21.03	22.38	22.35	22.08	21.72	21.70	22.04	21.32	19.79	21.73
C5 - Olefins	0.10	0.11	0.12	0.25	0.02	0.03	0.04	0.00	0.08	0.00	0.02	0.00
C6 - Parafins	18.06	18.56	18.10	18.36	17.54	17.84	18.01	18.42	18.06	17.38	16.98	17.82
C6 - Olefins	0.08	0.03	0.02	0.06	0.01	0.00	0.00	0.00	0.07	0.00	0.00	0.00
C7 - Parafins	11.19	11.23	12.21	11.44	10.77	11.28	11.40	11.53	11.24	11.23	11.59	11.27
C7 - Parafins	0.37	0.19	0.21	0.88	0.28	0.22	0.19	0.19	0.31	0.22	0.20	0.19

Table E.4: Detailed Conversion, Error and Rate Data for all Supported Palladium Loadings

Conversion Data (%)												
Reactor Number	WHSV ($g_{feed}/g_{acid.cat}.hr$)											Metal/Acid Ratio
	0.11	0.23	0.34	0.46	0.69	0.92	1.38	1.84	2.30	2.76	3.22	
1	90.52	30.78	22.26	18.94	11.01							0.0004
4	83.24	33.05	24.52	21.33	13.26							0.0013
2		83.73		39.49	23.07	18.05						0.0041
3						61.59	33.81	24.90	18.00	14.52	11.60	0.0403
1						99.77	58.43	42.60	29.11	24.59	23.24	0.1002
4						98.68	60.34	45.47	32.47	27.74	25.95	0.1692

Statistical Analysis - Percentage Error Values (for each conversion) (% error)												
Reactor Number	WHSV ($g_{feed}/g_{acid.cat}.hr$)											Metal/Acid Ratio
	0.11	0.23	0.34	0.46	0.69	0.92	1.38	1.84	2.30	2.76	3.22	
1	1.32	3.40	0.69	0.86	1.10							0.0004
4	4.06	1.33	1.21	0.98	0.56							0.0013
2		2.83		1.47	1.86	1.34						0.0041
3						1.15	1.07	1.60	1.19	0.82	1.01	0.0403
1						0.15	2.86	2.03	1.82	1.25	1.67	0.1002
4						0.05	1.44	3.75	3.43	1.00	2.62	0.1692

Rate Data (g_{feed} converted/$g_{acid.cat}.hr$)												
Reactor Number	WHSV ($g_{feed}/g_{acid.cat}.hr$)											Metal/Acid Ratio
	0.11	0.23	0.34	0.46	0.69	0.92	1.38	1.84	2.30	2.76	3.22	
1	10.40	7.07	7.67	8.70	7.59							0.0004
4	9.56	7.59	8.45	9.80	9.14							0.0013
2		19.24		18.15	15.91	16.59						0.0041
3						56.61	46.63	45.79	41.37	40.05	37.33	0.0403
1						91.72	80.58	78.32	66.90	67.81	74.77	0.1002
4						90.71	83.21	83.61	74.62	76.51	83.49	0.1692

Table E.5: Detailed Selectivity Data for the Three Lowest Palladium Metal Site / Acid Site Ratios

	Palladium metal/acid: 0,0004					Palladium metal/acid: 0,0013					Palladium metal/acid: 0,004			
Acid WHSV ($g_{feed}/g_{acid.cat}.hr$)	0.11	0.23	0.34	0.46	0.69	0.11	0.23	0.34	0.46	0.69	0.23	0.46	0.69	0.92
Metal WHSV ($g_{feed}/g_{metal.cat}.hr$)	153	306	460	613	919	43	86	129	172	258	27	54	82	109
Conversion (%)	90.52	30.78	22.26	18.94	11.01	83.24	33.05	24.52	21.33	13.26	83.73	39.49	23.07	18.05
C1	3.85	4.64	6.04	5.15	5.13	3.57	3.13	5.00	4.45	4.11	0.52	0.46	0.48	0.05
C2	1.17	0.25	0.00	0.00	0.00	0.57	0.17	0.00	0.00	0.00	0.22	0.12	0.04	0.00
C3	6.59	7.40	7.29	7.38	7.14	9.33	7.55	7.38	7.30	7.81	7.77	7.07	7.47	8.46
iso-C4	9.39	9.13	9.35	9.19	9.08	10.40	8.57	8.71	8.52	9.17	8.74	8.27	8.59	10.20
n-C4	12.18	11.30	11.03	11.03	10.51	14.03	12.10	11.66	11.55	11.66	12.48	11.52	11.43	13.41
iso-C5	9.80	9.83	10.14	10.12	10.68	9.54	9.70	10.16	10.16	11.09	10.29	10.58	10.74	11.79
n-C5	11.50	11.22	11.01	11.25	10.82	11.51	11.65	11.37	11.57	11.52	11.60	11.69	11.11	11.34
iso-C6	8.45	8.10	7.89	7.71	8.16	8.12	8.32	8.50	8.51	8.34	8.77	9.22	8.69	8.12
n-C6	8.38	8.39	8.50	8.77	9.05	6.75	8.46	8.44	8.84	8.66	8.44	8.96	8.68	8.19
iso-C7	7.24	7.02	7.13	7.25	7.85	6.24	6.75	6.87	7.02	7.04	7.24	7.49	7.75	7.59
n-C7	3.74	3.86	3.93	4.07	4.23	2.88	3.79	3.76	3.91	3.82	3.80	4.05	4.22	4.09
iso-C8	5.36	4.85	4.89	4.76	4.62	4.92	5.32	5.00	4.96	4.70	6.27	5.62	5.64	4.81
n-C8	1.74	1.84	1.90	1.89	2.06	1.23	1.68	1.56	1.62	1.69	1.85	1.78	1.88	1.93
iso-C9	3.61	3.54	3.45	3.26	2.70	3.64	3.70	3.41	3.32	3.01	3.76	3.88	3.91	2.87
n-C9	0.95	1.09	1.07	1.12	1.15	0.65	1.00	0.92	0.98	0.97	0.90	1.04	1.13	1.01
iso-C10	2.35	2.67	2.09	2.21	1.83	2.58	2.80	2.35	2.33	1.94	2.50	2.66	2.57	2.03
n-C10	0.59	0.84	0.76	0.89	0.95	0.24	0.74	0.72	0.78	0.82	0.54	0.76	0.86	0.85
iso-C11	1.59	1.60	1.26	1.17	0.95	1.67	2.04	1.73	1.52	1.02	1.76	2.03	1.85	1.26
n-C11	0.23	0.49	0.46	0.57	0.64	0.19	0.46	0.46	0.52	0.54	0.28	0.47	0.54	0.54
iso-C12	0.81	0.85	0.60	0.75	0.61	1.00	1.00	0.85	0.82	0.54	1.00	1.07	1.15	0.63
n-C12	0.10	0.24	0.25	0.31	0.34	0.07	0.22	0.23	0.28	0.29	0.12	0.22	0.27	0.27
iso-C13	0.21	0.16	0.11	0.10	0.06	0.40	0.21	0.12	0.12	0.05	0.47	0.27	0.17	0.04
n-C13	0.02	0.11	0.12	0.14	0.15	0.01	0.10	0.10	0.13	0.13	0.06	0.10	0.12	0.11
iso-C14	0.04	0.03	0.02	0.00	0.00	0.09	0.04	0.01	0.01	0.00	0.09	0.05	0.00	0.00
n-C14	0.01	0.02	0.03	0.02	0.00	0.01	0.03	0.00	0.01	0.00	0.02	0.03	0.00	0.00
iso-C15	0.01	0.00	0.00	0.00	0.00	0.05	0.00	0.00	0.00	0.00	0.08	0.01	0.00	0.00
n-C15	0.01	0.04	0.06	0.07	0.12	0.01	0.02	0.01	0.01	0.01	0.02	0.03	0.04	0.05
iso-C16	0.08	0.48	0.62	0.81	1.18	0.30	0.47	0.66	0.76	1.05	0.40	0.54	0.68	0.37
n-C16														
n- / iso- C4	1.30	1.24	1.18	1.20	1.16	1.35	1.41	1.34	1.36	1.27	1.43	1.39	1.33	1.31
n- / iso- C5	1.17	1.14	1.09	1.11	1.01	1.21	1.20	1.12	1.14	1.04	1.13	1.10	1.04	0.96
n- / iso- C6	0.99	1.04	1.08	1.14	1.11	0.83	1.02	0.99	1.04	1.04	0.96	0.97	1.00	1.01
n- / iso- C7	0.52	0.55	0.55	0.56	0.54	0.46	0.56	0.55	0.56	0.54	0.53	0.54	0.54	0.54
C3 - Parafins	6.34	6.98	6.76	6.86	6.43	9.30	7.38	7.09	6.99	7.28	7.57	6.79	7.06	7.87
C3 - Olefins	0.25	0.42	0.53	0.52	0.71	0.03	0.16	0.29	0.31	0.54	0.21	0.28	0.41	0.59
C4 - Parafins	20.24	18.48	18.04	17.81	16.40	24.22	19.97	19.17	18.72	18.44	20.14	18.44	18.16	20.66
C4 - Olefins	1.33	1.94	2.35	2.41	3.19	0.21	0.71	1.20	1.35	2.39	1.08	1.35	1.85	2.95
C5 - Parafins	19.19	18.14	17.69	17.73	16.42	20.77	20.27	19.84	19.78	19.16	20.30	20.31	19.21	18.87
C5 - Olefins	2.11	2.91	3.46	3.64	5.08	0.28	1.07	1.70	1.96	3.46	1.60	1.97	2.64	4.26
C6 - Parafins	15.63	14.95	14.52	14.55	14.36	14.65	16.23	16.07	16.29	15.21	16.30	17.09	16.01	14.14
C6 - Olefins	1.19	1.54	1.86	1.92	2.85	0.23	0.55	0.87	1.06	1.79	0.91	1.09	1.36	2.17
C7 - Parafins	9.65	9.38	9.47	9.60	9.67	8.73	10.03	9.95	10.14	9.62	10.07	10.60	10.85	9.83
C7 - Parafins	1.33	1.50	1.59	1.73	2.40	0.39	0.51	0.68	0.78	1.25	0.97	0.95	1.12	1.85

Table E.6: Detailed Selectivity Data for the Three Highest Palladium Metal Site / Acid Site Ratios

	Palladium metal/acid: 0,040						Palladium metal/acid: 0,100						Palladium metal/acid: 0,169					
Acid WHSV ($g_{feed}/g_{acid.cat}$·hr)	0.92	1.38	1.84	2.30	2.76	3.22	0.92	1.38	1.84	2.30	2.76	3.22	0.92	1.38	1.84	2.30	2.76	3.22
Metal WHSV ($g_{feed}/g_{metal.cat}$·hr)	11	17	22	28	33	39	4	7	9	11	13	16	3	4	5	7	8	9
Conversion (%)	61.59	33.81	24.90	18.00	14.52	11.60	99.77	58.43	42.60	29.11	24.59	23.24	98.68	60.34	45.47	32.47	27.74	25.95
C1	0.17	0.23	0.22	0.00	0.00	0.00	0.07	0.11	0.13	0.03	0.00	0.00	0.12	0.10	0.09	0.07	0.00	0.00
C2	0.07	0.00	0.00	0.00	0.00	0.00	0.06	0.01	0.00	0.00	0.00	0.00	0.06	0.03	0.00	0.00	0.00	0.00
C3	8.39	9.09	7.77	9.15	7.98	8.39	10.69	9.00	9.22	9.76	9.15	9.73	11.42	7.58	9.01	10.03	9.58	10.02
iso-C4	7.45	7.73	6.95	7.62	7.97	6.61	8.74	7.08	6.97	7.28	7.13	6.84	7.77	7.02	6.47	6.71	6.38	6.61
n-C4	13.00	13.84	12.74	13.58	14.37	11.79	14.79	13.89	13.60	14.61	13.32	13.77	14.95	14.45	14.18	14.30	14.00	14.14
iso-C5	11.34	11.75	11.14	11.43	12.00	10.90	12.98	12.05	11.59	11.89	11.32	11.36	12.56	12.05	12.31	11.76	11.91	11.34
n-C5	10.78	10.86	10.37	10.65	10.88	10.43	10.56	10.55	10.29	10.29	10.11	10.04	9.99	10.14	10.63	9.88	10.21	9.51
iso-C6	9.67	9.61	9.35	9.65	9.34	10.21	10.23	10.11	9.89	9.35	9.99	10.01	10.01	10.14	10.48	9.87	10.10	9.68
n-C6	8.19	7.99	8.12	8.37	7.98	8.91	7.56	7.97	7.94	7.50	8.16	8.10	7.52	7.76	8.17	7.66	7.78	7.57
iso-C7	7.72	7.37	8.09	7.79	7.51	8.29	7.58	7.89	7.87	7.35	8.11	8.06	7.63	8.11	8.30	7.99	7.72	8.17
n-C7	3.71	3.48	4.03	3.74	3.63	4.19	3.15	3.52	3.56	3.33	3.68	3.65	3.32	3.53	3.65	3.48	3.35	3.61
iso-C8	5.92	5.44	6.32	5.33	5.29	6.24	5.16	5.73	5.85	5.45	5.85	5.66	5.34	6.08	5.83	5.79	5.65	5.77
n-C8	1.52	1.42	1.74	1.48	1.51	1.78	1.02	1.30	1.40	1.36	1.43	1.41	1.12	1.32	1.33	1.32	1.34	1.43
iso-C9	3.99	3.75	4.36	3.55	3.58	3.87	3.19	3.79	3.92	3.86	3.81	3.78	3.31	4.07	3.52	3.82	4.01	4.13
n-C9	0.81	0.80	0.96	0.85	0.88	0.97	0.41	0.67	0.76	0.79	0.78	0.79	0.50	0.69	0.68	0.71	0.77	0.82
iso-C10	2.82	2.58	2.82	2.54	2.47	2.62	1.80	2.56	2.67	2.76	2.69	2.53	1.86	2.79	2.14	2.56	2.81	2.78
n-C10	0.52	0.56	0.68	0.65	0.67	0.77	0.17	0.43	0.52	0.58	0.59	0.59	0.25	0.44	0.45	0.51	0.56	0.60
iso-C11	1.82	1.60	1.73	1.28	1.26	1.34	1.04	1.65	1.78	1.72	1.67	1.56	1.15	1.80	1.31	1.69	1.73	1.76
n-C11	0.29	0.33	0.45	0.41	0.43	0.49	0.07	0.24	0.32	0.36	0.37	0.38	0.10	0.26	0.21	0.33	0.35	0.38
iso-C12	0.93	0.66	0.88	0.59	0.53	0.50	0.51	0.76	0.78	0.75	0.73	0.72	0.60	0.86	0.59	0.74	0.78	0.78
n-C12	0.12	0.15	0.21	0.20	0.22	0.26	0.02	0.09	0.15	0.17	0.18	0.19	0.04	0.10	0.10	0.16	0.18	0.20
iso-C13	0.23	0.03	0.05	0.03	0.02	0.01	0.14	0.17	0.17	0.03	0.03	0.03	0.21	0.20	0.12	0.04	0.03	0.03
n-C13	0.05	0.06	0.08	0.07	0.08	0.07	0.00	0.03	0.05	0.06	0.06	0.06	0.01	0.03	0.04	0.05	0.06	0.07
iso-C14	0.01	0.00	0.00	0.00	0.00	0.00	0.00	0.00	0.00	0.00	0.00	0.00	0.00	0.00	0.00	0.00	0.00	0.00
n-C14	0.01	0.00	0.00	0.00	0.00	0.00	0.00	0.00	0.00	0.00	0.00	0.00	0.00	0.00	0.00	0.00	0.00	0.00
iso-C15	0.03	0.00	0.00	0.00	0.00	0.00	0.02	0.00	0.00	0.00	0.00	0.00	0.03	0.01	0.00	0.00	0.00	0.00
n-C15	0.03	0.09	0.15	0.22	0.29	0.40	0.00	0.03	0.06	0.12	0.16	0.20	0.01	0.01	0.01	0.03	0.04	0.05
iso-C16	0.44	0.57	0.77	0.81	1.10	0.96	0.05	0.37	0.49	0.58	0.68	0.54	0.14	0.42	0.38	0.52	0.65	0.53
n-C16																		
n- / iso- C4	1.74	1.79	1.83	1.78	1.80	1.78	1.69	1.96	1.95	2.01	1.87	2.01	1.92	2.06	2.19	2.13	2.19	2.14
n- / iso- C5	0.95	0.92	0.93	0.93	0.91	0.96	0.81	0.88	0.89	0.87	0.89	0.88	0.80	0.84	0.86	0.84	0.86	0.84
n- / iso- C6	0.85	0.83	0.87	0.87	0.85	0.87	0.74	0.79	0.80	0.80	0.82	0.81	0.75	0.77	0.78	0.78	0.77	0.78
n- / iso- C7	0.48	0.47	0.50	0.48	0.48	0.51	0.41	0.45	0.45	0.45	0.45	0.45	0.43	0.44	0.44	0.44	0.43	0.44
C3 - Parafins	8.33	8.99	7.68	8.97	7.82	8.14	10.68	8.98	9.22	9.76	9.15	9.73	11.41	7.58	9.01	10.03	9.58	10.02
C3 - Olefins	0.06	0.09	0.09	0.18	0.16	0.25	0.00	0.02	0.00	0.00	0.00	0.00	0.01	0.00	0.00	0.00	0.00	0.00
C4 - Parafins	20.17	21.22	19.34	20.58	21.73	17.58	23.51	20.90	20.49	21.81	20.36	20.50	22.69	21.43	20.63	21.01	20.38	20.75
C4 - Olefins	0.28	0.35	0.36	0.62	0.62	0.82	0.02	0.06	0.08	0.07	0.09	0.11	0.02	0.03	0.02	0.00	0.00	0.00
C5 - Parafins	21.73	22.13	20.91	21.18	21.97	20.08	23.51	22.47	21.74	22.04	21.26	21.20	22.51	22.13	22.88	21.55	22.02	20.76
C5 - Olefins	0.38	0.48	0.61	0.90	0.92	1.25	0.02	0.13	0.14	0.15	0.16	0.20	0.03	0.06	0.06	0.08	0.10	0.10
C6 - Parafins	17.65	17.38	17.19	17.61	16.96	18.48	17.78	18.02	17.77	16.85	18.13	18.03	17.51	17.89	18.64	17.53	17.88	17.25
C6 - Olefins	0.21	0.22	0.28	0.41	0.35	0.64	0.01	0.05	0.06	0.00	0.01	0.07	0.02	0.02	0.01	0.00	0.00	0.00
C7 - Parafins	11.12	10.62	11.82	11.18	10.87	12.00	10.45	11.20	11.23	10.50	11.59	11.51	10.70	11.42	11.81	11.28	10.88	11.57
C7 - Parafins	0.31	0.23	0.30	0.35	0.27	0.48	0.27	0.21	0.19	0.18	0.20	0.20	0.25	0.22	0.15	0.20	0.19	0.20

Table E.7: Detailed Conversion, Error and Rate Data for all Supported Nickel Loadings

Conversion Data (%)											
Reactor Number	WHSV ($g_{feed}/g_{acid.cat}.hr$)										Metal/Acid Ratio
	0.11	0.23	0.34	0.46	0.57	0.69	0.92	1.15	1.38	1.61	
2	82.96	53.16	25.62	20.91	12.31						0.0041
3		97.90		50.42		21.55	23.28	10.39			0.0401
1				97.80		60.82	55.58	26.84	16.81	16.97	0.1000
4				99.27		82.39	60.59	35.43	23.55	23.83	0.1691

Statistical Analysis - Percentage Error Values (for each conversion) (% error)											
Reactor Number	WHSV ($g_{feed}/g_{acid.cat}.hr$)										Metal/Acid Ratio
	0.11	0.23	0.34	0.46	0.57	0.69	0.92	1.15	1.38	1.61	
2	1.54	2.41	1.42	1.03	0.17						0.0041
3		1.36		1.15		1.87	2.49	1.02			0.0401
1				1.10		1.36	0.94	0.49	1.48	1.92	0.1000
4				0.25		3.30	1.57	1.65	1.05	1.27	0.1691

Rate Data (g_{feed} converted/$g_{acid.cat}.hr$)											
Reactor Number	WHSV ($g_{feed}/g_{acid.cat}.hr$)										Metal/Acid Ratio
	0.11	0.23	0.34	0.46	0.57	0.69	0.92	1.15	1.38	1.61	
2	9.53	12.21	8.83	9.61	7.07						0.0041
3		22.49		23.17		14.85	21.40	11.93			0.0401
1				44.94		41.92	51.08	30.84	23.17	27.29	0.1000
4				45.62		56.79	55.69	40.70	32.46	38.33	0.1691

Table E.8: Detailed Selectivity Data for the Two Lowest Nickel Metal Site / Acid Site Ratios

	Nickel metal/acid: 0,004					Nickel metal/acid: 0,040				
Acid WHSV ($g_{feed}/g_{acid.cat}.hr$)	0.11	0.23	0.34	0.46	0.57	0.23	0.46	0.69	0.92	1.15
Metal WHSV ($g_{feed}/g_{metal.cat}.hr$)	20	40	59	79	99	4	8	12	16	20
Conversion (%)	82.96	53.16	25.62	20.91	12.31	97.90	50.42	21.55	23.28	10.39
C1	0.89	1.03	0.76	0.60	0.89	0.26	0.19	0.48	0.36	0.67
C2	0.81	0.30	0.19	0.12	0.00	0.56	0.11	0.01	0.02	0.00
C3	19.85	7.35	7.54	7.16	7.99	10.93	8.32	7.97	7.49	9.51
iso-C4	15.60	9.60	10.31	9.67	10.73	9.72	8.81	8.77	8.31	9.67
n-C4	21.15	11.11	11.16	10.85	11.38	13.75	12.72	12.59	12.42	12.49
iso-C5	10.18	9.99	11.14	10.63	12.18	9.48	9.90	10.51	10.42	10.99
n-C5	10.81	11.14	11.21	11.14	11.52	11.51	11.26	12.00	11.21	11.59
iso-C6	7.24	8.37	7.75	8.14	6.50	7.97	8.44	8.70	8.56	8.64
n-C6	2.91	8.47	8.71	8.66	8.97	8.05	8.60	9.14	8.73	9.39
iso-C7	4.15	7.54	7.95	7.62	7.91	6.31	6.91	6.98	7.53	7.07
n-C7	0.57	4.02	4.10	4.13	4.20	3.71	4.13	4.23	4.35	4.15
iso-C8	2.95	4.94	4.85	5.01	4.55	4.93	5.65	4.89	5.55	4.07
n-C8	0.09	2.00	2.15	2.15	2.17	1.58	1.93	1.83	1.87	1.66
iso-C9	1.62	3.74	3.41	3.71	2.42	3.50	4.02	3.34	3.92	2.64
n-C9	0.03	1.19	1.20	1.25	1.19	0.83	1.05	1.08	1.10	1.06
iso-C10	0.68	2.81	1.95	2.54	1.47	2.50	2.77	2.41	2.74	2.06
n-C10	0.02	0.88	0.94	1.01	0.98	0.45	0.67	0.79	0.79	0.83
iso-C11	0.19	2.05	1.15	1.56	1.09	1.80	1.96	1.61	1.86	0.99
n-C11	0.03	0.51	0.58	0.62	0.40	0.21	0.36	0.47	0.50	0.50
iso-C12	0.08	1.16	0.72	0.88	0.57	0.99	1.08	0.90	1.07	0.44
n-C12	0.03	0.26	0.30	0.32	0.32	0.07	0.16	0.23	0.25	0.25
iso-C13	0.01	0.47	0.20	0.20	0.05	0.43	0.35	0.09	0.16	0.00
n-C13	0.00	0.10	0.14	0.14	0.14	0.02	0.07	0.10	0.11	0.10
iso-C14	0.00	0.15	0.05	0.03	0.00	0.04	0.03	0.00	0.00	0.00
n-C14	0.00	0.04	0.06	0.05	0.00	0.01	0.01	0.00	0.00	0.00
iso-C15	0.01	0.03	0.00	0.00	0.00	0.14	0.03	0.00	0.00	0.00
n-C15	0.00	0.03	0.05	0.06	0.08	0.02	0.03	0.11	0.09	0.22
iso-C16	0.09	0.73	1.43	1.73	2.32	0.22	0.44	0.75	0.61	1.00
n-C16										
n- / iso- C4	1.36	1.16	1.08	1.12	1.06	1.41	1.44	1.44	1.50	1.29
n- / iso- C5	1.06	1.12	1.01	1.05	0.95	1.21	1.14	1.14	1.08	1.05
n- / iso- C6	0.40	1.01	1.12	1.06	1.38	1.01	1.02	1.05	1.02	1.09
n- / iso- C7	0.14	0.53	0.52	0.54	0.53	0.59	0.60	0.61	0.58	0.59
C3 - Parafins	19.80	6.89	6.85	6.56	7.01	10.87	8.19	7.73	7.26	9.05
C3 - Olefins	0.05	0.45	0.72	0.60	0.96	0.06	0.12	0.24	0.23	0.46
C4 - Parafins	36.64	18.56	18.07	17.58	17.25	23.16	20.98	20.32	19.84	20.22
C4 - Olefins	0.12	2.16	3.52	2.94	4.73	0.31	0.55	1.05	0.89	1.98
C5 - Parafins	20.86	17.69	16.76	17.25	16.26	20.58	20.37	20.88	20.33	19.24
C5 - Olefins	0.14	3.44	5.61	4.52	7.33	0.41	0.80	1.62	1.30	3.07
C6 - Parafins	9.99	14.99	13.20	14.36	11.89	15.77	16.61	17.03	16.63	16.42
C6 - Olefins	0.17	1.85	3.08	2.44	3.93	0.25	0.44	0.80	0.66	1.53
C7 - Parafins	3.95	9.69	9.28	9.56	8.67	9.60	10.62	10.63	11.35	10.39
C7 - Parafins	0.76	1.86	2.82	2.19	3.35	0.41	0.42	0.59	0.53	0.99

Table E.9: Detailed Selectivity Data for the Two Highest Nickel Metal Site / Acid Site Ratios

	Nickel metal/acid: 0,100						Nickel metal/acid: 0,169					
Acid WHSV ($g_{feed}/g_{acid.cat}.hr$)	0.46	0.69	0.92	1.15	1.38	1.61	0.46	0.69	0.92	1.15	1.38	1.61
Metal WHSV ($g_{feed}/g_{metal.cat}.hr$)	3	5	6	8	10	11	2	3	4	5	6	7
Conversion (%)	97.80	60.82	55.58	26.84	16.81	16.97	99.3	82.4	60.6	35.4	23.5	23.83
C1	0.10	0.14	0.17	0.23	0.40	0.55	0.04	0.13	0.15	0.22	0.25	0.37
C2	0.04	0.05	0.05	0.00	0.00	0.00	0.07	0.05	0.05	0.00	0.00	0.00
C3	11.50	9.22	9.00	9.28	9.25	8.04	11.19	9.32	9.41	9.50	9.69	8.42
iso-C4	9.91	8.01	7.83	7.80	7.68	7.05	11.29	8.13	7.54	7.47	7.61	7.10
n-C4	11.04	13.69	13.72	13.66	13.47	12.31	15.50	14.20	14.00	14.26	14.69	14.04
iso-C5	11.80	10.81	10.99	10.82	10.62	10.16	12.35	11.40	11.20	11.22	11.42	11.46
n-C5	12.19	11.36	11.14	11.50	11.36	11.31	11.89	11.53	11.16	11.19	11.48	11.70
iso-C6	9.53	9.15	9.20	9.08	8.88	9.32	9.56	9.45	9.36	9.20	9.15	9.15
n-C6	8.51	8.53	8.38	8.73	8.84	9.58	6.89	8.35	8.34	8.36	8.43	8.51
iso-C7	7.03	7.29	7.39	7.07	7.24	7.83	6.76	7.34	7.46	7.24	6.88	7.11
n-C7	3.56	3.88	3.80	3.79	4.04	4.42	2.47	3.59	3.78	3.76	3.53	3.79
iso-C8	4.75	5.41	5.56	5.17	5.16	5.56	4.41	5.29	5.57	5.35	4.77	5.40
n-C8	1.23	1.50	1.50	1.52	1.62	1.77	0.71	1.30	1.45	1.46	1.40	1.61
iso-C9	3.32	3.57	3.73	3.52	3.48	3.68	2.84	3.52	3.68	3.47	3.38	3.81
n-C9	0.51	0.77	0.81	0.85	0.90	0.98	0.21	0.62	0.74	0.76	0.81	0.90
iso-C10	2.10	2.52	2.62	2.50	2.43	2.50	1.70	2.31	2.45	2.44	2.37	2.38
n-C10	0.21	0.47	0.51	0.60	0.68	0.74	0.06	0.32	0.44	0.53	0.59	0.61
iso-C11	1.42	1.69	1.66	1.69	1.34	1.45	1.18	1.52	1.51	1.64	1.42	1.39
n-C11	0.07	0.25	0.24	0.37	0.42	0.46	0.03	0.15	0.23	0.31	0.36	0.37
iso-C12	0.68	0.85	0.86	0.82	0.77	0.83	0.55	0.75	0.76	0.75	0.77	0.80
n-C12	0.02	0.10	0.12	0.17	0.22	0.23	0.01	0.06	0.09	0.15	0.19	0.19
iso-C13	0.28	0.23	0.20	0.05	0.03	0.03	0.20	0.26	0.18	0.12	0.03	0.03
n-C13	0.01	0.04	0.04	0.07	0.08	0.09	0.00	0.02	0.03	0.06	0.07	0.07
iso-C14	0.00	0.01	0.00	0.00	0.00	0.00	0.00	0.01	0.00	0.00	0.00	0.00
n-C14	0.00	0.00	0.00	0.00	0.00	0.00	0.00	0.00	0.00	0.00	0.00	0.00
iso-C15	0.05	0.03	0.03	0.00	0.00	0.00	0.02	0.04	0.03	0.00	0.00	0.00
n-C15	0.01	0.02	0.02	0.07	0.13	0.13	0.00	0.02	0.01	0.02	0.03	0.02
iso-C16	0.15	0.43	0.40	0.65	0.95	0.99	0.05	0.32	0.37	0.53	0.70	0.75
n-C16												
n- / iso- C4	1.11	1.71	1.75	1.75	1.75	1.75	1.37	1.75	1.86	1.91	1.93	1.98
n- / iso- C5	1.03	1.05	1.01	1.06	1.07	1.11	0.96	1.01	1.00	1.00	1.01	1.02
n- / iso- C6	0.89	0.93	0.91	0.96	0.99	1.03	0.72	0.88	0.89	0.91	0.92	0.93
n- / iso- C7	0.51	0.53	0.51	0.54	0.56	0.56	0.36	0.49	0.51	0.52	0.51	0.53
C3 - Parafins	11.49	9.18	8.95	9.21	9.15	7.95	11.19	9.30	9.38	9.50	9.69	8.89
C3 - Olefins	0.00	0.04	0.04	0.07	0.10	0.09	0.00	0.02	0.02	0.00	0.00	0.00
C4 - Parafins	20.91	21.53	21.41	21.26	20.86	19.11	26.77	22.26	21.49	21.66	22.17	21.23
C4 - Olefins	0.04	0.17	0.15	0.19	0.30	0.26	0.01	0.07	0.06	0.07	0.13	0.09
C5 - Parafins	23.94	21.93	21.90	21.91	21.33	20.83	24.22	22.82	22.24	22.27	22.66	22.62
C5 - Olefins	0.05	0.25	0.23	0.41	0.65	0.64	0.01	0.11	0.12	0.14	0.24	0.21
C6 - Parafins	18.02	17.56	17.48	17.66	17.47	18.63	16.45	17.74	17.65	17.52	17.49	17.58
C6 - Olefins	0.02	0.12	0.11	0.15	0.24	0.26	0.00	0.07	0.05	0.03	0.09	0.05
C7 - Parafins	10.32	10.93	10.98	10.72	11.06	12.06	8.91	10.67	11.03	10.85	10.26	10.81
C7 - Parafins	0.27	0.23	0.21	0.14	0.22	0.20	0.32	0.26	0.21	0.15	0.14	0.15

Table E.10: Detailed Conversion, Error and Rate Data for all Supported Cobalt Loadings

Conversion Data (%)				
Reactor Number	WHSV ($g_{feed}/g_{acid.cat}.hr$)			Metal/Acid Ratio
	0.11	0.23	0.46	
2	61.73	24.59	17.96	0.00014
3	60.54	22.59	13.24	0.00121
4	85.99	54.83	32.08	0.00509
1	----	----	----	0.00302

Percentage Error Values (for each conversion) (% error)				
Reactor Number	WHSV ($g_{feed}/g_{acid.cat}.hr$)			Metal/Acid Ratio
	0.11	0.23	0.46	
2	4.14	1.29	2.37	0.00014
3	5.97	1.44	1.61	0.00121
4	4.33	2.43	2.25	0.00509
1	----	----	----	0.00302

Rate Data (g_{feed} converted/$g_{acid.cat}.hr$)				
Reactor Number	WHSV ($g_{feed}/g_{acid.cat}.hr$)			Metal/Acid Ratio
	0.11	0.23	0.46	
2	7.09	5.65	8.25	0.00014
3	6.96	5.19	6.08	0.00121
4	9.88	12.60	14.74	0.00509
1	----	----	----	0.00302

The loading at the M/A ratio of 0.003 was stopped as the reactor became blocked and the n-hexadecane feed was not reaching the catalyst but flowed into the safety catch pot.

Table E.11: Detailed Selectivity Data for all the Cobalt Metal Site / Acid Site Ratios

	Cobalt metal/acid: 0,00014			Cobalt metal/acid: 0,0021			Cobalt metal/acid: 0,00509		
Acid WHSV ($g_{feed}/g_{acid.cat}.hr$)	0.11	0.23	0.46	0.11	0.23	0.46	0.11	0.23	0.46
Conversion (%)	61.7	24.6	18.0	60.5	22.6	13.2	86.0	54.8	32.1
C1	15.81	17.21	6.23	19.26	19.27	11.18	3.96	7.08	8.67
C2	2.69	1.19	0.13	2.99	0.83	0.00	0.69	0.73	0.28
C3	6.58	0.43	5.64	6.71	0.38	4.27	11.32	4.83	5.12
iso-C4	8.33	8.75	9.62	7.89	8.77	9.27	5.50	9.08	8.43
n-C4	9.95	9.75	10.72	10.00	9.71	10.30	11.80	12.67	12.25
iso-C5	7.97	9.27	10.58	6.79	8.79	10.31	4.00	8.68	8.77
n-C5	9.52	10.70	11.24	9.30	9.92	11.34	13.71	12.02	11.40
iso-C6	6.77	7.24	7.94	6.39	7.04	7.62	10.91	8.01	7.37
n-C6	7.01	8.27	9.13	6.79	8.09	8.92	8.88	8.53	8.24
iso-C7	5.73	6.67	7.56	5.67	6.98	6.15	7.29	5.53	5.00
n-C7	3.21	3.81	4.21	2.41	4.09	3.92	3.25	3.88	3.88
iso-C8	3.90	3.89	4.48	4.05	4.26	3.69	5.93	4.63	4.87
n-C8	1.59	1.88	2.09	1.55	1.93	1.96	1.65	1.67	1.89
iso-C9	2.98	3.15	2.87	2.70	2.85	2.96	4.62	3.77	3.95
n-C9	1.02	1.09	1.17	1.06	0.99	1.26	0.66	0.94	1.10
iso-C10	2.69	2.57	2.77	2.63	2.23	2.83	3.32	3.06	3.58
n-C10	0.06	0.06	0.00	0.06	0.05	0.00	0.09	0.14	0.15
iso-C11	2.42	2.68	2.22	1.99	2.47	2.61	1.75	3.01	3.27
n-C11	0.11	0.12	0.10	0.09	0.11	0.13	0.07	0.14	0.14
iso-C12	0.73	0.72	0.74	0.78	0.66	0.75	0.23	0.73	0.79
n-C12	0.07	0.07	0.05	0.08	0.05	0.02	0.02	0.03	0.03
iso-C13	0.37	0.12	0.10	0.41	0.13	0.14	0.12	0.32	0.19
n-C13	0.00	0.00	0.00	0.00	0.00	0.00	0.00	0.00	0.00
iso-C14	0.07	0.00	0.00	0.03	0.00	0.00	0.02	0.04	0.02
n-C14	0.01	0.00	0.00	0.00	0.00	0.00	0.00	0.01	0.00
iso-C15	0.43	0.37	0.39	0.39	0.39	0.41	0.20	0.48	0.60
n-C15	0.00	0.00	0.00	0.00	0.00	0.00	0.00	0.00	0.00
iso-C16	0.00	0.00	0.00	0.00	0.00	0.00	0.00	0.00	0.00
n-C16									
n- / iso- C4	1.19	1.11	1.11	1.27	1.11	1.11	2.15	1.40	1.45
n- / iso- C5	1.19	1.15	1.06	1.37	1.13	1.10	3.43	1.39	1.30
n- / iso- C6	1.04	1.14	1.15	1.06	1.15	1.17	0.81	1.06	1.12
n- / iso- C7	0.56	0.57	0.56	0.42	0.59	0.64	0.45	0.70	0.78